Western U.S. Forest Carbon Balance in the 21st Century: Improving Projections with Improved Disturbance Monitoring and Modeling

A Dissertation

Presented in Partial Fulfillment for the Requirement for the

Degree of Doctor of Philosophy

with a

Major in Natural Resources

in the

College of Graduate Studies

University of Idaho

by

Jeffrey E. Stenzel

Major Professor: Tara W. Hudiburg, Ph.D.

Committee Members: Zachary E. Kayler, Ph.D.; Crystal Kolden, Ph.D.;

Timothy E. Link, Ph.D.

Department Administrator: P. Charles Goebel, Ph.D.

May 2021

Authorization to Submit Dissertation

This dissertation of Jeffrey E. Stenzel, submitted for the degree of Doctor of Philosophy with a Major in Natural Resources and titled "WESTERN U.S. FOREST CARBON BALANCE IN THE 21ST CENTURY: IMPROVING PROJECTIONS WITH IMPROVED DISTURBANCE MONITORING AND MODELING," has been reviewed in final form. Permission, as indicated by the signatures and dates below, is now granted to submit final copies to the College of Graduate Studies for approval.

Major Professor: _____ Date: _____
Tara W. Hudiburg, Ph.D.

Committee Members: _____ Date: _____
Zachary E. Kayler, Ph.D.

_____ Date: _____
Crystal Kolden, Ph.D.

_____ Date: _____
Timothy E. Link, Ph.D.

Department Administrator: _____ Date: _____
P. Charles Goebel, Ph.D.

Abstract

The forests of the western United States face profound impacts from shifts in climate, natural disturbance regimes, and land management in the 21st century. Under novel conditions, forest ecosystem services will be altered, including impacts to forest climate moderation, resource provision, and biodiversity. However, the complex processes that determine present-day observed forest structure and composition across the complex terrain of the region are incompletely understood. As a result, scientists and land managers are confronted with considerable uncertainty as to how widespread natural and human impacts upon forests will result in changed processes and states. This dissertation employs model-observation frameworks to examine and improve upon the understanding of how disturbance will impact western U.S. forest carbon balances from site to regional scales.

Chapter 1 addresses deficiencies in current process model representations of direct emissions and ecosystem mortality transfers during forest fire. In this study, I incorporate novel observations and modify an ecosystem biogeochemical model to compare to model default assumptions. Projected carbon balance impacts of observation-based vs model-based assumption are then quantified in: 1) A carbon dense forest via a modified Daycent biogeochemical model; 2) Across the western United States from 2000-2016. At the state level, model default assumptions lead to 50-110% overestimates in carbon emissions, primarily due to the unrealistic combustion of live tree bole biomass and compounded by a lack of standing-dead biomass pool representation. Projections demonstrate that emissions overestimates can increase to 300-500% in carbon dense forests (e.g. old growth) in the midterm (30 years) due to altered decomposition.

Chapter 2 quantifies the carbon and water balance impacts of an experimental selective thinning in a ponderosa pine forest in the University of Idaho Experimental Forest. I use automated and traditional ecosystem stock and flux measurements to estimate the impacts of treatments from 2016-2019 at contrasting tree and stand scales, with a focus on the balance between primary producer density reductions and mitigated summer drought stress. I then project the on and off-site carbon balance impacts of treatment through 2050 with a life cycle assessment (LCA) and with the Daycent biogeochemical model. Projections allow the exploration of whether carbon parity with control stands is reached within common emissions reduction time periods. Observations indicated an average 30% increase in thinned stand residual tree growth. In contrast to the control stand, treated stand tree transpiration persisted through the summer drought period. However, production and water use increases did not compensate for tree density reductions and both yearly Net Primary Production (NPP) and transpiration decreased in treatment stands. Projections demonstrated that large harvest-event emissions pulses from long-lived woody biomass pools led to long carbon deficit legacies; treatment carbon storage parity with control stands was not reached by 2050.

Chapter 3 employs a dynamic global vegetation model (DGVM) to simulate chapter 2 stand dynamics and examine model applicability for simulations across a northern Rocky Mountain ecoregion domain. The FATES DGVM simulates forest composition and structure, disturbance regimes, biogeochemistry, and biophysics, operating within the Community Land Model 5 (CLM5) of the Community Earth Systems Model (CESM). I examine FATES dynamics in the context of: 1) Variable intensity selective harvests; 2) Historical and future control and treatment stands; and, 3) sensitive input parameter variation.

Acknowledgments

I would like to thank Dr. Tara Hudiburg, my PhD and MS advisor, for the flexible encouragement that led to my completion of both anticipated (Chapter 2,3) and discovery-based (Chapter 1) studies. I greatly appreciate the support of the ITEAM graduate students and post-docs: Kristina Bartowitz, Danielle Berardi, Jeff Kent, and Eric Walsh. I thank my committee members: Drs. Zachary Kayler, Crystal Kolden, and Timothy Link for both your past input and anticipated future input on ongoing studies. Thank you Dr. Robert Keefe and UIEF work crews for thinning operations. Thank you Dr. Polly Buotte for extensive consultation on CLM FATES modeling. Thank you Melannie Hartman for the creation of Daycent with snags and Andrew Larson, Jim Lutz, and Mark Swanson for extensive YFDP observations. Funding for the research of this dissertation has been enabled by National Science Foundation award number DEB-1553049.

Table of Contents

List of Figures

List of Tables

Chapter 1: Fixing a snag in carbon emissions estimates from wildfires

Published in *Global Change Biology* as:

Stenzel, J. E., Lutz, J. A., Bartowitz, K. J., Hartman, M. D., Kolden, C. A., Smith, A. M. S., … Hudiburg, T. W. (2019). Fixing a snag in carbon emissions estimates from wildfires. Global Change, (March), 1–10. https://doi.org/10.1111/gcb.14716

Abstract

Wildfire is an essential earth-system process, impacting ecosystem processes and the carbon cycle. Forest fires are becoming more frequent and severe, yet gaps exist in the modeling of fire on vegetation and carbon dynamics. Strategies for reducing carbon dioxide (CO2) emissions from wildfires include increasing tree harvest, largely based on the public assumption that fires burn live forests to the ground, despite observations indicating that less than 5% of mature tree biomass is actually consumed. This misconception is also reflected though excessive combustion of live trees in models. Here, we show that regional emissions estimates using widely implemented combustion coefficients are 59%–83% higher than emissions based on field observations. Using unique field datasets from before and after wildfires and an improved ecosystem model, we provide strong evidence that these large overestimates can be reduced by using realistic biomass combustion factors and by accurately quantifying biomass in standing dead trees that decompose over decades to centuries after fire ("snags"). Most model development focuses on area burned; our results reveal that accurately representing combustion is also essential for quantifying fire impacts on ecosystems. Using our improvements, we find that western US forest fires have emit- ted 851 ± 228 Tg CO2

(~half of alternative estimates) over the last 17 years, which is minor compared to 16,200 Tg CO2 from fossil fuels across the region.

Introduction

Temperate forests of the western United States are significant carbon stocks (Buotte et al., 2019; Pan et al., 2011) and include some of the most carbon-dense forests on Earth (Hudiburg et al., 2009). Increasing forest fire activity threatens these carbon stores in parts of the region because larger burn areas can lead to more tree mortality (Abatzoglou & Williams, 2016; Hicke, Meddens, & Kolden, 2016; Westerling, Hidalgo, Cayan, & Swetnam, 2006). However, contemporary CO2 emissions to the atmosphere from fire are often significantly exaggerated because of public and policymaker misconceptions that forests commonly "burn to the ground" during fire and that mortality equals emissions (Figure 1) (Mater, 2017; Zinke, 2018). The reality is instead negligible stem combustion of live, mature trees (i.e., <5%; Figure 2), followed by gradual decomposition over years to centuries (Campbell, Donato, Azuma, & Law, 2007; Law & Waring, 2015). Modeled estimates of fire emissions reinforce public misconceptions, as tree mortality is often mistranslated into 30%–80% of tree carbon emitted immediately (van der Werf et al., 2010; Wiedinmyer & Neff, 2007), and is in conflict with observations (Lutz et al., 2017). It is important to rectify overestimates because governments are currently using mortality and emissions estimates from fire to inform land management decisions intended to mitigate climate change (California, Executive Department, 2018; Fears & Eilperin, 2019; Nunez, 2006; Oregon, 2005; UNFCCC, 2015; U.S. Executive Office of the President, 2018), emphasizing the need for model improvement using field observations.

While modeling research focuses primarily on improving representation of area burned due to the availability of validating satellite products (Hantson et al., 2016; Thonicke et al., 2010), it is critical to recognize that simulations can generate inaccurate estimates of combustion dynamics through a combination of (a) unrealistic combustion coefficients (i.e., the biomass

fraction that burns) and (b) misrepresentation of forest biomass (i.e., carbon) pools. Models use assumed fractions of biomass combusted (combustion coefficients) in fire and apply that to the biomass in the area burned. These de- fault combustion coefficients overestimate pool combustion when they exceed ranges of observed combustion across live and dead pools, effectively simulating events where forests "burn to the ground."

The largest discrepancies between modeled and observed combustion of aboveground biomass exist for live, mature trees, which are the dominant pool of aboveground carbon across western US forests (Ghimire, Williams, Collatz, & Vanderhoof, 2012; Hudiburg et al., 2009; Wilson, Woodall, &

Most models also lack standing dead tree carbon pools (snags; Table S2), essential for representation of forests in the context of disturbance and mortality (Edburg et al., 2012). High-severity fires can kill live trees, which become snags and the dominant stock of aboveground carbon in burned areas (Campbell et al., 2007; Figures 1d and 2). When trees die in a "no snag" model, the wood instead transfers to the forest floor, becoming downed-woody debris (Figure 1c). In drier climates, snags decompose at slower rates than downed-woody debris (Wirth, Gleixner, & Heimann, 2009), producing relatively slow emissions over decades

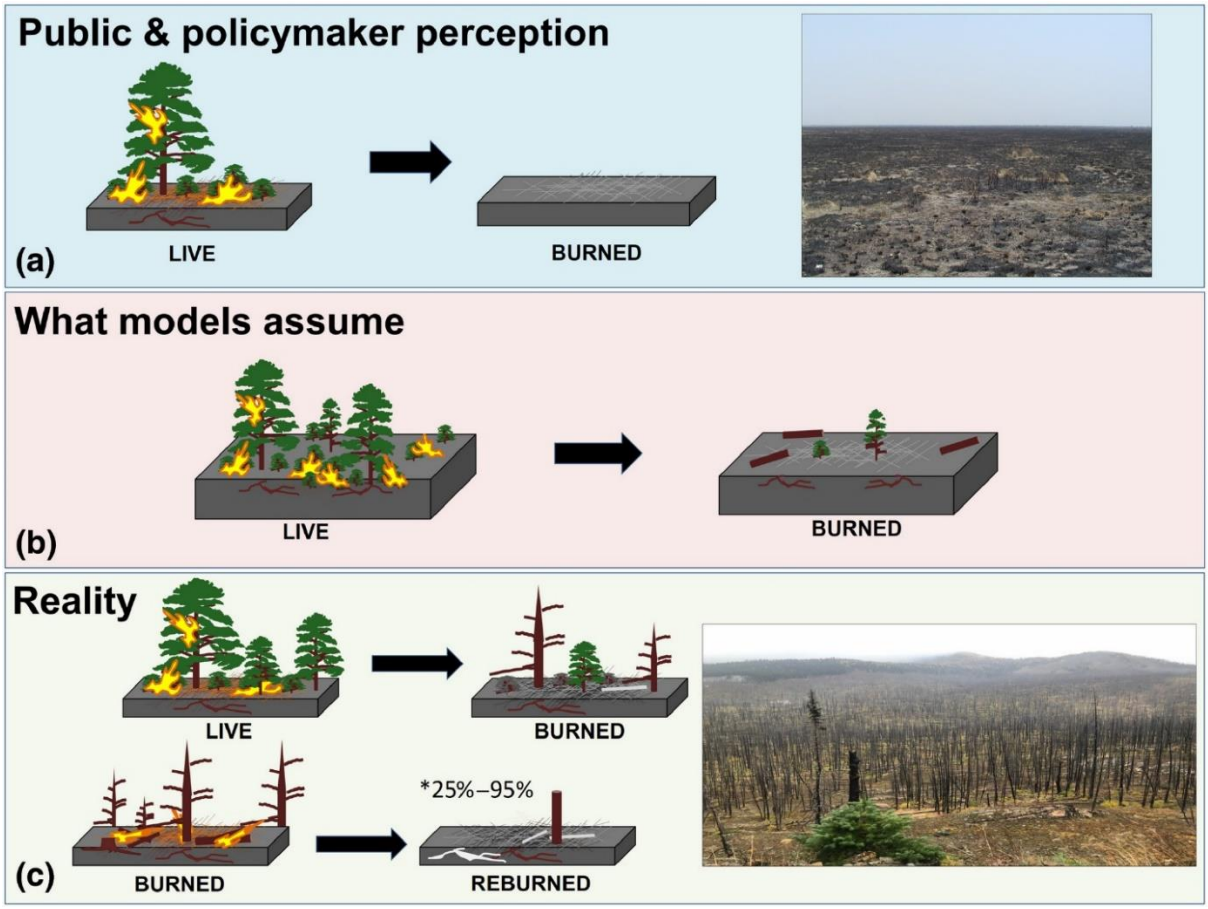

Figure 1. Conceptual diagram of realistic (observation-based) versus public perception and model implementation of live forest biomass combustion in high-severity forest fires. A common "public and policymaker perception" (U.S. Executive Office of the President, 2018; Zinke, 2018) (a), is that live, mature forests catastrophically "burn to the ground," with nearly all biomass emitted via combustion rather than remaining in the ecosystem as dead biomass (note: photograph from grassland). Flawed "model" fire implementations (b) are less extreme in their total ecosystem combustion, with the most significant misrepresentation being the over-combustion of live, mature trees. In "reality" (c), 80%–90% of live stems are killed but not combusted; their mass remains as substantial dead ecosystem carbon pools after the fire. *Short-return interval reburned stands can release additional carbon from dead biomass pools, ranging from ~25% (post-mature burn) to 95% (post-young burn)

Figure 2. Post-fire forest landscapes following different, varying severity fires in Oregon. (a) Ponderosa pine—low severity patch 4 years after the 2003 B&B Complex mixed severity fire (28,640 ha; photo by G. Meigs), (b) Mixed conifer—moderate severity patch 4 years after the 2003 B&B complex (photo by G. Meigs), (c) Ponderosa pine—high-severity patch 2 years after the 2002 Eyerly mixed severity fire (photo by T. Hudiburg) and (d) Ponderosa pine—high-severity patch 5 years after the 2002 Eyerly fire (photo by B.E. Law).

Table 1. Observed aboveground carbon stocks and combustion versus default model combustion. Note: All combustion percentages are equal to combustion coefficients except for the Rim Fire snag pool, where the percentage combines combustion and transfer of snag biomass to downed-wood pools. Bold italicized numbers highlight discrepancies between the range of model coefficients (Table S6, S7, S8; Lawrence et al., 2018; Sturtevant et al., 2009) and field observations for live trees. Field observations are from this study and previous studies (Campbell et al., 2007; Lutz et al., 2012). Standard deviation of YFDP subplots shown in parentheses where applicable.

Rim fire (YFDP) Pool	**Stock (Mg C/ha)**	**Combustion (%)**	**Model (%) (moderate-severity)**
Tree	281.3 (53.2)	***0.1 (0.0)***	
Foliage	–	–	***80–92***
Branch	–	–	***30–92***
Bark	–	–	***30–46***
Bolewood	–	–	***30–46***
Shrub	2.9	95.4	*na*
Snag	13.9 (3.0)	61.5 (8.8)	*na*
Coarse woody debris	39.5 (19.6)	58.3 (33.5)	28–50
Fine woody debris	3.3 (1.4)	94.4 (5.0)	50–100
Litter	11.9 (1.5)	90.4 (4.8)	50–100
Duff	43.6 (5.7)	88.5 (4.3)	50–100
Total	**396.4 (54.4)**	**21.9 (5.0)**	***na***
Biscuit fire (high-severity subset) Pool	**Stock (Mg C/ha)**	**Combustion (%)**	**Model (%) (high-severity)**
Tree	92.5	***8.7***	
Foliage	5.6	***73.0***	***80–100***
Branch	14.8	***7.9***	***30–100***
Bark	11.7	***21.0***	***30–80***
Bolewood	60.5	***0.6***	***30–80***
Snag	7.7	17.6	*na*
Coarse woody debris	7.6	34.1	28–80
Fine woody debris	1.1	78.0	50–100
Litter	9.2	100.0	50–100
Duff	6.0	99.0	50–100
Total	**124.0**	**22.5**	***na***

rather than acute, large pulses through combustion. Further, biomass location matters for reburn combustion (Campbell et al., 2007; Ghimire et al., 2012); simulating snags as downed-woody debris facilitates higher rates of combustion in subsequent fires.

Generally, model fire severity is defined by the amount of bio- mass killed and consumed. Representation of combustion in models varies from a single severity ("static severity," e.g., CLM 5.0; Lawrence et al., 2018) to a range from low-to-high ("variable severity," e.g., LANDIS-II; Sturtevant, Scheller, Miranda, Shinneman, & Syphard, 2009; Table 1, and Tables S1 and S2). These dynamic coefficients are either "categorical" or calculated through fire sub- models that largely depend on fuel moisture and tree or woody debris size class (Table S2). Default mortality and combustion coefficients can be "parameterized" to be more in line with observations; however, this is often not done, especially at large scales (Buotte et al., 2019; Liang, Hurteau, & Westerling, 2018; Tables S6, S7, and S8); modeling experiments instead often rely on restricting predicted burn area or fire occurrence to achieve realistic combustion (Hudiburg, Law, & Thornton, 2013; Hudiburg, Luyssaert, Thornton, & Law, 2013). There is also large variation in the biomass pools represented, with a persistent absence of snags. Even models that include dynamic combustion coefficients (e.g., LPJ-GUESS-SPITFIRE) or variable severity (e.g., LANDIS-II) can overestimate emissions because the rate at which standing wood becomes downed wood is too high without a snag pool (Figure 1c).

In this study, we compare a range of default combustion coefficients and forest structure representations of regional-to-global- scale models with observation-based combustion coefficients and a newly implemented model snag pool. Our observation-based

refinements utilize carbon stock datasets that span fire events, including new, detailed field observations from the 2013 Rim Fire in California (Lutz et al., 2017). We also simulate post-fire carbon cycle dynamics using an improved version of the globally recognized biogeochemical model DayCent (Hudiburg, Higuera, & Hicke, 2017; Parton, Hartman, Ojima, & Schimel, 1998) through addition of snag pools with varying combustion, decomposition, and fall rates (Figure S1). We then estimate 2000–2016 fire emissions across the western United States with our improved methods.

Materials and Methods

We calculated emissions from forest combustion in the western US states using site observations, the monitoring trends in burn severity (MTBS) burn perimeter database, and ecosystem modeling. Mortality and combustion coefficients were generated from plot data collected before and after fire in the region and from commonly used models. We developed a modified version of DayCent (Straube et al., 2018) that introduces a snag pool to improve representation of post-disturbance ecosystem structure and fluxes. DayCent was also used to simulate commonly used model combustion coefficients and mortality transfers in both snag-free and snag-enabled versions. Finally, we estimated recent western US forest emissions (2000–2016) for the same range of combustion and pool structures using forest inventory-derived plot biomass carbon estimates combined with the MTBS burn perimeter and severity database (Eidenshink et al., 2007).

Fire combustion coefficients from the 2013 Rim Fire were calculated using the Yosemite Forest Dynamics Plot (YFDP; CA; Lutz, Larson, Swanson, & Freund, 2012) dataset. The YFDP (37.77°N, 119.82°W) is part of the Smithsonian ForestGEO network of

spatially explicit monitoring plots (Anderson-Teixeira et al., 2015). The YFDP is a carbon-dense, mixed-conifer forest, where live trees contained ~70% of aboveground biomass pre-fire (Table 1 and Table S4). The YFDP (800 m × 320 m) was divided into ten, 160 m × 160 m quadrats, and pre- and post-fire aboveground carbon pools were calculated for each quadrat (Table 1, and Tables S3 and S4). The plot was burned in an unattended backfire set by Yosemite National Park to check the advance of the Rim Fire (Lutz, Larson, & Swanson, 2018; Lutz et al., 2017).

At plot inception (2009–2010), all trees were identified, mapped, and tagged. Snags were measured as to height, diameter, top diameter, and decay class. Shrub patches were delineated as poly- gons and shrub biomass was calculated by plot-specific allometric equations (Lutz et al., 2014). Due to the 113 year period of fire exclusion (Barth, Larson, & Lutz, 2015), herbaceous cover was de minimus. Each pre-fire year (2011–2013), trees were visited to ascertain their status in May–June, and therefore, the 2013 survey provided a com-prehensive inventory of standing stems. In May 2014, we performed the post-fire survey, noting tree death, whether tree canopies were scorched or combusted, and measuring dimensions of partially com- busted snags.

In 2011 and 2014, surface fuels were measured with 1,600 m transects following the methods of (Brown, 1974) with additional data taken on large woody debris (1,000 hr fuels, ≥10 cm diameter). Live biomass was calculated using the methods of Chojnacky, Heath, and Jenkins (2013). Snag biomass was calculated using the same equations as when trees were killed by fire when needles were only scorched. Pre-fire biomass of snags was calculated as the mass of the bole only, calculated as a conic frustum.

Combustion estimates were also used from published studies in mature Oregon forests. (Campbell et al., 2007, 2016; Meigs, Donato, Campbell, Martin, & Law, 2009; Figure 2; Table 1). Observations from the 2002 Biscuit Fire showed that live tree combustion was limited primarily to canopy combustion and bark scorching, resulting in a maximum 7% mature tree combustion at high (stand-replacing) severity. These datasets also contained reburned plots that burned 15 years earlier in the 1987 Silver Fire. The authors did not find any significant differences between the combustion coefficients of the aboveground pools in the reburn versus the initial burn; however, because significantly more of the carbon was in snag, downed wood, or small diameter tree pools, more aboveground carbon did combust.

Simulations were performed using a modified version (developed by the authors) of the biogeochemical model DayCent (Chen et al., 2016; Straube et al., 2018) that introduces standing dead pools and fluxes. DayCent is the daily time step of CENTURY, simulating fluxes of carbon and nitrogen between the atmosphere, ecosystem, and soil (for further model description see Figure S1). Our modified DayCent now incorporates standing dead pools of leaves, fine branches, and large wood into the forest submodel, as well as accompanying fluxes of carbon and nitrogen involved in both background senescence and prescribed fire and harvest events (Figure S1). Fluxes in and out of standing dead pools are governed by inputs from death of live pools, fall rates of standing dead material, decomposition, photodegradation, and removal by har- vest or fire. Attached dead leaves that fall to the ground are partitioned into surface structural and metabolic litter. When standing dead wood falls, it becomes coarse and fine woody debris. Live and dead material involved in fire events may now be returned to the system as charcoal.

Simulations were performed for each of the combustion and mortality parameter sets (Table S5) extracted from the YFDP 2013 Rim Fire, 2002 Oregon Biscuit Fire, and additional regional datasets of partial aboveground combustion (e.g., Fahnestock & Agee, 1983; Kauffman & Martin, 1989; Knapp, Keeley, Ballenger, & Brennan, 2005; Meigs et al., 2009). DayCent pre-fire carbon pools and fluxes were parameterized to the 2011 and 2013 carbon stocks of the YFDP (Table 1, and Tables S3 and S4; Lutz et al., 2012). Model spinup (2,000 years) was based on a pre-modern fire return interval of 29 years followed by 120 years of no fire, consistent with historical park records. Site soil characteristics were extracted from SSURGO (NRCS, 2010). Site climate (temperature and precipitation) was based on location data from PRISM (Daly, Taylor, & Gibson, 1997) for 1981–2017. Post-fire simulation periods in model experiments were driven with historical climate conditions. Mortality proportions were based on fire severity mortality classes (Campbell et al., 2016; Meigs et al., 2009) comparable to the mortality in the "variable-severity" model (below), facilitating comparison. Mortality classes include 0%–10%, 10%–50%, 50%–90%, and 90%–100% for very low-, low-, moderate-, and high-severity fire, respectively.

DayCent was also used to simulate default parameter sets from the Community Land Model v 5.0 (CLM; Lawrence et al., 2018; Oleson et al., 2013) and LANDIS-II with the Net Ecosystem Carbon and Nitrogen Succession (NECN) and Dynamic Fuels & Fire System (Sturtevant et al., 2009) (Scheller et al., 2007) (Tables S6, S7, and S8). These two models represent the range of coefficients and severities used by most other fire-enabled ecosystem, forest landscape, and dynamic vegetation models (Tables S1 and S2). In our results, CLM and LANDIS-II default parameters, respectively, inform our "static" and "variable" severity scenarios (combustion and mortality). In total, we performed 18 scenario simulations of the

YFDP representing the range of fire severity, pool combustion, and mortality transfer assumption scenarios.

CLM is the land model of the Community Earth System Model (CESM) and simulates the fluxes of energy, water, chemical elements, and trace gases between atmosphere, plants, and soil. As the land-model component of CESM, CLM is a globally utilized model in the effort to explore land-climate feedbacks, and has been used to research forest–climate interactions throughout the western United States (Buotte et al., 2019; Hudiburg, Law, et al., 2013; Hudiburg, Luyssaert, et al., 2013). During fire events, CLM employs single se- verity and mortality. Combustion is therefore governed by burn area. CLM first combusts litter, coarse woody debris, and live trees, and then transfers non-burned tree biomass to dead pools (Table S8).

LANDIS-II is a forest landscape model simulating growth and succession of tree species and age cohorts. LANDIS-II with NECN (derived from CENTURY/DayCent) is used to explore the potential effects of evolving climate, disturbance regimes, and management on ecosystem structure and composition. During a grid cell fire event, species cohort mortality is determined as a product of fire severity and species tolerance, with up to 100% of species cohorts killed and mortality occurring as death of all cohorts below a variable percentage of species longevity. Fire reduction parameters deter- mine emissions and specify reduction of dead wood and litter after the above mortality scheme kills and deposits biomass on the forest floor in the same time step (Tables S6 and S7). We calculated LANDIS-II equivalent biomass mortality estimates for the YFDP dominant stand species (White fir and Sugar pine).

Western US carbon stocks were calculated from over 80,000 forest inventory plots (FIA) containing over 2.5 million tree records in the region following methods developed in previous studies (Hudiburg et al., 2009; Hudiburg, Law, Wirth, & Luyssaert, 2011; Law et al., 2018; Law, Hudiburg, & Luyssaert, 2013). Uncertainty estimates for total regional emissions were calculated using a propagation of error approach accounting for error in biomass allometrics and the MTBS fire perimeters (Law et al., 2018).

Western US fire emissions were calculated from 2000 to 2016 using MTBS (Eidenshink et al., 2007) estimates of burn area and severity combined with FIA plot biomass data aggregated by ecoregion and forest type (30 m pixel resolution; Table S9) and severity-specific combustion factors for each pool (large stems, small stems, downed dead wood, understory, standing dead, litter pools (Campbell et al., 2007; Meigs et al., 2009; and Rim Fire values from this study). Areas of recurring severe fire based on the MTBS re- cord (less than 2% of total burn area included reburns from 1984 to 2016; Table S10) were combusted with modified biomass pools reflecting simulated post-fire conditions using combustion observations from reburned plots in the Biscuit Fire study (Campbell et al., 2007, 2016; Donato, Fontaine, & Campbell, 2016). Combustion factor scenarios were consistent with DayCent YFDP simulation sets by carbon pool (see Tables S5–S8). Observation-based and the variable-severity model-based sets were applied by severity. The static-severity model combustion percentages were applied across all severities within burn perimeters. Comparisons with fossil fuel emissions were done using Environmental Protection Agency state CO2 emissions data (EPA, 2018).

Results and Discussion

Fire emissions in carbon-dense forests

The YFDP experienced a mixed-severity burn in 2013, consuming 22% of aboveground carbon, with dead biomass producing 95% of estimated emissions (Table 1). The fire induced ~71% tree mortality (stems ≥1 cm dbh) within 1 year and combusted Observation-based combustion of aboveground carbon de- creased from 22% (80 Mg C/ha) to 6% (22 Mg C/ha) from high- to very low-fire severity, reflecting transitions between canopy and ground fire. With variable-severity model coefficients, aboveground carbon combustion decreased from a maximum of 87% to a minimum of 10%. This wide range is explained by large modeled de- creases in emissions with decreasing burn severity, averaging 20% of aboveground carbon per severity class (Figure 3a; dotted lines). By contrast, observation-based changes in emitted aboveground car- bon averaged 5% per severity class. The static- severity model simulation overestimated observation-based emissions by 59%–486% (high-low observed severity).

Thirty years' post-fire, the static-severity scenario carbon losses still exceeded those from observation-based severities by 39%– 1010% (Figure 3a). The difference in emissions estimates between the variable-severity model and observation-based scenarios margin- ally decreased over time due to a lack of remaining biomass to decom- pose (Figure S3). Nonetheless, the variable and static-severity models overestimated observation-based emissions by averages of 150% and 130%, demonstrating persistent unrealistic post-fire emissions over timescales relevant to greenhouse gas management. These results highlight that model estimates can both inflate fire emissions and the potential carbon benefits of severity-reduction strategies, such as thinning for fuels reduction. Further, static-severity

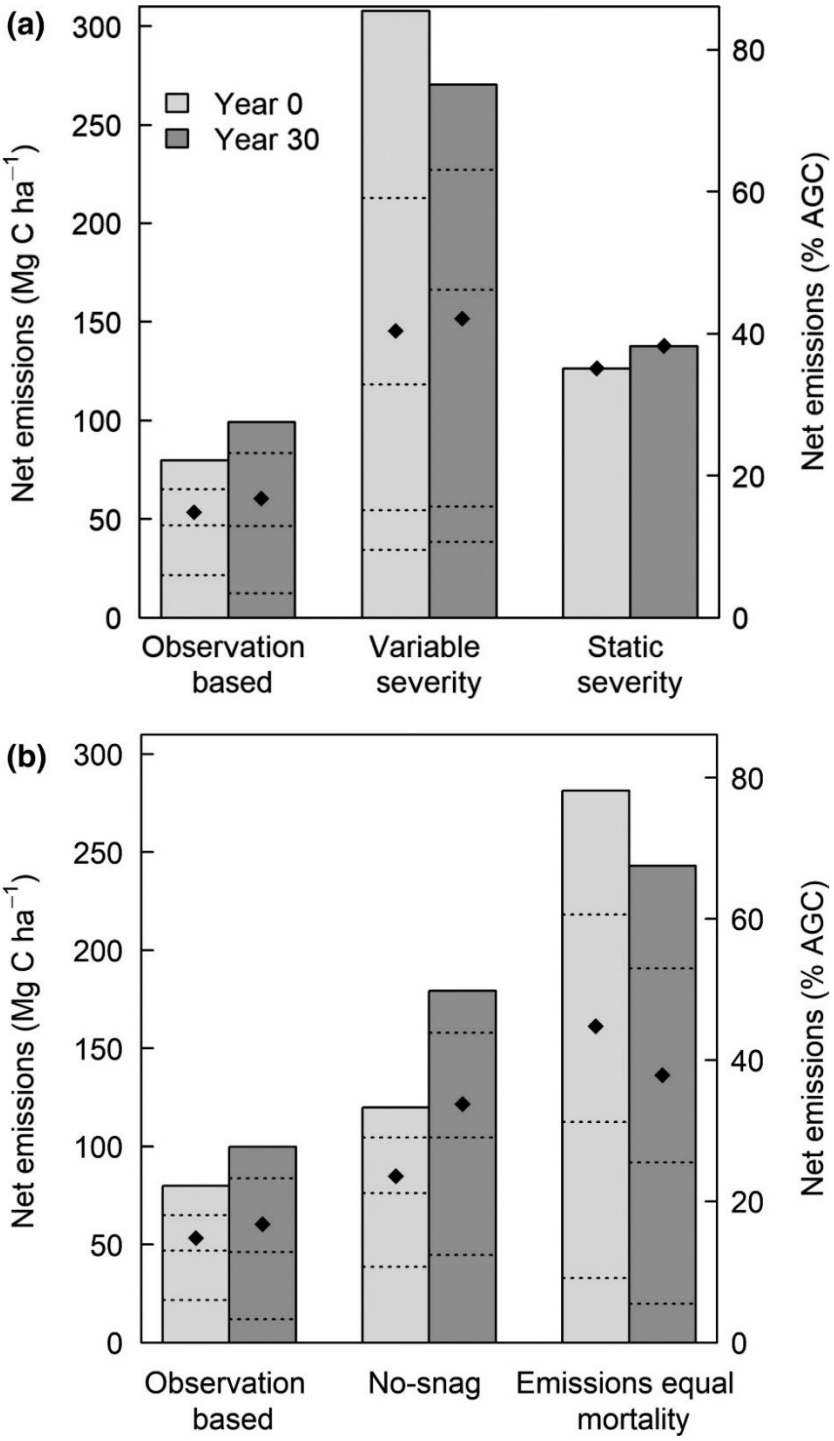

Figure 3. Simulated ecosystem carbon losses at the time of fire (Year 0) and 30 years post-fire at the YFDP. For scenarios with variable severity, full bars indicate emissions density at high severity. Dashed lines indicate emissions at very low-to-moderate severity. Points indicate scenario means (or static emissions). (a) Carbon losses for observation-based and model default parameterizations. (b) Carbon losses for observation-based, observation-based without snags, and "mortality = emissions" scenarios.

overestimates increase dramatically at lower severities, undervaluing the persistent carbon storage capacity of forests experiencing low-severity fire.

Omission of a snag pool resulted in increased combustion of downed-woody debris (vs. snags); net fire-event carbon losses were 50%–79% greater across no-snag scenarios (Figure 3b). Without snags, fire-killed biomass was deposited on the forest floor and decomposed at a faster rate than in the snag scenarios, where large quantities of killed biomass decayed in standing dead pools before reaching the ground (Figure S1). The combined effects of altered combustion and decomposition after 30 years yielded an average doubling of simulated net emissions across severities when snags were not represented.

From low-to-high severity, "mortality = emissions" scenarios ("public perception"; Figure 1b) exceeded observation-based emissions by 140%–253% (Figure 3b); these results were similar to variable-severity scenario results (Figure 3a). At neither 30 years nor 100 years, post-fire did the "mortality = emissions" scenario emissions decrease below the observation-based scenarios. Although up to 95% mortality was implemented in the observation-based scenarios, sub- sequent decomposition of dead biomass was largely compensated by regrowth. These results show that simulating mortality transfers that are distinct from combustion does not simply delay these carbon losses to the future (Figures S2 and S3); greenhouse gas emissions and impacts to the atmosphere are instead markedly decreased.

Emissions impacts across western US forest fires in the 21st century

Across the western United States, observation-based combustion emissions summed to 232 ± 62 Tg C from 2000 to 2016, emitting 23% of aboveground carbon stocks within ~11 million

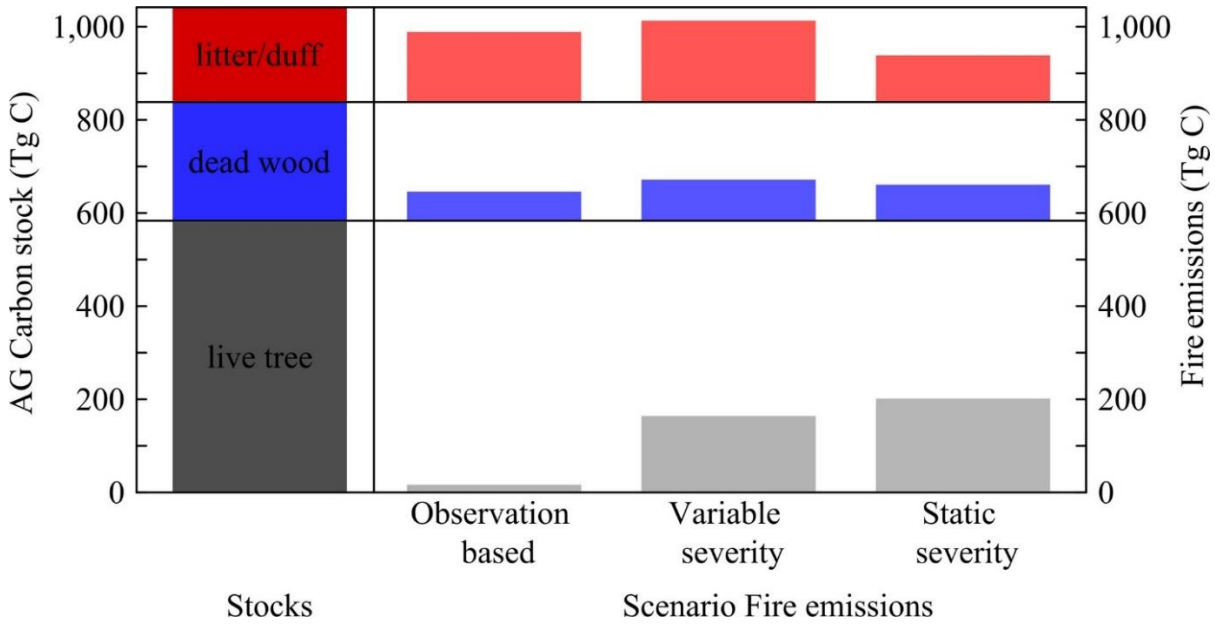

Figure 4. Western US aboveground carbon pools and pool fire emissions across scenarios, 2000–2016 forest burn area. Pre-fire aboveground carbon (AG) pool totals (opaque bars) are compared to fire-event pool carbon emissions (translucent bars). Litter/duff, dead wood, and live trees account for 21%, 26%, and 53% of aboveground stocks, respectively.

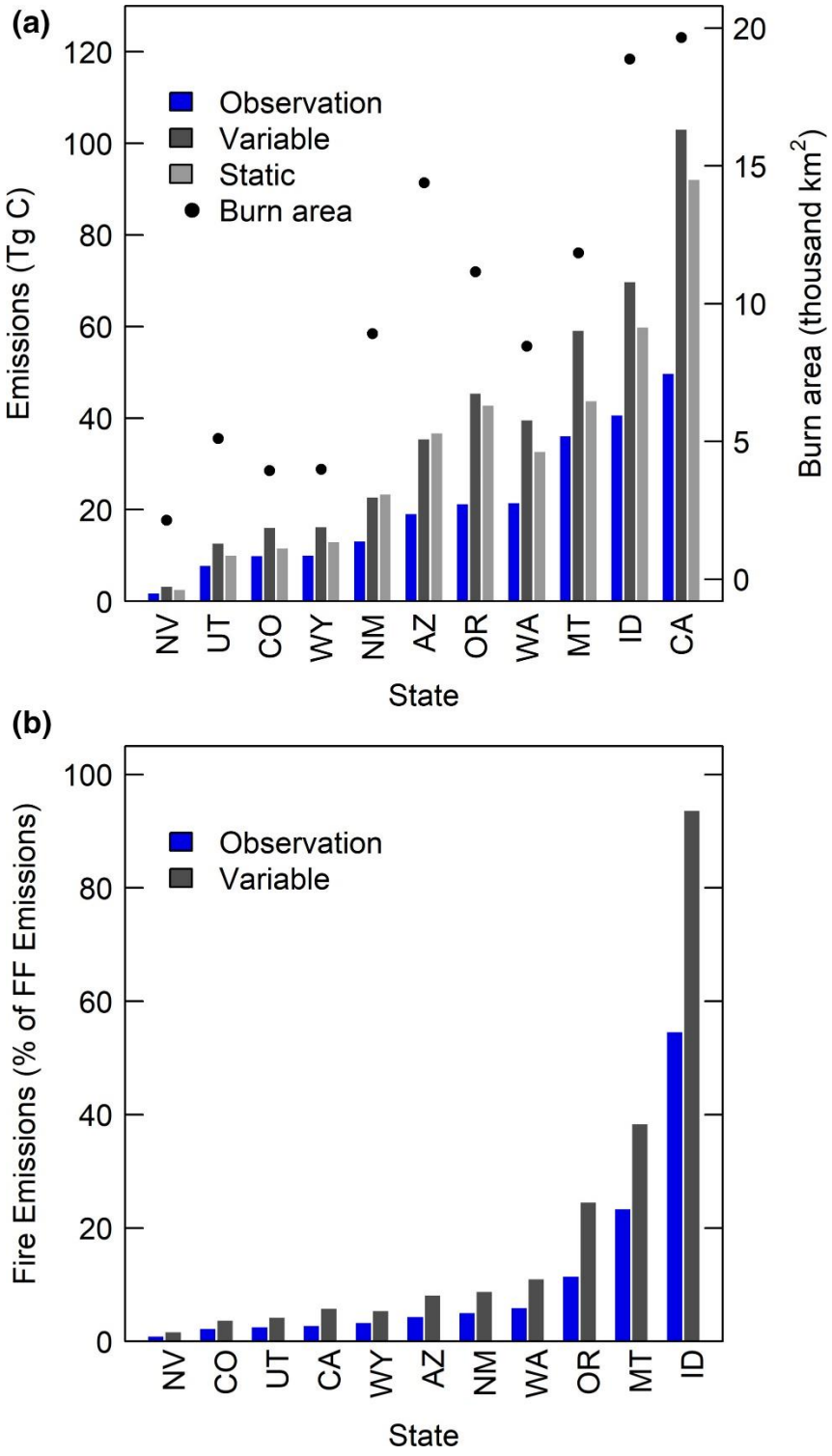

Figure 5. Total state emissions (2000–2016) estimated from observed combustion coefficients versus coefficients from variable and static-severity models. (a) Western state forest fire emissions and burn area. (b) Western state fire emissions as a proportion of fossil fuel (FF) emissions

hectares of burned area (Figures 4 and 5), in agreement with estimates for Oregon over similar time periods (Law, 2014; Meigs et al., 2009). As at smaller scales, model-based live tree combustion overestimated observation-based combustion by an order of magnitude (Figure 4), leading to regional emissions overestimates of 59% and 83%. Forest fires in California, Idaho, and Montana accounted for 54% of total combustion emissions (Figure 5), resulting from higher burned area and aboveground carbon density relative to southern interior states. Coastal-state (CA, OR, WA) model-based scenarios exceeded observation-based emissions by 81% and 103%, com- pared to overestimates of 35% and 67% in the Northern Rockies (ID, MT, WY). This difference stemmed from greater aboveground carbon density in coastal versus Northern Rocky states. Thus, carbon loss is most overestimated in forests with high tree biomass. Regional observation-based fire emissions totaled to 5% of fossil fuel emissions compared to twice that when using default coefficients (Figure 5b). Notably, Idaho and Montana fire emissions accounted for 55% and 24% of yearly fossil fuel emissions, respectively, highlighting the importance of correctly calculating fire emissions in the Northern Rockies due to large projected increases in fire (Westerling et al., 2006). Emissions in California and Washington were extremely low relative to fossil fuel emissions, likely because of population density (energy usage).

Implications

Our results illustrate that the use of inaccurate combustion coefficients in models can double forest fire emissions estimates across the western United States. Overestimates increase to three to four times in carbon-dense forests such as the YFDP, mostly because models incorrectly combust live trees. Treating carbon released over years to centuries as an

immediate emission by equating combustion with mortality is simply inaccurate. Omitting snag representation in models compounds this error, because of altered decay and combustion dynamics.

A warming climate and more frequently recurring fire (Westerling et al., 2006) may alter some regional forest carbon stocks from the present. The field data used in this study includes area in the 2002 Biscuit Fire that contained the 1987 Silver Fire (15 years earlier), where reburned plots showed an additional 26% reduction in standing and downed dead wood due to fire com- pared to mature single-burn plots but similar pool combustion coefficients across fires (Donato et al., 2016). New observations from reburned lodgepole pine stands in the Greater Yellowstone Ecosystem show that young stands can lose a majority of the aboveground carbon (basal diameter <4 cm; Turner, Braziunas, Hansen, & Harvey, 2019), consistent with Biscuit Fire observations for the small conifer pool (Campbell et al., 2007). This suggests a mechanism by which recurrent burning ("reburn") could in principle lead to state changes to treeless vegetation over the mid- term because of frequent, repeated combustion of aboveground stocks over time (Coop, Parks, McClernan, & Holsinger, 2016). The percentage of the regional forest landscape that has recently experienced such severe reburn is less than 1% (see regional methods), but could increase in the future with climate change (Dale et al., 2001; Turner et al., 2019), and disproportionally in some areas (e.g., Southern California and US Southwest). It will be essential to accurately estimate these emissions impacts in a regional context by quantifying shifting biomass pools (e.g., dead and young pools) upon which realistic combustion coefficients are applied.

Resolving modeled inaccuracies is critical because forest fire and CO2 emissions-reduction strategies are currently being implemented (California, Executive Department, 2018; U.S. Executive Office of the President, 2018). Overestimating forest fire emissions exacerbates public and policymaker misconceptions (Figure 1). Our simulations highlight the need for more studies on pre- and post-fire carbon pools over decadal durations in order to capture combustion dynamics in different forest types to provide observations for modelers to better constrain and validate their models. At present, even when models correctly estimate burned area, their ability to properly inform policy makers about the contributions of fires to greenhouse gas budgets can be inadequate, adding fuel to the fire when drafting forest management plans.

Acknowledgements

J.E.S., T.W.H., and K.J.B. were supported by National Science Foundation award number DEB-1553049 and DEB-1655183. A.M.S. and C.A.K. were supported by the National Science Foundation award DMS-1520873. A.M.S. was partially supported by the NASA Carbon Monitoring System Program Award NNH15AZ06I.

References:

Abatzoglou, J. T., & Williams, A. P. (2016). Impact of anthropogenic cli- mate change on wildfire across western US forests. Proceedings of the National Academy of Sciences, 113, 11770–11775. https://doi. org/10.1073/pnas.1607171113

Anderson-Teixeira, K. J., Davies, S. J., Bennett, A. C., Gonzalez-Akre, E. B., Muller-Landau, H. C., Joseph Wright, S., … Zimmerman, J. (2015). CTFS-ForestGEO: A worldwide network monitoring forests in an era of global change. Global Change Biology, 21(2), 528–549. https://doi. org/10.1111/gcb.12712

Barth, M. A. F., Larson, A. J., & Lutz, J. A. (2015). A forest reconstruc- tion model to assess changes to Sierra Nevada mixed-conifer forest during the fire suppression era. Forest Ecology and Management, 354, 104–118. https://doi.org/10.1016/j.foreco.2015.06.030

Brown, J. K. (1974). Handbook for inventorying downed woody material (24 p). General Technical Reports, INT-16. Ogden, UT: US Department of Agriculture, Forest Service, Intermountain Forest and Range Experiment Station.

Buotte, P. C., Levis, S., Law, B. E., Hudiburg, T. W., Rupp, D. E., & Kent, J. J. (2019). Near-future forest vulnerability to drought and fire var- ies across the western United States. Global Change Biology, 25(1), 290–303. https://doi.org/10.1111/gcb.14490

California, Executive Department. (2018). Executive Order B-52-18. Sacramento, CA.

Campbell, J., Alberti, G., Martin, J., & Law, B. E. (2009). Carbon dynam- ics of a ponderosa pine plantation following a thinning treatment in the northern Sierra Nevada. Forest Ecology and Management, 257(2), 453–463. https://doi.org/10.1016/j.foreco.2008.09.021

Campbell, J., Donato, D., Azuma, D., & Law, B. (2007). Pyrogenic carbon emission from a large wildfire in Oregon, United States. Journal of Geophysical Research: Biogeosciences, 112(G4), G04014. https://doi. org/10.1029/2007JG000451

Campbell, J. L., Fontaine, J. B., & Donato, D. C. (2016). Carbon emissions from decomposition of fire-killed trees following a large wildfire in Oregon, United States. Journal of Geophysical Research: Biogeosciences, 121, 718–730. https://doi.org/10.1002/2015JG003165

Chen, M., Parton, W. J., Adair, E. C., Asao, S., Hartman, M. D., & Gao, W. (2016). Simulation of the effects of photodecay on long-term litter decay using DayCent. Ecosphere, 7(12), e01631. https://doi. org/10.1002/ecs2.1631

Chojnacky, D. C., Heath, L. S., & Jenkins, J. C. (2013). Updated gener- alized biomass equations for North American tree species. Forestry, 87(1), 129–151. https://doi.org/10.1093/forestry/cpt053

Coop, J. D., Parks, S. A., McClernan, S. R., & Holsinger, L. M. (2016). Influences of prior wildfires on vegetation response to subsequent fire in a reburned southwestern landscape. Ecological Applications, 26(2), 346–354. https://doi.org/10.1890/15-0775

Dale, V. H., Joyce, L. A., Mcnulty, S., Neilson, R. P., Ayres, M. P., Flannigan, M. D., … Michael Wotton, B. (2001). Climate change and forest dis- turbances: Climate change can affect forests by altering the fre- quency, intensity, duration, and timing of fire, drought, introduced species, insect and pathogen outbreaks, hurricanes, windstorms, ice storms, or landslides. BioScience, 51(9), 723–734. https://doi. org/10.1641/0006-3568(2001)051[0723:CCAFD]2.0.CO;2

Daly, C., Taylor, G., & Gibson, W. (1997). The PRISM approach to map- ping precipitation and temperature. Paper presented at the Proc., 10th AMS Conf. on Applied Climatology.

Donato, D. C., Fontaine, J. B., & Campbell, J. L. (2016). Burning the legacy? Influence of wildfire reburn on dead wood dynamics in a temperate conifer forest. Ecosphere, 7(5), e01341. https://doi.org/10.1002/ ecs2.1341

Edburg, S. L., Hicke, J. A., Brooks, P. D., Pendall, E. G., Ewers, B. E., Norton, U., … Meddens, A. J. H. (2012). Cascading impacts of bark beetle-caused tree mortality on coupled biogeophysical and biogeochemical processes. Frontiers in Ecology and the Environment, 10(8), 416–424. https://doi.org/10.1890/110173

Eidenshink, J., Schwind, B., Brewer, K., Zhu, Z.-L., Quayle, B., & Howard, S. (2007). A project for monitoring trends in burn severity. Fire Ecology, 3(1), 3–21. https://doi.org/10.4996/fireecology.0301003 EPA. (2018).

Inventory of U.S. Greenhouse Gas Emissions and Sinks 1990–2016. Washington, DC: U.S. Environmental Protection Agency. April 2018. EPA 430-R-18-003. Retrieved from https://www.epa. gov/statelocalenergy/state-co2-emissions-fossil-fuel-combustion

Fahnestock, G. R., & Agee, J. K. (1983). Biomass consumption and smoke production by prehistoric and modern forest fires in western Washington. Journal of Forestry, 81(10), 653–657.

Fears, D., & Eilperin, J. (2019, January 14). Trump's executive order will aggressively cut more forest trees. The Washington Post.

Ghimire, B., Williams, C. A., Collatz, G. J., & Vanderhoof, M. (2012). Fire-induced carbon emissions and regrowth uptake in western U.S. forests: Documenting variation across forest types, fire severity, and climate regions. Journal of Geophysical Research: Biogeosciences, 117(G3). https://doi.org/10.1029/2011JG001935

Hantson, S., Arneth, A., Harrison, S. P., Kelley, D. I., Prentice, I. C., Rabin, S. S., … Yue, C. (2016). The status and challenge of global fire mod- elling. Biogeosciences, 13(11), 3359–3375. https://doi.org/10.5194/ bg-13-3359-2016

Hicke, J. A., Meddens, A. J., & Kolden, C. A. (2016). Recent tree mortality in the western United States from bark beetles and forest fires. Forest Science, 62(2), 141–153. https://doi.org/10.5849/forsci.15-086

Hudiburg, T. W., Higuera, P. E., & Hicke, J. A. (2017). Fire-regime vari- ability impacts forest carbon dynamics for centuries to millen- nia. Biogeosciences, 14(17), 3873–3882. https://doi.org/10.5194/ bg-14-3873-2017

Hudiburg, T. W., Law, B. E., & Thornton, P. E. (2013). Evaluation and improvement of the Community Land Model (CLM4) in Oregon forests. Biogeosciences, 10(1), 453–470. https://doi.org/10.5194/ bg-10-453-2013

Hudiburg, T. W., Law, B. E., Turner, D. P., Campbell, J., Donato, D. C., & Duane, M. (2009). Carbon dynamics of Oregon and Northern California forests and potential land-based carbon storage. Ecological Applications, 19(1), 163–180. https://doi.org/10.1890/07-2006.1

Hudiburg, T. W., Law, B. E., Wirth, C., & Luyssaert, S. (2011). Regional carbon dioxide implications of forest bioenergy production. Nature Climate Change, 1(8), 419–423. https://doi.org/10.1038/nclim ate1264

Hudiburg, T. W., Luyssaert, S., Thornton, P. E., & Law, B. E. (2013). Interactive effects of environmental change and management strat- egies on regional forest carbon

emissions. Environmental Science & Technology, 47(22), 13132–13140. https://doi.org/10.1021/es402903u

Kauffman, J. B., & Martin, R. (1989). Fire behavior, fuel consumption, and forest-floor changes following prescribed understory fires in Sierra Nevada mixed conifer forests. Canadian Journal of Forest Research, 19(4), 455–462. https://doi.org/10.1139/x89-071

Knapp, E. E., Keeley, J. E., Ballenger, E. A., & Brennan, T. J. (2005). Fuel reduction and coarse woody debris dynamics with early season and late season prescribed fire in a Sierra Nevada mixed conifer forest. Forest Ecology and Management, 208(1–3), 383–397. https://doi. org/10.1016/j.foreco.2005.01.016 Law,

B. E. (2014). Regional analysis of drought and heat impacts on for- ests: Current and future science directions. Global Change Biology, 20(12), 3595–3599. https://doi.org/10.1111/gcb.12651

Law, B. E., Hudiburg, T. W., Berner, L. T., Kent, J. J., Buotte, P. C., & Harmon, M. E. (2018). Land use strategies to mitigate climate change in carbon dense temperate forests. Proceedings of the National Academy of Sciences, 115(14), 3663–3668. https://doi.org/10.1073/ pnas.1720064115

Law, B. E., Hudiburg, T. W., & Luyssaert, S. (2013). Thinning effects on forest productivity: Consequences of preserving old forests and mitigating impacts of fire and drought. Plant Ecology & Diversity, 6(1), 73–85. https://doi.org/10.1080/17550874.2012.679013

Law, B. E., & Waring, R. H. (2015). Carbon implications of current and future effects of drought, fire and management on Pacific Northwest forests. Forest Ecology and Management, 355, 4–14. https://doi. org/10.1016/j.foreco.2014.11.023

Lawrence, D. M., Fisher, R. A., Koven, C. D., Oleson, K. W., Swenson, S. C., Bonan, G., … Fox, A. M. (2018). Technical note: CLM5 documenta- tion. Paper presented at the NCAR Technical Note.

Liang, S., Hurteau, M. D., & Westerling, A. L. (2018). Large-scale resto- ration increases carbon stability under projected climate and wildfire regimes. Frontiers in Ecology and the Environment, 16, 207–212. https:// doi.org/10.1002/fee.1791

Lutz, J., Larson, A., & Swanson, M. (2018). Advancing fire science with large forest plots and a long-term multidisciplinary approach. Fire, 1, 5. https://doi.org/10.3390/fire1010005

Lutz, J. A., Larson, A. J., Swanson, M. E., & Freund, J. A. (2012). Ecological importance of large-diameter trees in a temperate mixed-conifer forest. PLoS ONE, 7, https://doi.org/10.1371/journal.pone.0036131

Lutz, J., Matchett, J., Tarnay, L., Smith, D., Becker, K., Furniss, T., & Brooks, M. (2017). Fire and the distribution and uncertainty of carbon sequestered as aboveground tree biomass in Yosemite and Sequoia & Kings Canyon National Parks. Land, 6(1), 10. https://doi. org/10.3390/land6010010

Lutz, J. A., Schwindt, K. A., Furniss, T. J., Freund, J. A., Swanson, M. E., Hogan, K. I., … Larson, A. J. (2014). Community composition and al- lometry of Leucothoe davisiae, Cornus sericea, and Chrysolepis semper- virens. Canadian Journal of Forest Research, 44(6), 677–683. https:// doi.org/10.1139/cjfr-2013-0524

Mater, C. (2017). The surprising emissions from Oregon's forests (Guest opinion), Opinion. The Oregonian.

Meigs, G., Donato, D., Campbell, J., Martin, J., & Law, B. (2009). Forest fire impacts on carbon uptake, storage, and emission: The role of burn severity in the Eastern Cascades, Oregon. Ecosystems, 12(8), 1246–1267. https://doi.org/10.1007/s10021-009-9285-x NRCS. (2010).

Soil survey staff, natural resources conservation service, United States department of agriculture. Nunez, F. (2006). Assembly Bill 32: the California global warming solu- tions act of 2006. California State Assembly.

Oleson, K. W., Lawrence, D. M., Bonan, G. B., Drewniak, B., Huang, M., Koven, C. D., … Yang, Z.-L. (2013). Technical description of version 4.5 of the Community Land Model (CLM). Paper presented at the NCAR Technical Note.

Oregon. (2005). Oregon Senate Bill 1072 (73rd Oregon Legislative Assembly). Salem, OR.

Pan, Y., Birdsey, R. A., Fang, J., Houghton, R., Kauppi, P. E., Kurz, W. A., … Hayes, D. (2011). A large and persistent carbon sink in the world's forests. Science, 333, 988–993. https://doi.org/10.1126/scien ce.1201609

Parton, W. J., Hartman, M., Ojima, D., & Schimel, D. (1998). DAYCENT and its land surface submodel: Description and testing. Global and Planetary Change, 19(1–4), 35–48. https://doi.org/10.1016/s0921-8181(98)00040-x

Scheller, R., Domingo, J., Sturtevant, B., Williams, J., Rudy, A., Mladenoff, D., & Gustafson, E. (2007). Introducing LANDIS-II: Design and devel- opment of a collaborative landscape simulation model with flexible spatial and temporal scales. Ecological Modelling.

Smith, A. M. S., Sparks, A. M., Kolden, C. A., Abatzoglou, J. T., Talhelm, A. F., Johnson, D. M., … Kremens, R. J. (2016). Towards a new paradigm in fire severity research using dose–response experiments. International Journal of Wildland Fire, 25(2), 158–166. https://doi.org/10.1071/WF15130

Sparks, A. M., Smith, A. M., Talhelm, A. F., Kolden, C. A., Yedinak, K. M., & Johnson, D. M. (2017). Impacts of fire radiative flux on mature Pinus ponderosa growth and vulnerability to secondary mortality agents. International Journal of Wildland Fire, 26(1), 95–106. https:// doi.org/10.1071/WF16139

Straube, J. R., Chen, M., Parton, W. J., Asso, S., Liu, Y.-A., Ojima, D. S., & Gao, W. (2018). Development of the DayCent-Photo model and inte- gration of variable photosynthetic capacity. Frontiers of Earth Science, 12(4), 765–778. https://doi.org/10.1007/s11707-018-0736-6 Sturtevant, B.

R., Scheller, R. M., Miranda, B. R., Shinneman, D., & Syphard, A. (2009). Simulating dynamic and mixed-severity fire regimes: A pro- cess-based fire extension for LANDIS-II. Ecological Modelling, 220(23), 3380–3393. https://doi.org/10.1016/j.ecolmodel.2009.07.030

Thonicke, K., Spessa, A., Prentice, I. C., Harrison, S. P., Dong, L., & Carmona-Moreno, C. (2010). The influence of vegetation, fire spread and fire behaviour on biomass burning and trace gas emissions: Results from a process-based model. Biogeosciences, 7(6), 1991– 2011. https://doi.org/10.5194/bg-7-1991-2010

Turner, M. G., Braziunas, K. H., Hansen, W. D., & Harvey, B. J. (2019). Short-interval severe fire erodes the resilience of subalpine lodge- pole pine forests. Proceedings of the National Academy of Sciences, 201902841. https://doi.org/10.1073/pnas.1902841116

U.S. Executive Office of the President. (2018). Promoting active manage- ment of America's Forests, Rangelands, and other federal lands to improve conditions and reduce wildfire risk (Executive Order 13855). Washington, DC.

UNFCCC. (2015). Article 5. Paris agreement. Paris, France. Retrieved from https://treaties.un.org/pages/ViewDetails.aspx?src=TREAT Y&mtdsg_no=XXVII-7-d&chapter=27&cxml:lang=_en

van der Werf, G. R., Randerson, J. T., Giglio, L., Collatz, G. J., Mu, M., Kasibhatla, P. S., … van Leeuwen, T. T. (2010). Global fire emissions and the contribution of deforestation, savanna, forest, agricultural, and peat fires (1997–2009). Atmospheric Chemistry and Physics, 10(23), 11707–11735.

Westerling, A. L., Hidalgo, H. G., Cayan, D. R., & Swetnam, T. W. (2006). Warming and earlier spring increase western U.S. forest wildfire activity. Science, 313, 940–943. https://doi.org/10.1126/scien ce.1128834

Wiedinmyer, C., & Neff, J. (2007). Estimates of CO2 from fires in the United States: Implications for carbon management. Carbon Balance and Management, 2(1), 10. https://doi.org/10.1186/1750-0680-2-10

Wilson, B. T., Woodall, C. W., & Griffith, D. M. (2013). Forest carbon stocks of the contiguous United States (2000–2009). Wirth, C., Gleixner, G., & Heimann, M. (Eds.) (2009). Old-growth forests: Function, fate and value–an overview. In Old-growth forests (pp. 3–10). Berlin, Heidelberg: Springer.

Zinke, R. (2018). Wildfires seem unstoppable, but they can be prevented. Here's how, Opinion. USA TODAY.

Supporting Information:

Supporting Methods:

DayCent Model

DayCent requires the following inputs: vegetation cover, daily precipitation and air temperature (minimum and maximum), soil characteristics, and fire histories. DayCent calculates potential plant growth as a function of water, light, and soil temperature. Actual plant growth is limited based on soil nutrient availability and leaf area index, with allocation dependent on stand age, soil moisture, nutrient availability, and input parameters. DayCent has three soil organic matter (SOM) pools (active, slow, and passive), and two litter pools (structural and metabolic) each with different decomposition rates. All SOM pools and litter pools have above- and belowground components except for the passive pool. The active pool (microbial) has short turnover times (1–3 months), and the slow SOM pool (more resistant structural plant material) has turnover times ranging from 10 to 50 years depending on the climate. The passive pool includes physically and chemically stabilized SOM with turnover times ranging from 400 to 4000 years.

DayCent represents the following aboveground carbon pools: Foliage, fine branch, large live wood, large dead wood (course woody debris), fine dead branch (fine woody debris), structural litter, and metabolic litter. Plant material entering the litter layer is split into structural and metabolic material as a function of the lignin-to-nitrogen ratio of the litter (more structural with higher lignin-to-nitrogen ratios). DayCent removal events (including fire) are prescribed, allowing simulation of historical fire events with an array of combustion parameter sets in the context of site ecosystem dynamics.

FIA Biomass calculations

Live and dead tree biomass were calculated using ecoregion and species-specific allometric equations that use both height and diameter (DBH) for estimating bole and coarse root volume and bark, branch, fine root, and foliage biomass (Law et al., 2018; Li, Kurz, Apps, & Beukema, 2003). Ecoregion and species-specific wood density data are used to convert bole and coarse root volume to biomass. Standing dead tree carbon is based on recorded biomass and decay class and reduced over time by standing dead decay rates. Downed dead wood biomass is estimated using the line transect method and species- and size-specific wood densities reduced by decay class. Understory carbon was extracted from the FIA database where it was modeled from aboveground biomass, forest type, and other attributes (Burrill, 2017). Litter and duff biomass carbon estimates are also extracted from the FIA database as the product of plot average depth and material density that varies by forest type. For all calculations, in cases where an ecoregion and or species-specific equation or wood density is not available, substitutions can be made by genus, similar form, etc. Conversions to carbon are calculated based on carbon density of 0.5 for all pools

Table S1: Process Model Fire Module overview:

Model	Type	Use	Fire	Source
CLM 5.0	Process- based Earth System Model	Model emissions from historical to future fires	Li et al. 2014 model Glob-FIRM, Spitfire	Thonicke et al. 2001, Thonicke et al. 2010, Li et al. 2014
LPJ-GUESS	Process- based Earth System Model with DGVM (Individual or cohort-based)	Model emissions from historical to future fires	Prognostic; Glob-Firm Spitfire Blaze/Simfire	Smith et al. 2014 (Spitfire) Pellegrini et al. 2017 (Blaze/Simfire)
LPJ	Process- based Earth System Model with DGVM (Population- based)	Model emissions from historical to future fires	Prognostic; Glob-FIRM Spitfire LM-Fire	Sitch et al. 2003, Pfeiffer et al. 2013, Chaste et al. 2018
LANDIS-II	Process- based forest landscape model with DGVM	Model emissions from historical to future fires	Prognostic; LANDIS Dynamic Fire System Extension	
CLM-FATES	Process- based Earth System Model with DGVM	Model emissions from historical to future fires	Prognostic; Spitfire	Fisher et al. 2018
ORCHIDEE	Process- based Earth System Model with DGVM	Model emissions from historical to future fires	Prognostic; Spitfire	Yue et al. 2014 a, b
GFED	Emissions are calculated using CASA predicted biomass within fire perimeter and an assumed static combustion	MODIS collection 5 (500 m res)	Diagnostic, satellite-derived burned area estimate dataset	Giglio et al. 2013 van der Werf et al. 2017
JSBACH-Spitfire	Process-based Earth System Model	Land surface model simulating carbon and hydrological cycles	Prognostic, Spitfire	Lasslop et al. 2014

Model	Type	Use	Fire	Source
aDGVM	Process-based, individual-based ecosystem model (tropics)	Simulates physiological and biogeochemical	Prognostic, Semi-empirical (Higgins et al. 2008)	Higgins et al. 2008 Scheiter & Higgins 2009
MC2/MC1	Process-based regional biogeographic-biogeochemical DGVM model (based on MAPSS and CENTURY models)	Simulates species composition and C and nutrient dynamics	Prognostic; MCFIRE Module	Bachelet et al. 2001
'Snagged' DayCent (new version)	Ecosystem / Biogeochemical model	Model emissions from historical fires	Diagnostic; fire events are prescribed	This paper
DOS-TEM	Process-based ecosystem model (boreal)	Simulates soil and vegetation carbon and nitrogen cycling	Diagnostic; fire events are prescribed	Kelly et al. 2016
iLand	Process-based, individual-based forest landscape model	Simulates forest dynamics at landscape and watershed scales	Prognostic; iLand wildfire module	Seidl et al. 2012

Table S2. Fire Model Descriptions (adapted from [1])

FIRE MODEL	LAND MODEL	DESCRIPTION	VARIABLE FIRE INTENSITY	MORTALITY	COMBUSTION	SNAGS?	SOURCE
GFED	CASA	Satellite-derived burned severity and emissions. Empirical modeling between burnt area and satellite observations.	Yes.	Higher tree cover leads to higher tree mortality; lower tree/higher grass, lower tree mortality All ABG grass killed, 90% BG grass survives.	Dependent on fuel type (leaf, stem, root/ alive, dead), life-form. Killed plant material goes to litter pool.	No. Killed (but not combusted) enters litter pool.	2,3
GLOB-FIRM	CLM, LPJ	Empirical fire model. First global fire model.	No.	PFT-specific parameters for fractional mortality	All ABG litter and living biomass completely combusted. PFT-specific resistance factors for trees.	No. Killed stems (not combusted) enters litter pool.	4,5
SPITFIRE	LPJ-GUESS, LPJ, CLM-ED/FATES, ORCHIDEE, JSBACH	Process-based, rate-of-spread based fire model.	Yes. Fuel combustion separated by PFTs. Fire intensity influences tree mortality from ground fires.	Residence time influence tree mortality from ground fires via crown scorching, cambial damage. Flame height determines crown scorch. Thicker bark trees have greater survival rate.	Dynamic process for combustion completeness. Depends on fire characteristics and the fuel class moisture content (PFT & fuel type specific combustion).	No. C retained by the surviving, resprouting PFTs. Scorched woodmass enters litter pool.	6,7

FIRE MODEL	LAND MODEL	DESCRIPTION	VARIABLE FIRE INTENSITY	MORTALITY	COMBUSTION	SNAGS?	SOURCE
LM-FIRE	LPJ	Process-based, rate-of-spread based fire model.	Yes. Fuel combustion separated by PFTs.	Size cohorts in each PFT	Dynamic process for combustion completeness. Depends on fire characteristics and the fuel class moisture content (PFT and fuel type specific combustion).	No. C retained by the surviving, resprouting PFTs. Scorched woodmass enters litter pool.	8,9
LANDIS DYNAMIC FIRE SYSTEM EXTENSION	LANDIS-II	Rate of spread fire module	Yes.			No.	10
LI ET AL. 2013	CLM 4.5, 5.0	Based off CTEM fire module.		PFT-specific mortality factors.	Combustion transfers C from leaves, stems, roots and ABG litter to the atmosphere. PFT-specific combustion factors for C pools (leaf, stem, root).	No. Post-fire mortality transfers C (leaves, stems and roots) killed by fire to the litter pool.	11,12
SIMFIRE	LPJ-GUESS	Semi-empirical fire model		Individuals of woody PFTs within each patch selected at random to be killed/survive based on PFT's fire resistance	100% of dead leaves, 46-59% live and dead ABG grasses burn. In woody vegetation, 100% of dead leaves, 46-59% of live leaves burn. 20% dead and 0% live wood.	*Transfer of live to dead biomass pools following a fire (LPJ-GUESS doesn't have snags.)*	13

FIRE MODEL	LAND MODEL	DESCRIPTION	VARIABLE FIRE INTENSITY	MORTALITY	COMBUSTION	SNAGS?	SOURCE
BLAZE	LPJ-GUESS	Process-based, rate-of-spread based fire model.	Yes. BLAZE calculates fire-line intensity from meteorological data and fuel loads (from land model).	Mortality occurs following low or negative growth efficiency, age, or due to a change in climate to conditions beyond the plant functional type's (PFT's) bioclimatic limits.	Combustion based on intensity-dependent combustion factors.	*Transfer of live to dead biomass pools following a fire (LPJ-GUESS doesn't have snags.)*	14
MCFIRE	MC1 & MC2	Process-based, rate-of-spread based fire model.	Yes. Fire intensity influences tree mortality from ground fires (crown scorching, cambial damage).	Residence time influence tree mortality from ground fires via crown scorching and cambial damage. Canopy height/flame height determines crown scorch. Thicker bark trees have greater chance of surviving fire of given residence time.	Dynamic process for ıbustion completeness. ends on fire racteristics and the fuel s moisture content & fuel type specific ıbustion).	No. Scorched wood goes to litter pool	15,16
CTEM FIRE MODULE	CTEM	Process-based, rate-of-spread based fire model.		PFT-specific mortality factor.	PFT-specific combustion parameters for different woody pools (leaf, litter, stem, root, 0-70%).	No. Killed (but not combusted) goes to litter pool	17

FIRE MODEL	LAND MODEL	DESCRIPTION	VARIABLE FIRE INTENSITY	MORTALITY	COMBUSTION	SNAGS?	SOURCE
LPX FIRE MODULE	LPX (based on LPJ-SPITFIRE)	Process-based, rate-of-spread based fire model.	Fire intensity influences tree mortality from ground fires (from crown scorching, cambial damage).	Residence time influence tree mortality from ground fires via crown scorching and cambial damage. Canopy height/flame height determines crown scorch. Thicker bark trees have greater chance of surviving fire of given residence time.	Fuel combustion split into PFTs.	No. Killed (but not combusted) goes to litter pool.	18

Table S3. Yosemite Forest Dynamics Plot (YFDP) subplot biomass pool combustion (transfer) proportions. Calculated 2013 Rim Carbon pool combustion in the YFDP is based on biomass inventories[19,20] for each of ten, 160 m × 160 m quadrats (see 'methods' for pool specific methods). Tree accounting entailed tracking of all stems ≥1 cm dbh. Ground fuel calculations are based on 160 m of fuel transects per quadrat. The snag field accounts for the decrease in biomass of tracked standing dead stems (≥10 cm dbh); however, these stems were not individually followed to ground pools, leading to this field more appropriately representation a combination of transfer and combustion rather than combustion alone. *Shrub biomass is based on the aggregate values for the 25.6 ha YFDP. Minor tree combustion was measured that was not large enough to be displayed as non-zero values here.

Subplot	Litter	Duff	1-Hour	10-Hour	100-Hour	CWD	Tree	Shrub*	Snag
1	0.87	0.81	0.94	0.92	1.00	0.96	0.00	0.95	0.62
2	0.92	0.84	0.70	0.80	1.00	0.58	0.00	0.95	0.73
3	0.81	0.92	0.97	0.88	0.91	0.71	0.00	0.95	0.68
4	0.90	0.85	0.79	0.80	1.00	0.87	0.00	0.95	0.65
5	0.94	0.90	0.83	1.00	1.00	0.56	0.00	0.95	0.66
6	0.98	0.87	1.00	1.000	1.00	0.80	0.00	0.95	0.67
7	0.92	0.88	1.00	1.00	1.00	0.01	0.00	0.95	0.46
8	0.92	0.93	1.00	0.96	1.00	0.92	0.00	0.95	0.54
9	0.91	0.94	0.96	0.83	1.00	0.15	0.00	0.95	0.66
10	0.87	0.91	0.84	0.78	1.00	0.28	0.00	0.95	0.49

Table S4. Yosemite Forest Dynamics Plot (YFDP) subplot pre-fire biomass pools. Biomass stocks (Mg ha^{-1}) for each of ten, 160 m × 160 m quadrats of the YFDP, pre-Rim Fire burn. Inventories are from 2011 & 2014. See 'methods' for pool inventory methods. *Shrub biomass is based on the aggregate values for the 25.6 ha YFDP. Study carbon stocks were calculated as 0.5 times biomass.

Subplot	Litter	Duff	1-Hour	10-Hour	100-Hour	CWD	Tree	Shrub	Snag
1	23.79	78.49	0.38	2.56	3.90	26.51	757.06	5.88	21.44
2	20.74	81.06	0.73	3.68	2.68	90.97	501.86	5.88	28.96
3	23.15	112.37	1.35	3.04	5.60	176.84	563.13	5.88	35.56
4	24.89	81.18	0.81	3.52	4.87	61.95	669.49	5.88	37.98
5	30.92	80.17	0.59	2.29	8.28	72.50	502.22	5.88	23.01
6	23.64	92.96	0.41	1.70	2.19	78.61	673.02	5.88	31.76
7	21.07	90.08	0.50	1.28	1.70	59.97	579.39	5.88	28.59
8	24.10	98.46	0.74	2.50	3.17	59.57	484.03	5.88	22.70
9	23.83	81.42	0.27	1.23	1.22	71.76	451.61	5.88	27.89
10	21.17	76.27	0.35	1.70	2.19	91.94	443.34	5.88	20.96

Table S5. **Observation-based combustion coefficients**. Based on regional aboveground carbon pool inventory spanning fire, including the 2013 Yosemite Rim Fire[20] and the 2002 Biscuit Fire[21,22].

foliage	live branch	live large wood	bark	fwd	cwd	litter	duff
0.69	0.05	0.005	0.2	0.95	0.6	1	0.99
0.27	0.02	0.001	0.06	0.9	0.55	0.9	0.9
0.08	0.005	0	0.03	0.7	0.35	0.75	0.65
0.02	0	0	0.01	0.5	0.05	0.5	0.45

Table S6. **Landis II default cohort fire mortality reductions (variable severity)**, from the fire damage table of the Dynamic Fire System Extension[10,23]. The proportion of cohorts killed by a fire event is determined by the severity – species fire tolerance differential. All cohorts equal to or below the threshold age percentage are killed. The percentage refers to maximum species longevity, a user set parameter. Note: This is not a biomass reduction, which is mediated by the prognostic species age and biomass distributions.

Cohort Ages Killed (% of species longevity)	Severity - Species Fire Tolerance Differential
≤ 20%	-2
≤ 50%	-1
≤ 85%	0
≤ 100%	1

Table S7. Landis-II default Fire Reduction Parameters (variable severity), Net Ecosystem Carbon & Nitrogen Succession (formerly Century Succession)[24,25]. Note: Wood and litter reduction include biomass killed in the same fire event, which is transferred to the ground and combusted.

Fire Severity	Wood Reduction	Litter Reduction
1	0	0.5
2	0.05	0.75
3	0.2	1.0
4	0.5	1.0
5	0.8	1.0

Table S8. **Default Combustion and Mortality Factors, CLM V5.0[12] (static severity)**. Mortality transfers occur as transfer of uncombusted leaf and stem pools, and thus do not include live material removal by combustion.

Pool	Combustion Factor	Mortality Factor
leaf	0.8	0.8
stem	0.3	0.15
dead wood	0.28*	*na*
litter	0.5*	*na*

Table S9. Western U.S. state aboveground forest carbon pools (mean & SD) and fire statistics, 2000-2016. Statistics are estimated for burned forest area[26-28].

State	Live AGC (% AGC)	AGC (Mg ha^{-1})	Burn Area (km2)	Mod-High Severity Fire (% fire area)
Arizona (AZ)	60 (11)	75 (24)	14385	34
California (CA)	62 (9)	133 (54)	19663	48
Colorado (CO)	48 (16)	80 (18)	3945	53
Idaho (ID)	46 (6)	88 (11)	18883	42
Montana (MT)	45 (5)	98 (28)	11843	51
New Mexico (NM)	57 (8)	77 (27)	8912	27
Nevada (NV)	57 (12)	34 (30)	2143	52
Oregon (OR)	62 (13)	111 (59)	11154	40
Utah (UT)	37 (5)	57 (21)	5105	47
Washington (WA)	55 (8)	110 (34)	8461	46
Wyoming (WY)	41 (7)	90 (25)	3999	44

Table S10. Western U.S. forest burned area that experienced multiple moderate-high severity burns, 1986-2016. Based on MTBS fire severity products[27] and forest cover from Hicke *et al* 2013 [29].

Region	Severe successive reburn (%)
AZ/CO/NM/NV/UT	1.0
CA	3.4
ID/MT/WY	1.6
OR/WA	1.8

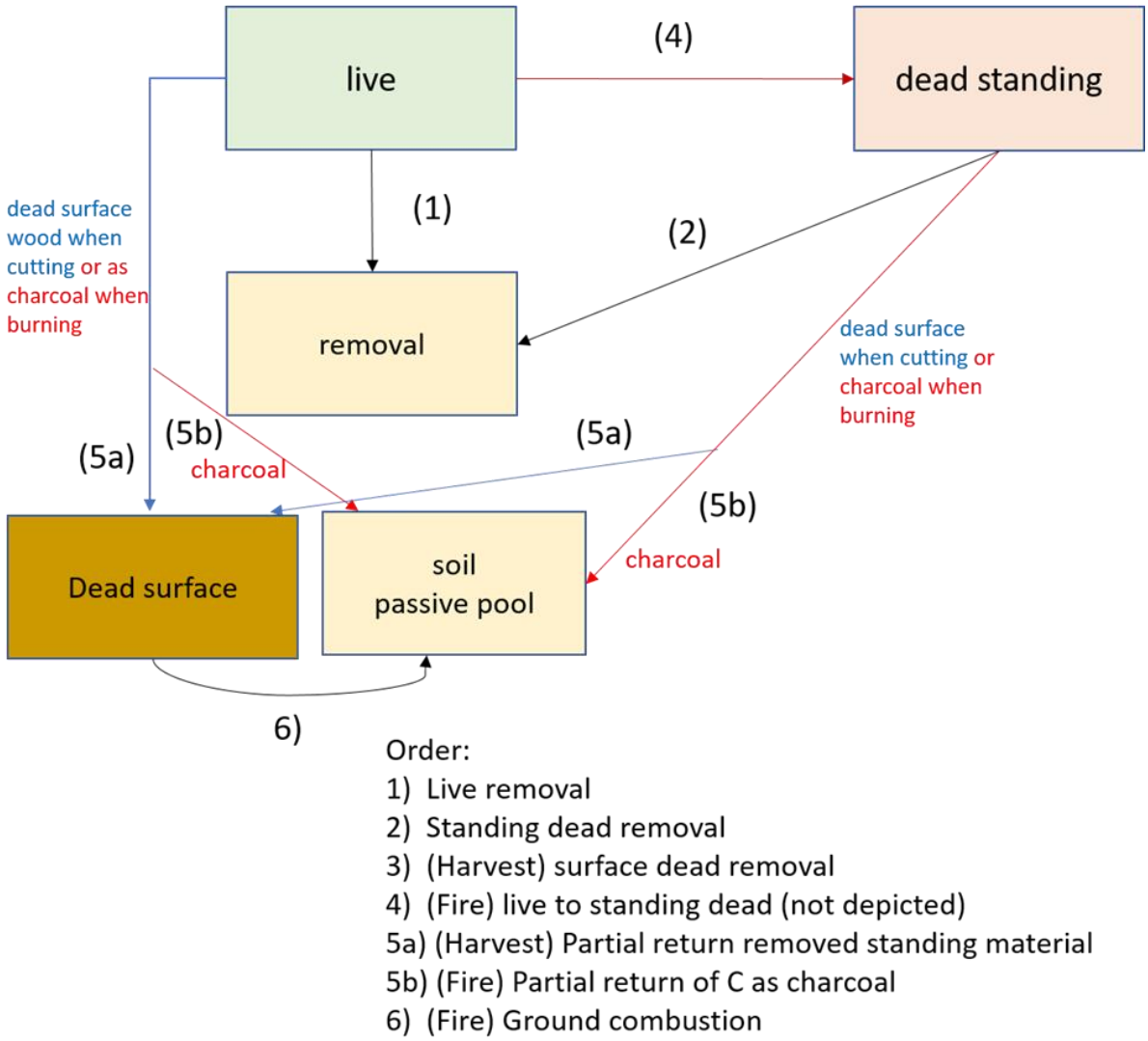

Figure S1. Diagram of modified Daycent standing dead modifications for carbon removals during disturbance events. Generalized diagram of carbon pools and removal flows (fire or harvest) in the modified Daycent version used in this study. Actual carbon pools correspond to live standing, dead standing, and ground pools for large wood, branches, and leaves. Non-disturbance fluxes include temperature and moisture moderated decomposition and photodegradation for dead pools and senescence for live pools. Modified nitrogen structure not depicted here.

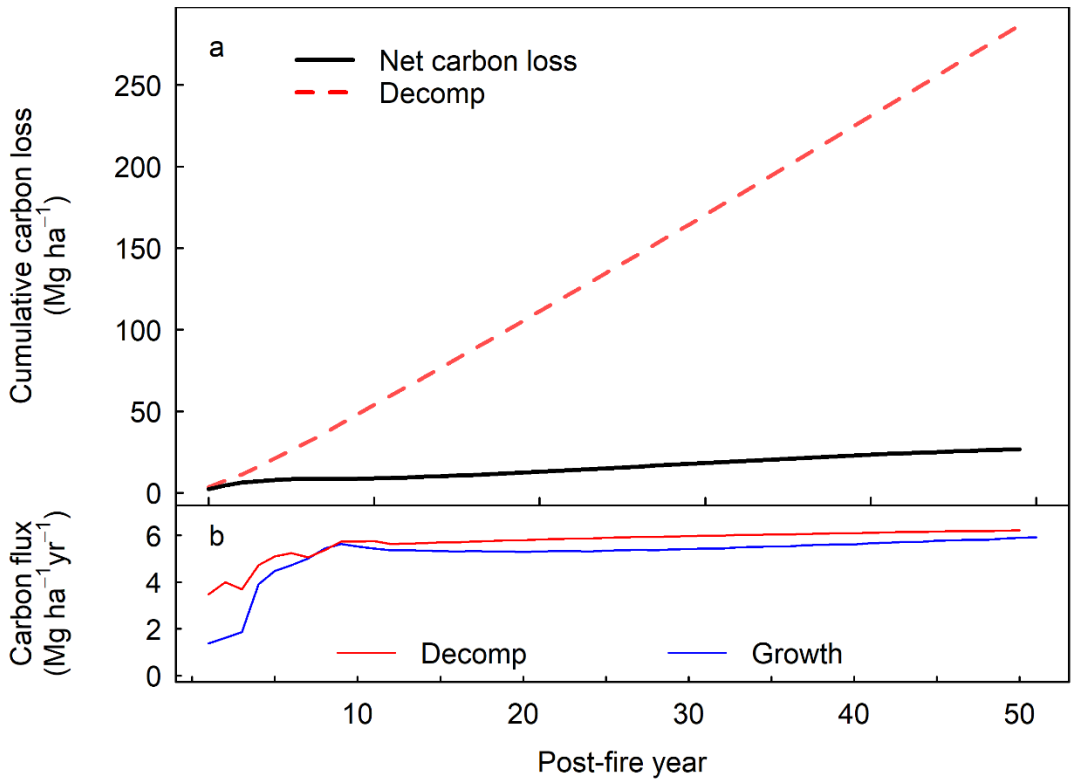

Figure S2. Post-fire emissions as the balance between growth and decomposition. Post-fire net carbon losses related to tree mortality are the balance of dead mass decomposition and forest regrowth (i.e. Net Primary Production; NPP). Slow decomposition, caused in part by standing dead matter, yields post-fire emissions that are largely compensated by rapid growth. **a.** Example of post-high-severity fire cumulative decomposition and total ecosystem carbon losses (i.e. emissions) for a simulation with high tree mortality but low tree combustion. **b**. Post-fire growth (i.e. Net Primary Productivity) and decomposition fluxes in the high mortality, low combustion scenario.

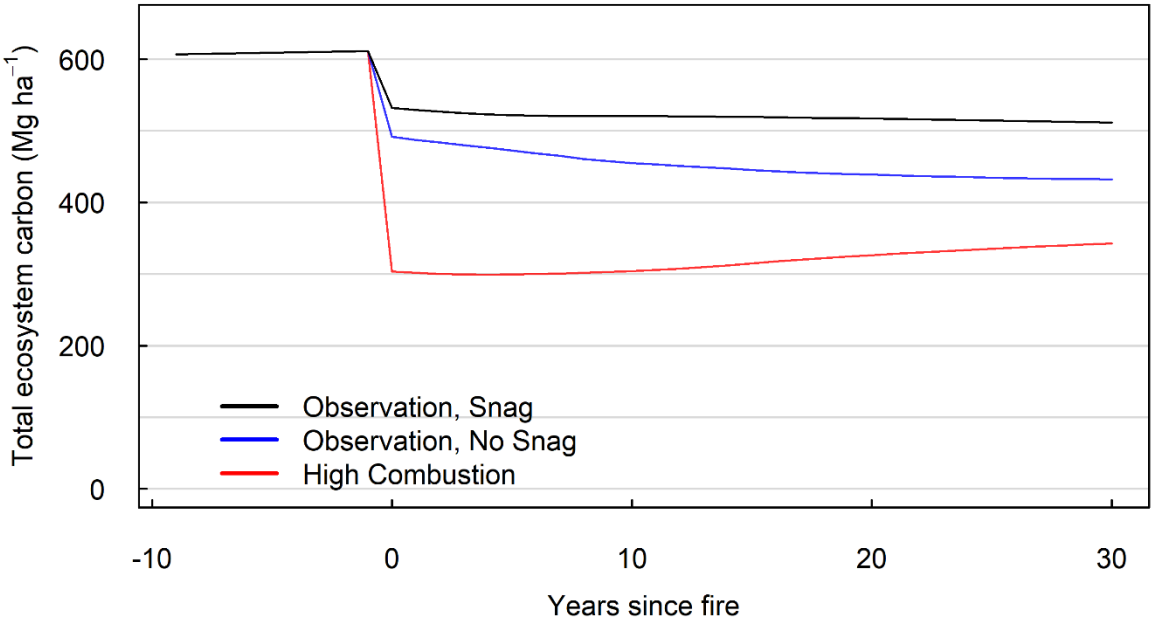

Figure S3. Scenario total carbon losses due to combustion and decomposition. Example high-severity fire ecosystem carbon losses under observation based (with snags, no snags) and high combustion, variable-severity model-based scenarios. All scenarios faced high tree mortality (95%) by mass. The high combustion scenario experienced most mortality as fire-event combustion; observation-based scenarios experienced lower event combustion and post-fire carbon loss trajectories that were affected by decomposition with or without snags. Post-fire losses are a balance of component fluxes, as depicted in **Figure S2**.

Supplementary References

1 Hantson, S. *et al.* The status and challenge of global fire modelling. *Biogeosciences* **13**, 3359-3375 (2016).

2 Potter, C., Klooster, S. & Genovese, V. Carbon emissions from deforestation in the Brazilian Amazon Region. *Biogeosciences* **6**, 2369-2381 (2009).

3 Giglio, L., Randerson, J. T. & van der Werf, G. R. Analysis of daily, monthly, and annual burned area using the fourth-generation global fire emissions database (GFED4). *Journal of Geophysical Research: Biogeosciences* **118**, 317-328 (2013).

4 Sitch, S. *et al.* Evaluation of ecosystem dynamics, plant geography and terrestrial carbon cycling in the LPJ dynamic global vegetation model. *Global change biology* **9**, 161-185 (2003).

5 Thonicke, K., Venevsky, S., Sitch, S. & Cramer, W. The role of fire disturbance for global vegetation dynamics: coupling fire into a Dynamic Global Vegetation Model. *Global Ecology and Biogeography* **10**, 661-677 (2001).

6 Lasslop, G., Thonicke, K. & Kloster, S. SPITFIRE within the MPI Earth system model: Model development and evaluation. *Journal of Advances in Modeling Earth Systems* **6**, 740-755, doi:10.1002/2013MS000284 (2014).

7 Thonicke, K. *et al.* The influence of vegetation, fire spread and fire behaviour on biomass burning and trace gas emissions: results from a process-based model. *Biogeosciences* **7**, 1991-2011 (2010).

8 Pfeiffer, M., Spessa, A. & Kaplan, J. O. A model for global biomass burning in preindustrial time: LPJ-LMfire (v1. 0). *Geoscientific Model Development* **6**, 643-685 (2013).

9 Chaste, E. *et al.* The pyrogeography of eastern boreal Canada from 1901 to 2012 simulated with the LPJ-LMfire model. *Biogeosciences* **15** (2018).

10 Sturtevant, B. R., Miranda, B. R., Scheller, R. M. & Shinneman, D. LANDIS-II Dynamic Fire System Extension (v2. 0) User Guide.

11 Li, F., Levis, S. & Ward, D. Quantifying the role of fire in the Earth system–Part 1: Improved global fire modeling in the Community Earth System Model (CESM1). *Biogeosciences* **10**, 2293-2314 (2013).

12 Lawrence, D. M. *et al.* in *NCAR Technical Note* (National Center for Atmospheric Research, 2018).

13 Knorr, W., Jiang, L. & Arneth, A. Climate, CO 2 and human population impacts on global wildfire emissions. *Biogeosciences* **13**, 267-282 (2016).

14 Pellegrini, A. F. *et al.* Fire frequency drives decadal changes in soil carbon and nitrogen and ecosystem productivity. *Nature* **553**, 194 (2018).

15 Lenihan, J. M. & Bachelet, D. Historical climate and suppression effects on simulated fire and carbon dynamics in the conterminous United States. *Global Vegetation Dynamics: Concepts and Applications in the MC1 Model*, 17-30 (2015).

16 Bachelet, D. *et al.* MC1: a dynamic vegetation model for estimating the distribution of vegetation and associated ecosystem fluxes of carbon, nutrients, and water. *Pacific Northwest Station General Technical Report PNW-GTR-508* (2001).

17 Arora, V. K. & Boer, G. J. Fire as an interactive component of dynamic vegetation models. *Journal of Geophysical Research: Biogeosciences* **110** (2005).

18 Prentice, I. *et al.* Modeling fire and the terrestrial carbon balance. *Global Biogeochemical Cycles* **25** (2011).

19 Lutz, J. A., Larson, A. J., Swanson, M. E. & Freund, J. A. Ecological importance of large-diameter trees in a temperate mixed-conifer forest. *PLoS ONE* **7**, doi:10.1371/journal.pone.0036131 (2012).

20 Lutz, J., Larson, A. & Swanson, M. Advancing Fire Science with Large Forest Plots and a Long-Term Multidisciplinary Approach. *Fire* **1**, 5, doi:10.3390/fire1010005 (2018).

21 Campbell, J. L., Fontaine, J. B. & Donato, D. C. Carbon emissions from decomposition of fire-killed trees following a large wildfire in Oregon, United States.

Journal of Geophysical Research: Biogeosciences **121**, 718-730, doi:10.1002/2015JG003165 (2016).

22 Campbell, J., Donato, D., Azuma, D. & Law, B. Pyrogenic carbon emission from a large wildfire in Oregon, United States. *Journal of Geophysical Research: Biogeosciences* **112**, G04014, doi:10.1029/2007JG000451 (2007).

23 Sturtevant, B. R., Scheller, R. M., Miranda, B. R., Shinneman, D. & Syphard, A. Simulating dynamic and mixed-severity fire regimes: a process-based fire extension for LANDIS-II. *Ecological Modelling* **220**, 3380-3393 (2009).

24 Scheller, R. M., Hua, D., Bolstad, P. V., Birdsey, R. A. & Mladenoff, D. J. The effects of forest harvest intensity in combination with wind disturbance on carbon dynamics in Lake States Mesic Forests. *Ecological Modelling* **222**, 144-153 (2011).

25 Liang, S., Hurteau, L., S., Hurteau, M. D., & Westerling, A. L. (2018). Large-scale restoration increases carbon stability under projected climate and wildfire regimes. Frontiers in Ecology and the Environment, 16(4), 207–212. https://doi.org/10.1002/fee.1791Matthew D. & Westerling, A. L. Large-scale restoration increases carbon stability under projected climate and wildfire regimes. *Frontiers in Ecology and the Environment* **16**, 207-212, doi:10.1002/fee.1791 (2018).

26 Law, B. E. *et al.* Land use strategies to mitigate climate change in carbon dense temperate forests. *Proceedings of the National Academy of Sciences*, 201720064 (2018).

27 Eidenshink, J. *et al.* A project for monitoring trends in burn severity. *Fire ecology* **3**, 3-21 (2007).

28 Ruefenacht, B. *et al.* Conterminous U.S. and Alaska Forest Type Mapping Using Forest Inventory and Analysis Data. *Photogrammetric Engineering & Remote Sensing* **74**, 1379-1388, doi:10.14358/PERS.74.11.1379 (2008).

29 Hicke, J. A., Meddens, A. J., Allen, C. D., & Kolden, C. A. (2013). Carbon stocks of trees killed by bark beetles and wildfire in the western United States. *Environmental Research Letters*, *8*(3), 035032.

Chapter 2: Restoration Thinning in a Drought-Prone Idaho Forest Creates a Persistent Carbon Deficit

Published in *Journal of Geophysical Research: Biogeosciences* as:

Stenzel, J. E., Berardi, D. B., Walsh, E. S., & Hudiburg, T. W. (2021). Restoration thinning in a drought-prone Idaho forest creates a persistent carbon deficit. Journal of Geophysical Research: Biogeosciences, 1–18. https://doi.org/10.1029/2020jg005815

Abstract

Western US forests represent a carbon sink that contributes to meeting regional and global greenhouse gas targets. Forest thinning is being implemented as a strategy for reducing forest vulnerability to disturbance, including mortality from fire, insects, and drought, as well as protecting human communities. However, the terrestrial carbon balance impacts of thinning remain uncertain across regions, spatiotemporal scales, and treatment types. Continuous and in situ long-term measurements of partial harvest impacts to stand-scale carbon and water cycle dynamics are nonetheless rare. Here, we examine post-thinning carbon and water flux impacts in a young ponderosa pine forest in Northern Idaho. We examine in situ stock and flux impacts during the 3 years after treatment as well as simulate the forest sector carbon balance through 2050, including on and off-site net emissions. During the observation period, increases in tree-scale net primary production (NPP) and water use persistence through summer drought did not overcome the impacts of density reduction, leading to 45% annual reductions of NPP. Growth duration remained constrained by summer drought in control and thinned stands. Ecosystem model and life cycle assessment estimates demonstrated a net forest sector carbon deficit relative to control stands of 27.0 Mg C ha^{-1} in 2050 due to emissions from dead biomass pools despite increases to net ecosystem production. Our results demonstrate dynamics resulting in carbon losses from forest thinning, providing a baseline

with which to inform landscape-scale modeling and assess tradeoffs between harvest losses and potential gains from management practices.

Introduction

Removal of atmospheric CO2 by the world's forests is now an essential component of limiting global warming to 1.5°C–2°C in addition to large reductions in fossil fuel emissions (IPCC, 2018). Forests remove atmospheric carbon via photosynthesis, accumulating large quantities of carbon in long-lived, lignin-dominated pools, most notably tree wood and soils. This is particularly evident in regions recovering from historically high levels of harvest (Hudiburg et al., 2019; Law et al., 2018). In the Western US, decreases in net carbon uptake (i.e., net ecosystem production [NEP]) due to drier conditions in water-limited environments and in- creases in mortality events from fire, insects, and drought (Abatzoglou & Williams, 2016; Allen et al., 2010; Hicke et al., 2012; Schwalm et al., 2012; van der Molen et al., 2011) may decrease global greenhouse gas (GHG) mitigation potential of forests by increasing carbon losses relative to gains. In part due to concerns over declining carbon sink strength in some areas, forest thinning is being explored and implemented as a wide scale mitigation strategy (State of California, 2018), particularly in states with GHG reduction man- dates (California, Oregon, Washington). However, in situ observations of thinning impacts on carbon and water dynamics are limited, especially with measurements spanning the important temporal and spatial scales at which these impacts occur (from seconds to years and leaves to landscapes).

Forest thinning has become a common strategy for reducing individual tree stress and potentially decreasing tree mortality (Franklin et al., 2018; Liang et al., 2018; Sohn et al., 2016; U.S. Executive Office of the Pres- ident, 2018), yet thinning is a management practice

with inherent carbon costs because live trees are killed, reducing primary producer density and increasing dead biomass available for decomposition or combustion (both within and outside of the ecosystem) (James et al., 2018; Law et al., 2013). To justify specific removal treatments for carbon storage benefits, the net emissions costs of thinning must be lower than the costs of inaction at the temporal and spatial scales of focus, regardless of an ecosystem's baseline sink or source strength (Hudiburg et al., 2011; Law et al., 2013; Mitchell et al., 2012; Naudts et al., 2016). However, the carbon balance impacts of treatments remain uncertain across tree, ecosystem, and regional scales due to large variations in ecosystem processes, stochastic landscape disturbances, unclear assessment time scales, variable treatment and accounting methods, and historically unprecedented climate. This complexity precludes a "one size fits all" approach to prescriptions (Brown et al., 2004; DellaSala et al., 2013; Hudiburg et al., 2019; Law et al., 2018). Moreover, sufficient continuous measurements of before and after carbon stocks and fluxes in control and thinned stands are often lacking (Tsamir et al., 2019), especially measurements that can be used to improve and validate the mechanics of the larger scale modeling (M. D. Hurteau et al., 2016; Liang et al., 2018; McCauley et al., 2019) that is essential to evaluating landscape outcomes.

Natural and human disturbances, including fire, insects, drought, and harvest, can reduce NEP through altering the balance between ecosystem gross primary production (GPP, i.e., photosynthesis) and total eco- system respiration (ER) (Chapin et al., 2006). NEP can be reduced in the absence of tree mortality due to greater sensitivity of GPP than respiration to stressors, as shown from eddy covariance estimates during turn of the 21st century drought in western North America and Europe (Ciais et al., 2005; Schwalm et al., 2010, 2012; Zhao & Running, 2010). Mortality events generate large reductions in net primary pro- duction (NPP)

(i.e., growth, or GPP minus autotrophic respiration) via decreases in live plant density and pulses of dead biomass decomposition that may last years to centuries (J. L. Campbell et al., 2016; van der Molen et al., 2011). The net ecosystem carbon balance (NECB) represents the total ecosystem carbon balance and includes losses from fire emissions or human removals. In the case of forest fire, direct emissions result from combustion of biomass stocks, but typically account for less than 30% of aboveground carbon, are small in relation to subsequent decomposition after high-severity fire, and are primarily limited to dead biomass on the forest floor (J. Campbell et al., 2007; J. L. Campbell et al., 2016; Harris et al., 2019; Meigs et al., 2009; Stenzel et al., 2019).

In examining disturbance from harvest, however, it is important to recognize that NECB is an ecosystem mass balance and does not account for the net emission of ecosystem-derived carbon to the atmosphere. In other words, “out-of-site” is not “out-of-mind” when accounting for net emissions because all removed bio- mass eventually decomposes or is combusted (Harmon et al., 1996). The Net Forest Sector Carbon Balance (NSCB; Hudiburg et al., 2019) accounts for net emissions of ecosystem carbon from NEP, on-site combustion, and off-site emissions estimated via life cycle assessment (LCA).

Thinning for disturbance mitigation is intended to generally increase residual tree resistance to stressors, increasing individual tree carbon and water status and decreasing probability of mortality. However, killing live tree biomass can decrease ecosystem carbon storage over baseline conditions on decadal scales (Goetz et al., 2012), with storage losses, time until recovery, and residual tree growth positively correlated with thinning intensity (Zhou et al., 2013). These processes vary regionally and there are few studies that have continuously measured water and carbon fluxes both before and after thinning, measured at

stand scales, and included control plots (Dore et al., 2010, 2012). Instead, studies have primarily relied on single or periodic carbon stock inventories and modeling. This is important because modeling studies should be validated against data (measurements) of the process-based responses before quantifying carbon emissions for entire regions.

Thinning can impact forest response to stressors through modifying the availability of water, light, and nutrients to the remaining trees as well as altering microclimates. Particularly in water limited forests, changes to soil water availability and timing can have significant impacts on tree photosynthesis and growth (Tepley et al., 2020). In addition to direct impacts on canopy transpiration, thinning has been shown to result in changes to snowmelt volumes and infiltration through less canopy interception and subsequent sublimation (Krogh et al., 2020; Tague et al., 2019; Varhola et al., 2010). These hydrological changes can change soil water availability via altering the partitioning of evaporation, transpiration, and runoff, most significantly during the spring and summer, when warming temperatures and longer daylengths allow for more substantial photosynthesis in higher latitudes. For forests that experience summer drought, soil water availability in deeper soil layers is also crucial (Brooks et al., 2002) and is affected by the persistence of site snowpack in the spring and timing of snowmelt at higher elevations.

Forest thinning emissions result primarily from the harvest and eventual decomposition or combustion of killed above and belowground biomass. Because harvests differ from natural disturbances in that large quantities of stem biomass are often removed and are emitted off site, conducting a LCA of biomass fates is critical to estimating carbon emissions, as no biomass is stored indefinitely (Goetz et al., 2012; Hudiburg et al., 2011, 2019). Avoided emissions (e.g., combustion during a subsequent or avoided fire) should also

be accounted for, but because fire is stochastic, and will occur in only a fraction of a treated landscape during treatment lifespans, these avoided emissions are difficult to quantify (J. L. Campbell & Ager, 2013). More- over, the emissions avoided can be less than emissions associated with harvest, depending on the harvest intensity (Berner et al., 2017).

To address the biogeochemical impacts of thinning, we performed a density reduction treatment (thinning) on a ponderosa pine forest in the Northern Rocky Mountains, a region that is underrepresented in long- term forest research networks (e.g., AmeriFlux, LTER, NEON) yet contains some of the most carbon dense forests in the western US. The region is also characterized by seasonal drought stress and forests with high vulnerability to disturbance (Buotte, Law, et al., 2020; Buotte, Levis, et al., 2020). We utilize a novel integration of automated tree and soil measurements, traditional inventory techniques, LCA, and ecosystem modeling to examine response at multiple spatiotemporal scales. Multidecadal ecosystem carbon trajectories in the 21st century are simulated with Daycent (Parton et al., 1998), the daily timestep version of the CEN- TURY model, to evaluate the consequences of thinning at stand and landscape scales through 2050. Our study addresses the following: What are the impacts of forest thinning on (1) tree-scale carbon and water dynamics, (2) ecosystem scale carbon and water dynamics, and (3) net forest sector carbon balance through 2050? In the short term, we hypothesized that moderate live tree removals would increase individual tree water use and production yet reduce stand carbon uptake due to reductions in live tree density and increases in dead belowground biomass. Moreover, considering the immediate and eventual emissions of biomass removals, we expect that carbon parity with the control stands would take several decades.

Materials and Methods

Study Site Description

The study site is a 35-year old (2015) ponderosa pine (Pinus ponderosa) plantation located in the University of Idaho Experimental Forest in Northern Idaho (46.846°N−116.716°W, Figure 1). Pretreatment average basal area was 36 m2 ha^{-1} and density was 824 trees ha−1. Average tree diameter-at-breast-height (DBH) and height were 23 cm and 15 m. Site elevation is ~970 m with slopes from 0° to 5° and aspects ranging from ~135° to 270° southeast to west. The 30-years average annual air temperature and precipitation are 8.3°C and 883 mm, respectively (DayMet; (Thornton, 2012). The previous 40 years mean frost free growing period is 113 days, with every year after 2012 being above average (Hegewisch & Abatzoglou, 2020). Typically, this region experiences prolonged summer drought with consecutive rain free days ranging from 40 to 100 days, resulting in a late-summer drought period in which rooting depth soil moisture is depleted and vapor pressure deficits are high (SNOTEL; Schaefer & Paetzold, 2001). Soils at this location are a silty loam with a volcanic ash layer. Understory shrubs consist of ninebark (Physocarpus malvaceus), oceanspray (Holodiscus dumosus), and common snowberry (Symphoricarpus albus). Understory tree regeneration is largely nonexistent.

Study Design

Six 0.4-ha (1-acre, 35.7 m radius) plots were installed in the Fall of 2016. In each plot, four subplots (10 m radius) were established following the FAO Terrestrial Carbon Observations protocol (Law et al., 2008), with one subplot in the center and the remaining three 15-m from center in the directions of 0°, 120°, and 240°. Three plots were thinned to 6

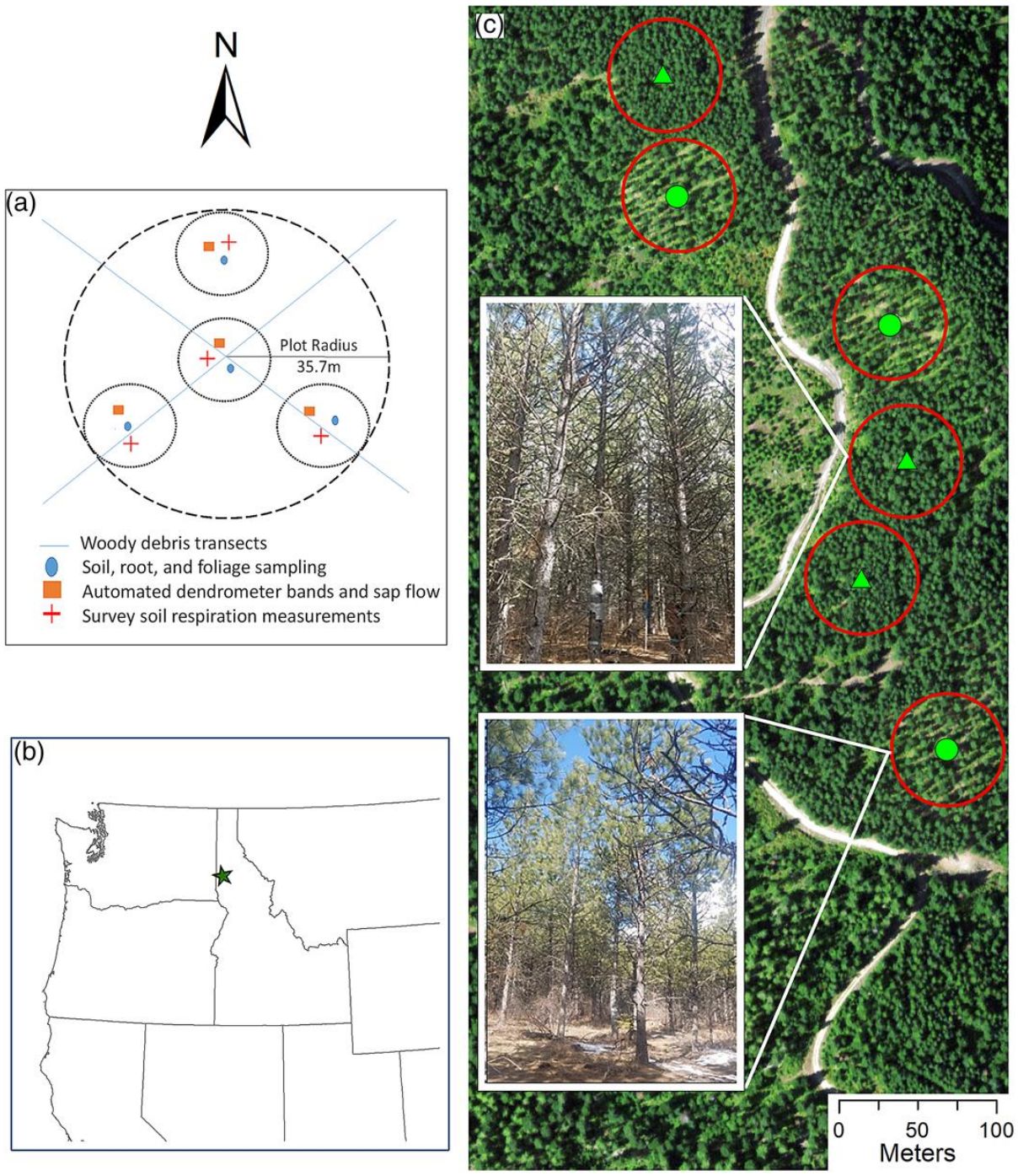

Figure 1. Study location and design. (a) Plot diagram. Locations of sap flow sensors and dendrometers were randomly distributed within 4, 10 m radius subplots. (b) Study location in the Northern Rockies ecoregion near Moscow, ID, USA. (c) Annotated image of study sites within the University of Idaho Experimental Forest, June 2020 (ArcGIS World Imagery, 1.2 m). Red circles indicate plot locations (center circles = thinned, triangles = control). Representative photographs were taken shortly after the thinning treatment in Spring, 2017 (photo credit: T. Hudiburg).

m spacing and a 50% reduction in basal area from December 2016 to April 2017, while the remaining three plots remained as control plots. Woody debris and slash from the thinned plots were removed, piled, and burned in accordance with University of Idaho Experimental Forest protocols to prevent fuels build-up and bark beetle habitat. To capture the stand dynamics associated with thinning, we estimated pre and post thinning carbon stocks, carbon fluxes, and water dynamics. We statistically modeled stocks, fluxes, and water dynamics as a function of time, seasonality, and environmental covariates (Tables S2–S4) to identify data patterns and explain intraannual responses. We projected long- term effects of thinning on forest ecosystem carbon balance with a biogeochemical model (DayCent) and life cycle analysis of harvested carbon.

Carbon Stock and Biometric Measurements

Sampling size and frequency differed for the measured biomass pools (see Table 1). For all biomass pools, conversions to carbon are calculated based on a carbon to biomass ratio of 0.5. Live and dead tree biomass were calculated using regional and species-specific allometric equations that use height and DBH for estimating bole and coarse root volume, bark, branch, fine root, and foliage biomass (Means et al., 1996). Site-specific wood density was used to convert bole and coarse root volume to biomass. Standing dead tree carbon is based on recorded biomass and decay class and reduced over time by standing dead decay rates.

Understory woody shrub biomass was estimated using site-specific allometric equations based on in situ samples of shrubs. We estimated percent cover and height classes

Table 1. Carbon stock and biometric field sampling structure.

Inventory	Year	Season	Scale	Samples (n per Plot)
Tree	2016, 2019	Summer	Subplot	Complete
Understory	2016, 2019	Summer	Subplot	Complete
Woody Debris	2016, 2019	Summer	Plot	A 10-m (fine) and 45-m (coarse) (2)
Soil	2016	Summer	Plot	4 per plot (4)
Litter and Duff	2019	Fall	Plot	4 per plot (4)
Roots	2016, 2017, 2018, 2019	Spring, Fall	Subplot	3 per subplot (12)

Standard deviations are in parentheses. All carbon pools are in Mg C ha^{-1} while NPP is in g C m^{-2} yr^{-1}.

Table 2. Average plot-level pre- and post-thinned carbon pools and NPP. Standard deviations are in parentheses. All carbon pools are in Mg C ha^{-1} while NPP is in g C m^{-2} yr^{-1}.

	Total Tree (live and dead)	Woody debris	Understory Vegetation	Litter / Duff	Soil	Total Ecosystem Carbon	NPP
2012 - 2016							
Control	102.2 (3.9)	33.1 (1.6)	5.4 (0.2)	16.2 (3.8)	56.1 (8.4)	213.1 (13.1)	784.9 (84.8)
Thinned	101.6 (15.9)	34.8 (4.6)	5.5 (0.8)	16.9 (6.7)	51.4 (8.4)	210.2 (19.3)	794.7 (67.1)
2017 - 2019							
Control	104.6 (4.0)	33.1 (1.6)	5.4 (0.2)	16.2 (11.9)	NA	215.4 (13.2)	760.7 (83.8)
Thinned	53.8 (9.1)	40.5 (2.6)	1.4 (0.2)	16.9 (6.7)	NA	164.0 (13.7)	550.9 (61.8

for a sample of shrubs, then harvested, dried, and weighed samples to develop the biomass equations. Subsequently, all shrub percent cover and height class within each subplot were measured to estimate total shrub biomass of each plot. Thinning operations destroyed over 85% of shrub biomass with negligible re-sprout prior to the 2019 sampling. Herbaceous and grass biomass were negligible in all the plots and not included in our estimates. Plot level fine and coarse woody debris carbon pools were estimated using line-transects that extended in each cardinal direction from the center of the plots (Law et al., 2008; Van Wagner, 1968), with density modifiers by species and decay class. All stump diameters, heights, species, and decay classes were recorded for each plot. Stump volume was calculated as a cylinder and converted to biomass with a decay-class constant modifier for density.

Soil samples (10 cm2) were measured for carbon and nitrogen content at 0–5 cm, 5–10 cm, 10–20 cm, and 20–30 cm. Litter and duff were separated from these samples (Chojnacky et al., 2009), dried, and weighed in the laboratory. Field depth of litter and duff was measured and bulk density was calculated; biomass to carbon conversion factors of 0.37 and 0.49, respectively were used to estimate carbon stocks of each (M. Hurteau & North, 2009).

Root biomass cores were collected from the top 20-cm of the soil profile. Roots were separated from the soil, dried, sorted into size classes (<2 mm, 2–5 mm, and >5 mm), and weighed to get seasonal biomass of fine and coarse roots. Root biomass was used to estimate the carbon pool size of roots as well as fine root turnover.

Carbon and Water Flux Measurements

Automated measurements of soil moisture, soil temperature, sap flow, bole circumference growth, and soil respiration occurred from 2017 to 2019. Primary data collection occurred through the months of March through November and is the focus of analysis.

Meteorological data were captured through a combination of on-site sensors and nearby meteorological stations. On site climate and soil measurements were augmented with precipitation and air temperature from the Moscow Mountain SNOTEL station located on the same ridge as the study site (Schaefer & Paetzold, 2001). Air temperature and relative humidity within the mid-canopy (4.5–6 m) of 1 tree per plot were measured using MicroDAQ LogTag model HAXO-8 humidity and temperature recorders (MicroDAQ.com Ltd., Contoocook, NH, USA). Soil moisture and temperature were measured at half hourly intervals with CS650 sensors (Campbell Scientific, Logan, UT, USA). Probes were placed in the soil, horizontally at 10, 30, and 80 cm in the soil profile in each plot in a location where slope and canopy coverage were representative of the majority of the plot.

Sap flow was measured in seven trees per plot using paired thermal dissipation sap flow probes (Granier et al., 1996) installed to a depth of 2-cm into the sapwood. The upper probe was continuously heated while voltage differential between the two probes was measured at 5-min intervals using CR1000 dataloggers (Campbell Scientific, Logan, UT, USA). Sap flow measurements were reduced to three trees per plot for the winter months (November–March) each year due to solar power limitations. Time series data were cleaned and converted from differential voltage via the TRACC package for R (Ward et al., 2017). A

rolling baseline zero flow was calculated with a zero-flow vapor pressure deficit (VPD) threshold of 0.1 kPa on nights in which this threshold was met for a minimum of 2 h and linearly interpolated for periods of higher VPD.

Stand sap flux (Et; cm d−1) was calculated with additional inputs of stand inventory observations, including tree DBH and sapwood depth. Plot sap flow was calculated as canopy transpiration (Ec; cm m-2 d−1; at ≥ daily scale) divided by area. Canopy transpiration was calculated as a product of sap flow (cm h−1), sapwood area, and leaf area at daily and greater scales. To account for flow attenuation at depths greater than 2 cm, relative flux by sapwood depth was calculated according to similarly aged ponderosa pine stands (Irvine et al., 2004). We did not find a relationship between tree size and sap flow at 2 cm (the range of DBH in the stands was narrow in the even aged stand). For trees without sensors in each plot, we estimated flow based on average flow rates adjusted by tree-size-specific estimates of sapwood area and flow attenuation across sapwood depth.

Stand canopy conductance (Gc; cm s−1; Equation 1) was calculated from stand sap flow, intracanopy temperature and relative humidity, and stand LAI, and restricted to periods when VPD greater than or equal to 0.6 kPa. (Drake et al., 2011; Ewers et al., 2001):

(1) $$G_C = K_g(T) \times \frac{E_c}{(VPD \times LAI)},$$

Where *T* is temperature (Celsius), VPD is vapor pressure deficit (kPa), LAI is stand leaf area index (unitless) and K_g is the conductance coefficient (Drake et al.,). Based on Fick's law, carbon uptake can be calculated a function of $G_C$and the leaf-atmosphere CO_2 gradient. We therefore also assessed the degree to which light-saturated leaf CO_2 concentrations (C_i) were

conserved in the study stand (Drake et al., ; G. Katul et al.,). C_i across the growing season was estimated via leaf starch $\delta^{13}C$, which is the ratio of stable isotopes ^{13}C–^{12}C relative to a standard reference and reflects carbon isotope discrimination associated with photosynthesis (Equations and ; Farquhar et al.). Mid- and upper canopy sunlit needles were collected across plots during the spring and summer drought period of 2018 (n = 38) via the shotgun method, reflecting the isotopic composition of recent photosynthate relative to the standard reference. Needles were dried and ground and starch was extracted via methanol/chloroform/water extraction (Wanek et al.,), then packaged in tin capsules. Analysis of $\delta^{13}C$ was performed using a coupled elemental analyzer (ECS 4010, Costech Analytical, Valencia, CA) and continuous flow isotope ratio mass spectrometer (Delta PlusXP, Thermo Finnigan, Bremen, Germany), reported relative to VPD. C_i was calculated as:

(2) $$\Delta = \frac{\delta^{13}C_{\text{air}} - \delta^{13}C_{\text{plant}}}{1 + \delta^{13}C_{\text{plant}}},$$

(3) $$\Delta = a + \left(b - a\right) \times \frac{c_i}{c_a},$$

Where Δ is discrimination relative to air and a and b are the fractionation due to diffusion and carboxylation (4.4 and 27)‰. We assumed a δ13Cair of −8‰ and that atmospheric CO2 was a stable 415 ppm during day- time hours (G. G. Katul & Albertson, 1999).

The seasonality of tree growth was determined using self-logging dendrometer bands. TreeHugger auto- mated dendrometer bands (Global Change Solutions, LLC) were installed on sap flow trees in each plot by March of 2017, ∼2 months prior to typical growing season initiation. TreeHugger dendrometer bands record bole circumference changes via shifting

stylus depression of a soft potentiometer pad. Dendrometer accuracy is ±10 μm and measurement resolution is 6 μm. Prior to installation, outer stem bark was smoothed with a rasp and chisel. Bands were installed at ~2-m in height (above sap flow probes) and appropriate spring tension for proper stylus-potentiometer overlap was verified. Circumference and band/logger temperature were recorded at 30-min intervals by a dedicated logger associated with each band. Band data was analyzed for determining the seasonality (i.e., rate of growth, start and cessation) of bole wood NPP and reconciled with increment core data to determine annual bole wood NPP.

Current and historical estimates of wood NPP were derived from measuring radial growth increments from 20 trees in each plot, including sap flow trees. NPP of woody components is computed from the difference in biomass at two points in time divided by the measurement interval. Previous DBH (calculated from the wood increment cores) and height (modeled using site-specific diameter height equations) for each tree are used to calculate the previous biomass. Foliage NPP was calculated as foliage biomass divide by plot-specific average leaf retention times (Hudiburg et al., 2011). We were unable to detect significant changes in live and dead root biomass pools between spring and fall sampling periods, and therefore could not calculate fine root NPP in our samples. We used the literature reported average fine root turner over time for North American conifers (0.641; Li et al., 2003) multiplied by fine root biomass to determine fine root NPP.

Total soil respiration (Rs; including both autotrophic [Ra] and heterotrophic [Rh] contributions) was were measured using both automated and survey measurements. Shallow 10-cm diameter collars were installed to a depth of 2-cm at each subplot in March of 2017.

Automated measurements of Rs were taken hourly using eosFD forced diffusion chambers (Eosense, Nova Scotia, Canada). Two chambers each were installed at two of the thinned plots and one control plot. Automated measurements were primarily used to evaluate and develop diurnal gap filling techniques for the survey data and for winter Rs measurements while the chambers were under snow and the sites were inaccessible.

Survey measurements of Rs were taken weekly from April–early November between 10:00 a.m. and 2:00 p.m. using an EGM-5 SRC portable gas analyzer (PP Systems, Amesbury, MA, USA). Survey measurements were gap-filled to attain daily, weekly, monthly, and annual totals of Rs using linear interpolation (Gomez-Casanovas et al., 2013). Linear interpolation was selected because it outperformed soil temperature and soil moisture based models (Reichstein et al., 2003) when compared to automated data for periods in which automated Rs data were available.

Biogeochemical Model Description, Evaluation, and Simulations

An updated and improved version of the DayCent ecosystem model (Parton et al., 1998; Stenzel et al., 2019) was implemented to estimate future NEP dynamics post thinning and estimate the NSCB along with a LCA. DayCent is the globally recognized daily timestep version of the biogeochemical model CENTURY, widely used to simulate the effects of climate and disturbance on ecosystem processes including forests worldwide (Bai & Houlton, 2009; Bartowitz et al., 2019; Hartman et al., 2007; Hudiburg et al., 2017). The current version (Stenzel et al., 2019) now includes a standing dead tree pool (i.e., snag pool) because of the important biogeochemical consequences of having standing dead wood versus live wood that dies and immediately becomes downed coarse woody debris.

Required inputs for the model include vegetation cover, daily precipitation and air temperature, surface soil texture, site coordinates (for solar inputs), and disturbance histories. DayCent calculates potential plant growth as a function of water, light, and soil temperature, and limits actual plant growth based on soil nutrient availability. The model includes three soil organic matter (SOM) pools (active, slow, and passive) with different decomposition rates, above- and below-ground litter pools, and a surface microbial pool as- sociated with the decomposing surface litter. Plant material is split into structural and metabolic material as a function of the lignin to nitrogen ratio of the litter. The active pool (microbial) has short turnover times (1–3 months) and the slow SOM pool (more resistant structural plant material) has turnover times ranging from 10 to 50 years depending on the climate. The passive pool includes physically and chemically stabilized SOM with turnover times ranging from 400 to 4,000 years. Model outputs include soil C and N stocks, live and dead biomass, above- and below-ground NPP, heterotrophic respiration, fire emissions, and NEP, defined as the difference between NPP and heterotrophic respiration. While Daycent does not explicitly represent individual trees, it implicitly represents the effects of stand competition, particularly with regards to the availability of mineral nitrogen and soil moisture.

Site simulations were driven with historic (1950–2005) and projected future climate (daily maximum temperature, minimum temperature, and precipitation) through 2050 under RCP 8.5 (Figure S5). In- put data was obtained as 4 km statistically downscaled CCSM4 (CMIP5 GCM ensemble member) data from MACAv2-METDATA (https://climate.northwestknowledge.net/MACA/data_csv.php; Abatzoglou & Brown, 2012). MACA is a statistical downscaling method that has been evaluated for local analysis while retaining a large set of climate variables. Parameterization of point runs was based on species

and local observation-based ecophysiological traits (e.g., Leaf retention time, leaf nitrogen concentration, maximum leaf area index) and site and area specific soil characteristics (observations and SSURGO; Abatzoglou & Brown, 2012; NRCS, 2010). Disturbance history was prescribed based on the experimental thinning and most recent recorded clear cut of the stand in the late 20th century. Model evaluation within the observation period was based on comparison with measured live and dead carbon stocks, aboveground NPP, and seasonal soil volumetric water content (Table S6, Figures S3 and S4). For 2018–2019, model VWC r2 was 0.72 (Figure S3); in particular, the timing of summer soil dry down followed observations and in turn led to model NPP downregulation. From 2008 to 2016, the r2 of the modeled aboveground live carbon stock was 0.90, reflecting similar model-observation live-tree trajectories following the 20th century clear cut.

In addition to prognostic future NEP, the emissions tradeoffs between thinning losses and potentially enhanced forest resilience to mortality were evaluated with additional disturbance prescriptions. A range of mass mortality scenarios were prescribed for the higher density unthinned stands only. Scenarios were intended to represent stress related mortality events in which most killed live biomass remains on site (e.g., drought, insect, pathogen, and other chronic stress-related mortality), and thus did not include combustion losses. The future timing (2020–2045) and intensity (50%–90%) of a single mass mortality event was varied and compared to an undisturbed control and thinned stand net emissions by 2050 (Table S1).

Life-Cycle Assessment and Net Forest Sector Carbon Balance

A LCA was employed to account for the storage and emission of killed harvested biomass that was removed from site or combusted on site. Branches and foliage mass from harvested trees were burned as slash on site within 1 year of the thinning. Removed biomass

was divided into product pools including wood and paper products with half-lives of 75 and 2.5 years (Dymond, 2012; Skog, 2008; Smith et al., 2006), respectively. Wood waste (i.e., mill wood that does not become a product) is assumed to be burned onsite with energy recapture or to decay within 1 year. Fossil fuel emissions for all harvesting activities and transport to the mill are also included. We define the Net Forest Sector Carbon Balance (NSCB; see Hudiburg et al., 2019) as the net terrestrial balance of carbon within or derived from the forest ecosystem (NEP—Fire Emissions—wood product chain emission; Table S5). In comparison to NECB (NEP—Fire Emissions—Harvested Biomass), NSCB accounts for net vertical transfers of carbon between the atmosphere and land, delaying the subtraction of removed carbon until it is combusted or decomposes at the end of the product chain lifespan. NEP was modeled with the Daycent ecosystem model, and included decomposition of stumps, course roots, and fine roots killed during harvest.

Statistical Analyses

Flux differences (except stand scale NPP) between treatments were evaluated using generalized linear mixed-effects tree models (GLMM Tree; Fokkema et al., 2018). These models estimate a global random effects model, recursively partition the data with respect to a set of covariates using model-based recursive partitioning (MOB; Zeileis et al., 2008), and apply localized linear mixed-effects models (LMM; Bates et al., 2014) to partitioned data, that is, MOB terminal nodes. Global linear mixed-effects models did not describe the data well (except for stand scale NPP), partly because of the nonlinear nature of response variables within years. The MOB aided in identification of treatment-subgroups, which was beneficial for non- arbitrary data partitioning into temporally similar responses and improving LMM covariate fitting. Stand scale NPP was modeled for all nontreatment plots for the period 2008–

2018 to detect effects of climate with- out treatment effects. An LMM without the MOB modeling was fit to these data after the MOB model failed to detect subgroupings on the partitioning covariates. Model selection for each flux was based on nested covariate models and assessment of AIC, BIC, and interpretation of model fit. Covariate significance within the selected LMM models was determined using 95% confidence intervals. The nested set of covariates with respect to the fixed effects, random effects, and the MOB models differed among the fluxes (Tables S2–S4). R was used for data analysis, with the glmertree package used for estimation of the GLMM Tree (Fokkema et al., 2018) and the lme4 package used for the LMM.

Uncertainty estimates in model predictions were quantified using a propagation of error approach that combines the observation uncertainty (i.e., NPP, biomass) with uncertainty in model input parameters and forcing datasets (i.e., climate). Because our climate data was specific to our site for historical simulations, we had no reason to assign any uncertainty for validation with observations. Moreover, because the model was parameterized exclusively with site data, most of our model uncertainty was attributed to variation in our site observations for leaf retention time and belowground biomass.

Results

Pre- and Post-treatment Carbon Stocks

Thinning reduced tree biomass by 47 ± 13% across treatment plots, resulting in a density of 232 ± 23 trees ha−1. Postthinning spacing increased from ∼13 to 21 ft (3.3–6.6 m). Residual tree DBH in thinned plots increased from 23 cm prethinning to 27 cm and heights from 14.8 to 16.5 m. Woody debris increased in the thinned plots primarily because of

removal operations increased the number of stumps (from ~4.5 to 9.1 Mg C ha−1; Table S1). Thinning reduced understory vegetation biomass by 75%; however, understory vegetation was a minor portion of aboveground live biomass pretreatment (<5%) in all plots. Killed course root mass was the largest source of on-site dead biomass inputs, ranging from 11 to 13 Mg C ha−1 per plot. Moderate winter windthrow occurred in treatment plot 6, resulting in 7% mortality of remaining live trees. No additional mortality has been observed in control or treatment plots since observations began in 2016. In total, an estimated 60% of killed aboveground biomass was removed from the site, while most of the remaining portion was piled and burned.

Net Primary Production

Tree-Level Response to Thinning In thinned plots, average individual tree NPP increased 70% ± 12% (2017–2019 growth vs. 2012–2016 growth), with the largest increases observed immediately after thinning in 2017 (Figure 2b). In comparison, control plot average tree growth declined by 1%–5% in the same period. Increased average tree growth in thinned plots was a result of both increased growth of remaining individuals (i.e., within-tree NPP increased on average 31% ± 8%) as well as a greater proportion of larger, higher productivity trees. Trees remaining after treatment had been on average 30% more productive and 5 cm larger in DBH than the prethin plot tree average. In remaining trees, there was not a strong relationship between diameter and radial growth ($r = 0.05$). However, consistent radial growth across size classes translated to a geometric positive effect of tree size on volume growth (Figure 2a). Treatment response magnitude and direction was variable; 20% of thinned stand trees did not display increases in radial growth, 50% displayed increases of less than 25%, and 15% of trees displayed increases of over 100% (Figure 2a).

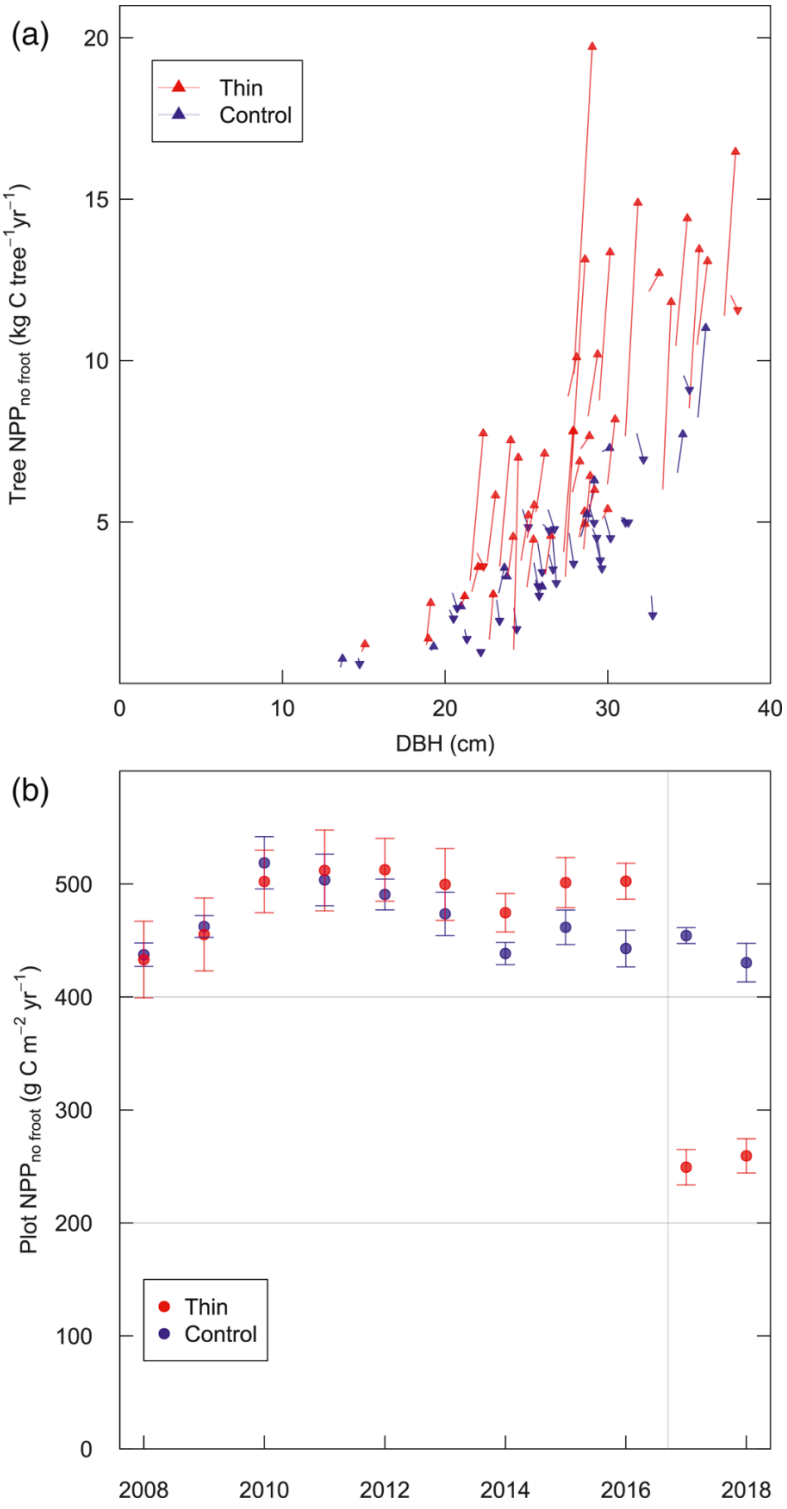

Figure 2. Tree and stand level thinning NPP response. (a) Tree NPP response by DBH. Triangles indicate mean 2017–2018 NPP, triangle direction indicates increases (up) or decreases (down) from the 2015–2016 tree NPP mean, represented by the start of each line. (b**)** Plot level NPP by treatment. Bars indicate SE. Vertical dashed line indicates thinning treatment.

At the stand scale, decreases in tree density were not compensated by the increases in tree growth, and NPP decreased by 45% in thinned stands, (−245 ± 23 g C m^{-1} yr^{-1}, $p < 0.05$, paired T-test) (Figure 2b). During the same period, control plot NPP declined by 3% (−25 ± 11 g C m^{-1} yr−1). Before treatment, average yearly NPP from 2012 to 2016 across all plots was 790 ± 75 g C m^{-1} yr−1. Through the pretreatment period, NPP sensitivity to yearly climate was relatively low (Figure 2b). NPP excluding fine roots peaked in 2010 (∼500 g C m^{-1} yr−1) and declined modestly through 2016, with apparent declines in radial growth approximately balancing increases in tree size and stand biomass. The primary driver of pretreatment stand-level NPP variation was stand age rather than seasonal cli- mate variables (Table S2, LME). Even so, site-wide NPP estimates ranged by only 50 g C m^{-1} yr^{-1} from 2008 to 2016. Though 2015 was an exception- ally hot and dry year, with the longest soil drought period within the observation period, stand NPP nonetheless increased over 2014 (Figure 2b).

Automated dendrometer measurements indicated that stem radial growth occurred from early May until the beginning of August from 2017 to 2019 (Figure 3; ∼3 months), a period receiving an average 11% of yearly precipitation during the last decade (2010–2019 Moscow Mountain SNOTEL). Spring rain was not sufficient for preventing continual declines in soil moisture to 30 cm following snow melt (Figure 3). Neither growth start nor end dates varied significantly by treatment ($p < 0.05$, two-sided t-tests), despite tree level differences in treatment growth magnitude (Figure 2a). Growth initiation was more rapid (days) than cessation (weeks) and corresponded to the period of soil and air temperature increase immediately after snowmelt. Growth cessation was gradual (ap- proximately the month of July) and corresponded with the depletion of rooting depth VWC. Drought-period

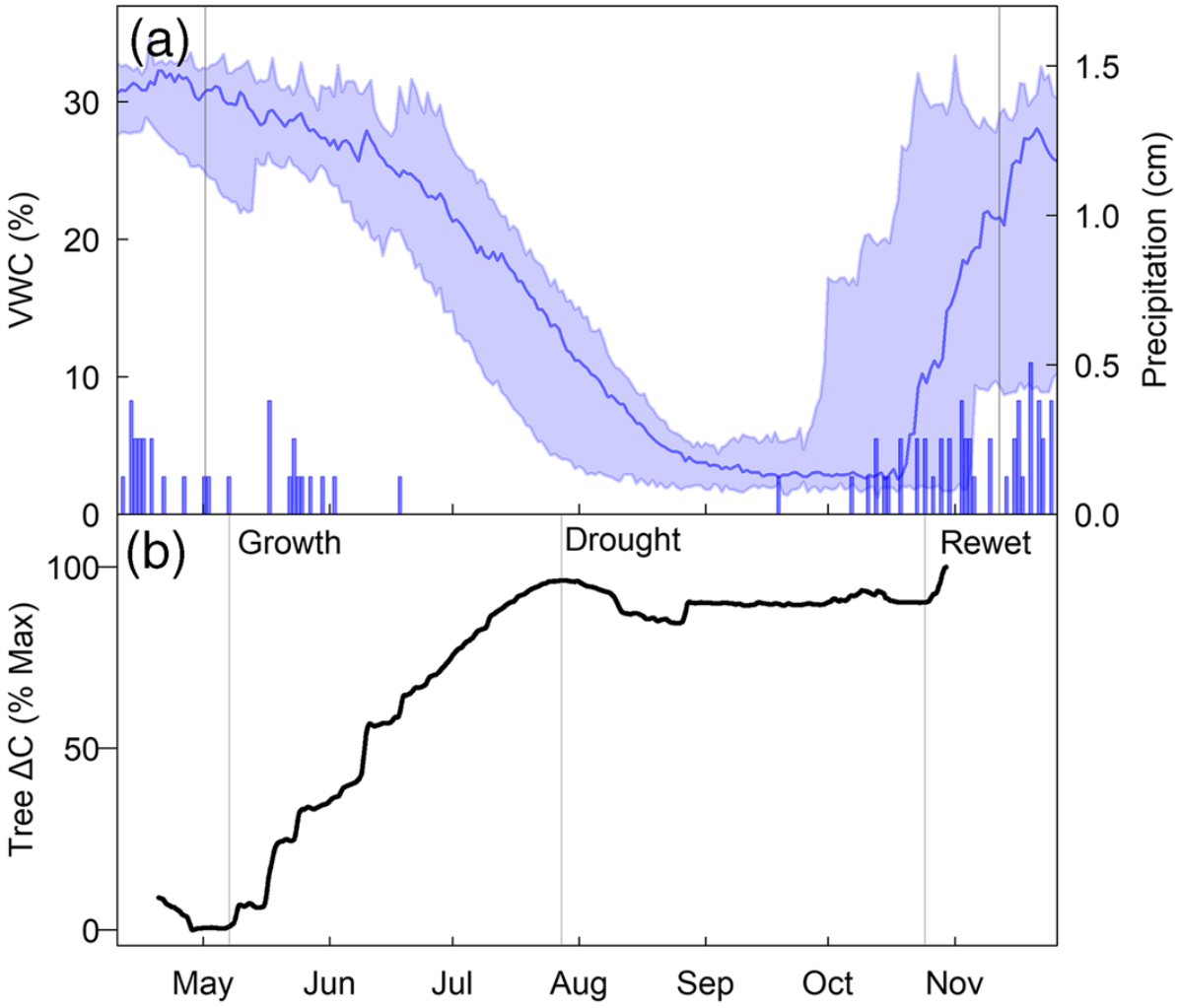

Figure 3. Tree growth and seasonal moisture. (a) 2010–2019 VWC at 20 cm depth (median and range) and daily precipitation (daily median). Vertical gray lines indicate median boundaries of the snow-covered season. Moscow Mountain SNOTEL station. (b) Example dendrometer Δ stem circumference series (ΔC; from early spring minimum) for the study site.

circumference shrinkage occurred followed growth cessation and continued until the first major fall rain events, when rapid (i.e., hours to days) circumference recovery occurred upon (Figure 3).

Respiration

Soil respiration (Rs) between control and treatment plots was similar from weekly to annual time scales (Figure 4), with some seasonal variation. Total annual soil respiration did not significantly vary between treatments during 2018 or 2019 (Table S3 and t-test, $p > 0.05$). However, there were periods when control plot means differed from thinned plot means. Rs varied significantly during July and August of 2018 with higher Rs in the thinned stands. Annual Rs ranged from ~830 to 1230 g C m-2 yr^{-1} across plots in 2018–2019. Across all years and treatments, concurrent with stem growth, Rs peaked from May through July and declined strongly with de- clines in VWC from August onwards (LMM; Table S3).

Modeled estimates of component soil respiration fluxes showed a concurrent increase in Rh and decrease in Ra in the thinned plots for several years after thinning, followed by soil Ra recovery and gradual course root decomposition. In both periods, the result was negligible net change in total Rs (Figure S1).

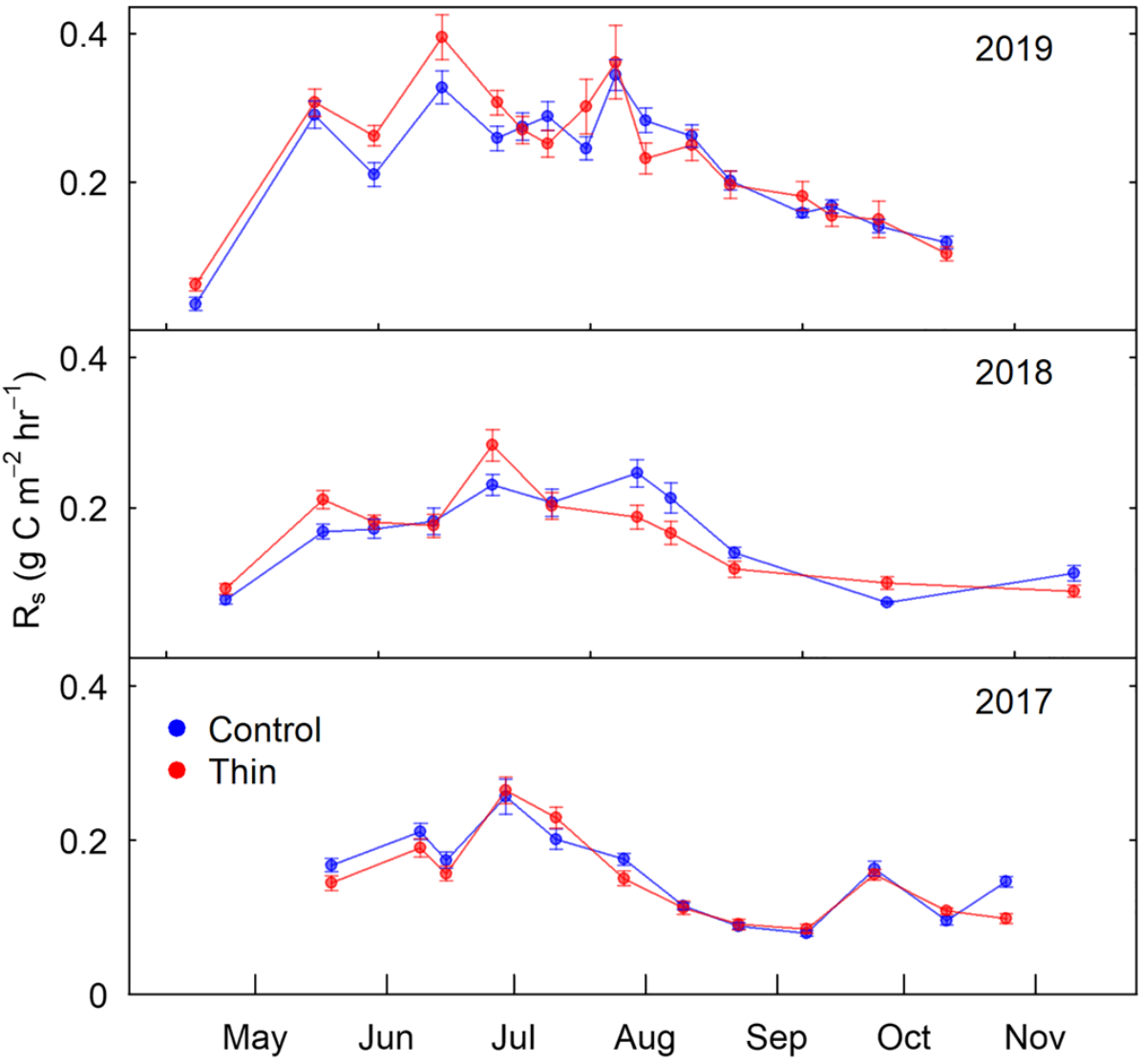

Figure 4. Survey soil respiration observations for control and thinned plots from 2017 to 2019. Error bars represent the standard error for plot-level mean values on each measurement day.

Sap Flow and Canopy Conductance

Tree-level sap flow (i.e., at sensor depth) from May-October was 55% and 46% higher in thinned versus control plots in 2018 and 2019, with distinct predrought and drought periods (Figures 5c and 5d, significant treatment effects during all 2018 and 2019 periods, Table S4). In thinned plots, tree sap flow was on average 18% & 26% higher until week 28 in 2018 and week 29 in 2019, when significant drought divergence was observed (Figures 5c and 5d). Spring and early summer sap flow patterns were similar between treatments, with flow under well-hydrated conditions corresponding to variations in temperature and VPD,

Declines in sap flow occurred during rapid soil dry-down (Figure 3) from July through August. While trees in all plots demonstrated declines in sap flow along with declines in site VWC, control-tree flow declined by ~65% from predrought maximum flow by August, while treatment-tree flow declined by ~33%. Continued declines were observed through September, with 87% and 63% decreases for control and treated plots, respectively, relative to mid-season maximums. As a result, tree-level sap flow for trees in the thinned stands from mid-July through October were on average 133% and 90% higher than control stand trees sap flow during 2018 and 2019. For control and thinned plot trees, this drought period represented an average 31%–32% and 40%–48% of measurement period sap flow. Flow past October remained low, though temperatures and VPD declined during this period. During all growing season periods evaluated, treatment and VPD were significant covariates, while VWC was significant across most periods (Table S4).

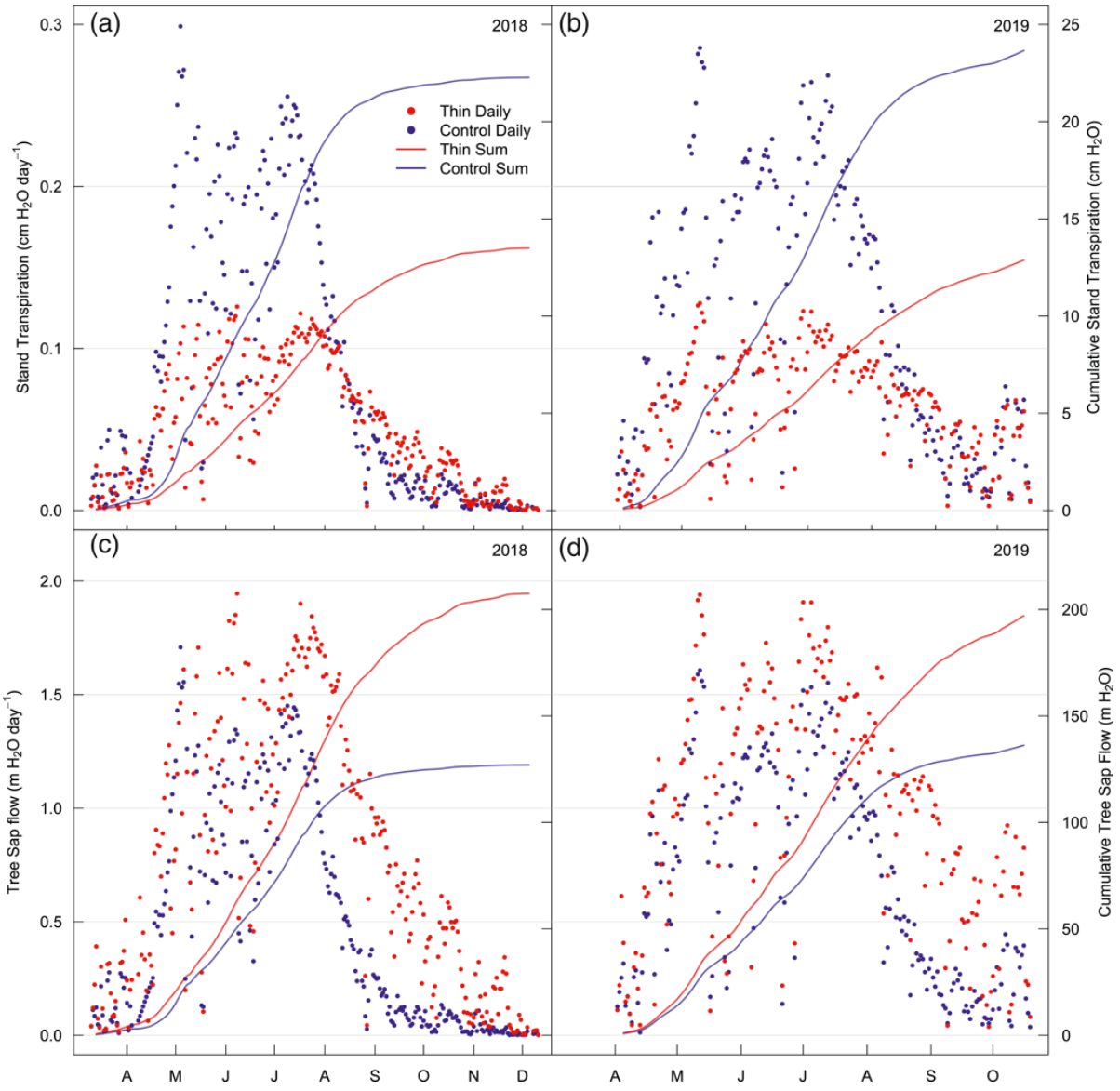

Figure 5. Tree and stand scale sap flow, 2018–2019. (a) Daily and (b) cumulative mean stand transpiration. (c) Daily and (d) cumulative mean tree sap flow.

In 2019, Gc was estimated with the addition of intracanopy temperature and relative humidity measurements. High spring Gc was achieved across treatments by late March to early April, with average daytime Gc 19% higher in thinned stand trees (Figure S1). Daytime Gc for both treatments began to decline sharply in late July (~doy 200) and diverged in magnitude by early August. Thinned stand Gc was on average 165 % higher than in control plots from August through mid-October, with peak differences occurring in early September, after which air temperature and VPD declined through the Fall. During the fall, Gc rose despite consistently low sap flow due to lowered VPD. Spring and Summer δ13C was also evaluated as a proxy for the intraleaf concentration of CO2 and intrinsic water use efficiency (i.e., Ci/ Ca). Values of δ13C did not vary significantly between treatments or across the spring and summer drought period ($p < 0.05$, paired and unpaired t-tests).

Stand-Level Transpiration

Decreased tree density, sapwood area, and leaf area in the thinned stand (Table 1) resulted in lower stand-level transpiration compared to control plots from May-October (Figures 5a and 5b). Transpiration in the control plots was 74% higher than the thinned plots, varying from 115% higher in early July to 19% more in late October. This difference was greater than 100% in the predrought period, when tree-level sap flow was similar be- tween treatments. In 2018 and 2019, stand-level sap flow approximately converged beginning in August and control stand-level flow decreased below treatment flow in September only (Figures 5a and 5b).

Net Forest Carbon Balance (NEP and LCA)

Thinning resulted in an average 48 and 10 Mg C ha^{-1} of killed above and belowground biomass, with 37.4 Mg C ha^{-1} removed from site (Table 1). ~35% of killed biomass remained on site, 18% was combusted as slash or left as debris, and 65% was removed.

Ecosystem partial harvest was simulated in DayCent to investigate trends through 2050 under a warming climate with consistent annual precipitation (Figure S5). Through the observation period, modeled tree component carbon stocks and seasonal patterns of soil moisture driving summer growth cessation com- pared well to measurements (r2 = 0.90 and 0.72 respectively. Figures S3 and S4). During the first 5 years postharvest, modeled NEP in thinned stands was lower than control stands, resulting in a maximum post- treatment relative NEP deficit of 12.1 Mg ha^{-1} (Figure 6a). The NEP deficit relative to control stands was overcome by 2035. Low or negative NEP in the first 5 years postharvest resulted from killed belowground biomass decomposition as well as reduced leaf area and NPP (Figure 6a). By 2050, total posttreatment NEP in the thinned stand was 4.6 Mg ha^{-1} higher than control stands, a relative recovery of 16.7 Mg ha^{-1} compared to the posttreatment minimum. Increases in NEP resulted both from increases in NPP and in- creased allocation to low-turnover wood pools that occurred in part due to increased availability of mineral nitrogen. Decomposition of killed course roots occurred over several decades and a pulse of postharvest respiration was primarily apparent from the smaller fine root pool. Compared to the control simulation through 2050, differences in stand carbon stocks declined but did not disappear. Aboveground live and total ecosystem carbon in the thinned stand amounted to 75% and 84% of the control in 2050.

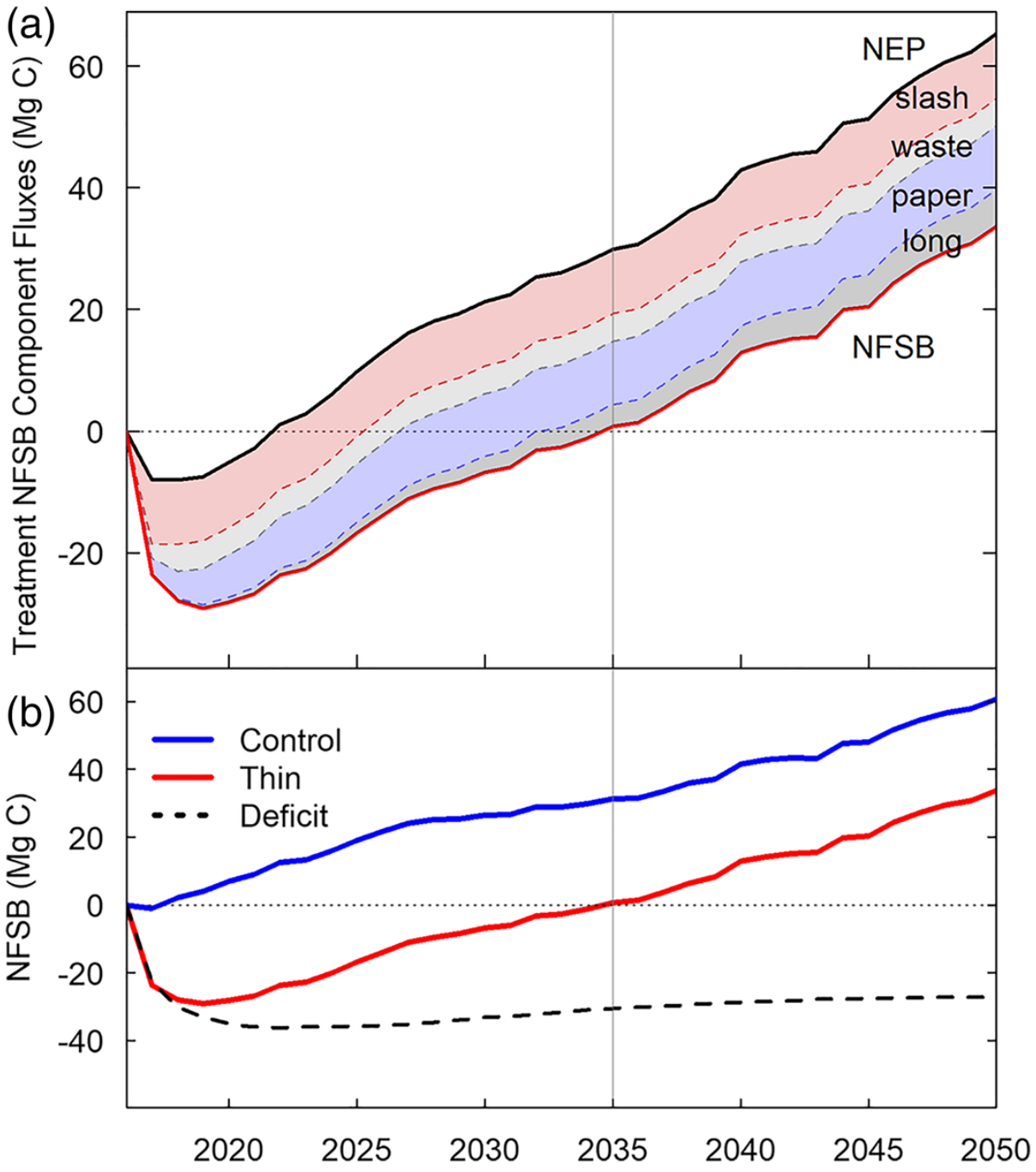

Figure 6. Modeled NFSB post treatment (2017–2050). Vertical gray lines indicate treatment stand recovery to pretreatment total ecosystem carbon stock. (a) Cumulative treatment stand NEP and NFSB and component product emissions. (b) Cumulative treatment and control NFSB. Dotted line indicates thin NFSB deficit relative to control.

Combustion of slash and waste products resulted in 15 Mg C ha^{-1} of har- vested biomass emissions within the first 5 years of treatment (Figure 6a). By 2050, 21.0 Mg C ha^{-1} (56%) of removals and 31.6 Mg C ha^{-1} (66%) of killed aboveground biomass had been emitted. Most remaining product carbon remained in long-term pools, which retained 73% (16.4 Mg C ha−1) of inputs in 2050. The NSCB was −26.7 and 33.7 Mg C ha^{-1} in 2021 (5 years) and 2050, representing the net balance of stand-derived carbon both on and off site relative to pretreatment. Thinned stand carbon parity with pretreatment carbon stocks (2016) occurred in less than 20 years. However, the NSCB deficit relative to the control stand was 27.0 Mg C ha^{-1} in 2050, representing the simulated net emissions to the atmosphere relative to control (Figure 6b).

Scenarios with prescribed future mass tree mortality in unthinned stands indicated that most mortality events before 2050 would not exceed the 27.0 Mg C ha^{-1} relative emissions estimated for thinned stands by 2050 (Table S1). Mortality of 50%–95% of tree biomass before 2035 led to control-relative emissions that were 40%–70% of treatment stand relative emissions by 2050. Events of 75%–90% and from ∼2035 to 2045 approximately matched or exceeded site 2050 thinning-related relative emissions (maximum increase of 22%). In all cases, while high mortality yielded greater than 40 Mg C ha^{-1} killed biomass, gradual on-site decomposition as well as regrowth or improved residual forest growth led to control-relative 2050 emissions equivalent to less than 25% of killed biomass.

Discussion

Forest thinning in a young ponderosa pine plantation resulted in observed and modeled decreases in ecosystem and forest sector carbon storage over unmanaged control plots through the year 2050. Despite increased tree-level production and water use in a

location characterized by growing season drought stress, this study affirms inherent site tradeoffs between individual tree vigor and stand carbon storage over time. We estimate that thinned plot carbon stocks will return to prethinned levels by 2035 (Figure 6), but forest sector carbon parity (Mitchell et al., 2012) with untreated plots will not occur by 2050 and therefore represents a relative carbon source to the atmosphere in the absence of disturbance.

After treatment (2017–2019), decreased tree density reduced observed stand biomass and NPP over control (Figure 2b, Table 2), while soil respiration remained similar (Figure 4). Modeled results suggested that thinned stand NEP would exceed control NEP in subsequent years following several years of canopy recovery due to increases in available mineral nitrogen and increased allocation of carbon to wood (and a resulting decrease in biomass turnover). However, a carbon deficit relative to control remained due to the removal of ~40% of live ecosystem carbon as well as the subsequent release of ~60% of removed biomass by 2050. Despite the continued storage of a portion of removed biomass in long-lived wood products, large immediate and short-term emissions were associated with slash combustion, on-site decomposition, and short-term product chain emissions (i.e., waste and paper), and do not represent avoided emissions through 2050. A multidecadal ecosystem biomass (i.e., carbon) deficit following moderate and heavy partial harvest is supported by most analyses of mid to long-term thinning structural impacts (James et al., 2018; Zhou et al., 2013), though we note a general paucity of long-term observations of carbon stocks specific to variable thinning treatments and regions (Williams & Powers, 2019). We highlight that moderate removals in the productive, even aged study stand (vs. thinning from below, e.g., North & Hurteau, 2011) led to net emissions due to biomass removal and turnover that was rapid relative to yearly ecosystem production (i.e., “slow in, “fast out," Law et al., 2018).

Thinning increased average tree size, diameter growth, and NPP (Figure 2a). Increases in average NPP were a function of both increases in individual tree production as well as altered stand structure (i.e., lower productivity trees being removed; e.g., M. Ryan et al., 1997). A ~70% increase in average tree growth was associated with a more modest ~30% increase in residual tree production. This result highlights the need to differentiate increases in tree production (and, presumably, resilience) from averages that are dependent on structural changes alone when interpreting previous research and anticipating stand and landscape level carbon sequestration and storage (e.g., D'Amato et al., 2013; Sohn et al., 2016; Zhou et al., 2013). Longitudinal observations of individual trees (e.g., Anderson-Teixeira et al., 2015) are generally necessary to isolate tree responses to disturbance and determine the extent to which mean responses are representative of over- all stand function and resilience.

Tree growth magnitude within years was not strongly related to growth duration across treatments and individuals, as growth was similarly constrained by mid-summer VPD and VWC (Figure 3). However, thinned plot trees displayed higher sap flow and canopy conductance through the late summer and early fall drought period, implying higher photosynthesis. High-seasonal variability in canopy conductance and a lack of strong variation in Ci/Ca are consistent with conductance as the primary determinant of assimilation in our stands (Drake et al., 2011). These results are also consistent with higher sensitivity of growth (i.e., NPP) than photosynthesis (and GPP) to seasonal moisture stress, a temporary decoupling of carbon supply and carbon demand (Körner, 2003; Muller et al., 2011; Sala et al., 2012), and a likely improved carbon supply of thinned stand trees through the fall and winter. At an individual tree scale, the largest increases in NPP were observed in the growing season immediately after the winter thinning treatment. Though growing seasons 2018–2019

were preceded by markedly improved tree fall and yearly average gas exchange in treatment plots, continued increases in annual stem growth over 2017 were not observed, possibly suggesting altered carbon allocation responses across treatments that were not resolved by our measurements (Körner et al., 2005; M. Ryan et al., 1997).

While observed growing season length and growing season stand water use were similar between treatments, thinned plot trees displayed less severe downregulation of drought-period water use (Figure 5). This implies improved tree carbon and water status during drought moisture stress and winter periods, and the potential for improved resistance to mortality from regional drought or other disturbance (Adams et al., 2017; N. McDowell et al., 2008; Schlesinger et al., 2016; Sevanto et al., 2014). However, the only nat- ural tree mortality observed since 2015 has been mild windthrow in treatment plots. It will be essential to continue current monitoring in order to observe the long-term impacts of thinning on carbon and water status and how those dynamics effect potential decreases in mortality from disturbance (D'Amato et al., 2013; Sohn et al., 2016; Tepley et al., 2020; van der Molen et al., 2011) that were not prescribed in our modeling. To date, our site observations have been based on treatments in even aged stands of codominant young trees (<40 years). As the stands age, the increased relative size and performance of thinned stand trees (Sohn et al., 2016) may contribute to stand structure that is more resistant to disturbance impacts (Agee & Skinner, 2005). However, forest vulnerability to drought is also complicated by vulnerabilities associated with larger trees that have been related to hydraulic limitations, canopy characteristics, and other factors impacting carbon source strength or sink demand (Bennett et al., 2015; N. G. McDowell & Allen, 2015; Pangle et al., 2015; M. G. Ryan et al., 2006) and can reverse the direction of responses to density as stands age (D'Amato et al., 2013).

Carbon balance tradeoffs between reduced biomass density and increased forest resilience to disturbance are uncertain in large part due to the uncertainty of future natural disturbances occurring in treated areas. Our simulated mass mortality scenarios indicated that 2050 thinning emissions approximately equaled the 2050 emissions from stand mortality events greater than 75% and occurring after 2035. In these experiments, the gradual decomposition of large pools of killed biomass remaining on site highlighted that the emissions consequences of near-term natural disturbances will in part be realized beyond current GHG reduction timelines (e.g., 2035 or 2050, IPCC, 2018). Thus, when managing for forest carbon storage, the timing and magnitude of potential carbon gains or losses, which may be offset in time from disturbance events, must be considered. In our simulations, the near-parity in carbon emissions from thinning and high natural disturbance late in the simulation period occurred at the stand level. However, at the landscape level, the encounter rates between treatments and disturbance are typically low (J. L. Campbell et al., 2012). Greater areas of forest must therefore be treated than will encounter a disturbance, in turn increasing any carbon cost to benefit ratio estimated at the stand scale. Due to the infeasibility of landscape level treatment experiments, landscape level predictions of disturbance impacts are generally simulated with earth systems models (Buotte, Levis, et al., 2020), which remain limited in their ability to represent stochastic disturbance such as wildfire

Thinning treatment impacts will vary across spatiotemporal scales, meaning our results are both site-specific and have future uncertainty. Furthermore, while our experiment entailed a single thinning intensity, it is possible that lower biomass harvest would have resulted in enhanced residual tree function at lower carbon cost (nonlinear benefits; North & Hurteau, 2011; Zhou et al., 2013). Future work in the region should also better characterize

snow accumulation and melt (e.g., SWE) and soil water availability both onsite and at higher elevations to better understand how changes in hydrology will affect thinned and unthinned stands (Krogh et al., 2020).

This study indicated that moderate forest thinning at a northern Rocky Mountain site improved tree function during summer drought at the cost of reduced forest sector carbon balance through 2050. Following treatment, growth and water use increased at the tree scale but decreased at the stand scale due to density reductions. Ecosystem modeling and LCA demonstrated near-term carbon emissions from on and off-site killed biomass that were large relative to annual NPP and therefore unlikely to be overcome in the near- term of GHG mandates (e.g., Hudiburg 2019); this highlights the importance of accounting for the fates of harvested biomass. At a stand level, our results demonstrate that thinning strategies to reduce carbon emissions in the next decades (IPCC, 2018) must either overcome inherent and persistent carbon deficits over nonmanagement or be sufficiently justified for services other than carbon storage (i.e., wood production, human hazard reduction). However, treatments intended to increase carbon storage over business-as-usual should also show that they can do so at the landscape scale and within potentially limited treatment life- times (J. L. Campbell et al., 2012). Because the locations of stochastic disturbances (e.g., fire) will occur over only a fraction of a treated area, further landscape (vs. stand) level analyses are ultimately necessary to integrate the prevalence and magnitude of carbon balance impacts from human versus natural disturbances in managed landscapes. It is particularly important to account for region-specific ecosystem carbon density, productivity, and vulnerability to disturbance to establish where treatments may successfully mitigate car- bon losses (Buotte, Law, et al., 2020).

Acknowledgments

This work was supported by National Science Foundation award number DEB-1553049. We thank Seth Parker for field data collection and Robert Keefe for providing the harvest operations and advice. The authors declare no competing financial conflicts of interests or other affiliations with conflicts of interest with respect to the results of the paper. Any real or perceived financial conflicts of interests for any author.

References:

Abatzoglou, J. T., & Brown, T. J. (2012). A comparison of statistical downscaling methods suited for wildfire applications. International Journal of Climatology, 32(5), 772–780.

Abatzoglou, J. T., & Williams, A. P. (2016). Impact of anthropogenic climate change on wildfire across western US forests. Proceedings of the National Academy of Sciences, 113, 11770–11775. https://doi.org/10.1073/pnas.1607171113

Adams, H. D., Zeppel, M. J., Anderegg, W. R., Hartmann, H., Landhäusser, S. M., Tissue, D. T., et□al. (2017). A multi-species synthesis of physiological mechanisms in drought-induced tree mortality. Nature Ecology and Evolution, 1(9), 1285–1291.

Agee, J. K., & Skinner, C. N. (2005). Basic principles of forest fuel reduction treatments. Forest Ecology and Management, 211(1–2), 83–96. https://doi.org/10.1016/j.foreco.2005.01.034

Allen, C. D., Macalady, A. K., Chenchouni, H., Bachelet, D., McDowell, N., Vennetier, M., et□al. (2010). A global overview of drought and heat-induced tree mortality reveals emerging climate change risks for forests. Forest Ecology and Management, 259(4), 660–684.

Anderson-Teixeira, K. J., Davies, S. J., Bennett, A. C., Gonzalez-Akre, E. B., Muller-Landau, H. C., Joseph Wright, S., et□al. (2015). CT-FS-ForestGEO: A worldwide network monitoring forests in an era of global change. Global Change Biology, 21, 528–549. https://doi.org/10.1111/gcb.12712

Bai, E., & Houlton, B. Z. (2009). Coupled isotopic and process-based modeling of gaseous nitrogen losses from tropical rain forests. Global Biogeochemical Cycles, 23, 1–10. https://doi.org/10.1029/2008GB003361

Bartowitz, K. J., Higuera, P. E., Shuman, B. N., McLauchlan, K. K., & Hudiburg, T. W. (2019). Post-Fire Carbon Dynamics in Subalpine Forests of the Rocky Mountains. Fire, 2(4), 58. https://www.mdpi.com/2571-6255/2/4/58

Bates, D., Mächler, M., Bolker, B., & Walker, S. (2014). Fitting linear mixed-effects models using lme4. arXiv preprint arXiv:1406.5823.

Bennett, A. C., McDowell, N. G., Allen, C. D., & Anderson-Teixeira, K. J. (2015). Larger trees suffer most during drought in forests world-wide. Nature Plants, 1(10), 15139.

Berner, L. T., Law, B. E., Meddens, A. J. H., & Hicke, J. A. (2017). Tree mortality from fires, bark beetles, and timber harvest during a hot and dry decade in the western United States (2003–2012). Environmental Research Letters, 12(6), 065005. http://stacks.iop.org/1748-9326/12/i=6/a=065005

Brooks, J. R., Meinzer, F. C., Coulombe, R., & Gregg, J. (2002). Hydraulic redistribution of soil water during summer drought in two con-trasting Pacific Northwest coniferous forests. Tree Physiology, 22(15–16), 1107–1117. https://doi.org/10.1093/treephys/22.15-16.1107

Brown, R. T., Agee, J. K., & Franklin, J. F. (2004). Forest restoration and fire: principles in the context of place. Conservation Biology, 18(4), 903–912.

Buotte, P. C., Law, B. E., Ripple, W. J., & Berner, L. T. (2020). Carbon sequestration and biodiversity co-benefits of preserving forests in the western United States. Ecological Applications, 30(2), e02039. https://doi.org/10.1002/eap.2039

Buotte, P. C., Levis, S., Law, B. E., Hudiburg, T. W., Rupp, D. E., & Kent, J. J. (2019). Near-future forest vulnerability to drought and fire varies across the western United States. Global Change Biology, 25(1), 290–303.

Campbell, J., Donato, D., Azuma, D., & Law, B. (2007). Pyrogenic carbon emission from a large wildfire in Oregon, United States. Journal of Geophysical Research: Biogeosciences, 112(G4), G04014. https://doi.org/10.1029/2007JG000451

Campbell, J. L., & Ager, A. A. (2013). Forest wildfire, fuel reduction treatments, and landscape carbon stocks: A sensitivity analysis. Journal of Environmental Management, 121, 124–132.Campbell, J. L., Donato, D. C., & Fontaine, J. B. (2016). Effects of post-fire logging on fuel dynamics in a mixed-conifer forest, Oregon, USA: a 10-year assessment. International Journal of Wildland Fire, 25(6), 646–656. https://doi.org/10.1071/wf15119

Campbell, J. L., Fontaine, J. B., & Donato, D. C. (2016). Carbon emissions from decomposition of fire-killed trees following a large wildfire in Oregon, United States. Journal of Geophysical Research: Biogeosciences, 121, 718–730. https://doi.org/10.1002/2015JG003165

Campbell, J. L., Harmon, M. E., & Mitchell, S. R. (2012). Can fuel-reduction treatments really increase forest carbon storage in the western US by reducing future fire emissions?. Frontiers in Ecology and the Environment, 10, 83–90. https://doi.org/10.1890/110057

Chapin, F., Woodwell, G., Randerson, J., Rastetter, E., Lovett, G., Baldocchi, D., et al. (2006). Reconciling carbon-cycle concepts, terminol-ogy, and methods. Ecosystems, 9, 1041–1050. http://dx.doi.org/10.1007/s10021-005-0105-7

Chojnacky, D., Amacher, M., & Gavazzi, M. (2009). Separating duff and litter for improved mass and carbon estimates. Southern Journal of Applied Forestry, 33(1), 29–34.

Ciais, P., Reichstein, M., Viovy, N., Granier, A., Ogee, J., Allard, V., et al. (2005). Europe-wide reduction in primary productivity caused by the heat and drought in 2003. Nature, 437(7058), 529–533. http://www.nature.com/nature/journal/v437/n7058/suppinfo/nature03972_S1.html

D'Amato, A. W., Bradford, J. B., Fraver, S., & Palik, B. J. (2013). Effects of thinning on drought vulnerability and climate response in north temperate forest ecosystems. Ecological Applications, 23(8), 1735–1742.

DellaSala, D. A., Anthony, R. G., Bond, M. L., Fernandez, E. S., Frissell, C. A., Hanson, C. T., & Spivak, R. (2013). Alternative views of a restoration framework for federal forests in the Pacific Northwest. Journal of Forestry, 111(6), 420–429.

Dore, S., Kolb, T. E., Montes-Helu, M., Eckert, S., Sullivan, B., Hungate, B. A., et al. (2010). Carbon and water fluxes from ponderosa pine forests disturbed by wildfire and thinning. Ecological Applications, 20(3), 663–683.

Dore, S., Montes-Helu, M., Hart, S. C., Hungate, B. A., Koch, G. W., Moon, J. B., et al. (2012). Recovery of ponderosa pine ecosystem carbon and water fluxes from thinning and stand-replacing fire. Global Change Biology, 18(10), 3171–3185.

Drake, J. E., Davis, S. C., Raetz, L., & Delucia, E. H. (2011). Mechanisms of age-related changes in forest production: the influence of phys-iological and successional changes. Global Change Biology, 17(4), 1522–1535.

Dymond, C. C. (2012). Forest carbon in North America: annual storage and emissions from British Columbia's harvest, 1965–2065. Carbon Balance and Management, 7, 8. https://doi.org/10.1186/1750-0680-7-8

Ewers, B. E., Oren, R., Phillips, N., Strömgren, M., & Linder, S. (2001). Mean canopy stomatal conductance responses to water and nutrient availabilities in Picea abies and Pinus taeda. Tree Physiology, 21(12–13), 841–850.

Farquhar, G. D., Ehleringer, J. R., & Hubick, K. T. (1989). Carbon isotope discrimination and photosynthesis. Annual Review of Plant Biology, 40(1), 503–537.

Fokkema, M., Smits, N., Zeileis, A., Hothorn, T., & Kelderman, H. (2018). Detecting treatment-subgroup interactions in clustered data with generalized linear mixed-effects model trees. Behavior Research Methods, 50(5), 2016–2034. https://doi.org/10.3758/s13428-017-0971-x

Franklin, J. F., Johnson, K. N., & Johnson, D. L. (2018). Ecological forest management. Waveland Press.

Goetz, S. J., Bond-Lamberty, B., Law, B. E., Hicke, J. A., Huang, C., Houghton, R. A., et al. (2012). Observations and assessment of forest carbon dynamics following disturbance in North America. Journal of Geophysical Research, 117. https://doi.org/10.1029/2011jg001733

Gomez-Casanovas, N., Anderson-Teixeira, K., Zeri, M., Bernacchi, C. J., & DeLucia, E. H. (2013). Gap filling strategies and error in estimat-ing annual soil respiration. Global Change Biology, 19(6), 1941–1952.

Granier, A., Biron, P., Bréda, N., Pontailler, J. Y., & Saugier, B. (1996). Transpiration of trees and forest stands: short and long-term moni-toring using sapflow methods. Global Change Biology, 2(3), 265–274.

Harmon, M. E., Harmon, J. M., Ferrell, W. K., & Brooks, D. (1996). Modeling carbon stores in Oregon and Washington forest products: 1900–1992. Climatic Change, 33(4), 521–550.

Harris, L. B., Scholl, A. E., Young, A. B., Estes, B. L., & Taylor, A. H. (2019). Spatial and temporal dynamics of 20th century carbon storage and emissions after wildfire in an old-growth forest landscape. Forest Ecology and Management, 449, 117461.

Hartman, M. D., Baron, J. S., & Ojima, D. S. (2007). Application of a coupled ecosystem-chemical equilibrium model, DayCent-Chem, to stream and soil chemistry in a Rocky Mountain watershed. Ecological Modelling, 200(3), 493–510.

Hegewisch, K. C., & Abatzoglou, J. T. (2020). Historical climate tracker' web tool. NW Climate Toolbox. Retrieved from: https://climate-toolbox.org/

Hicke, J. A., Allen, C. D., Desai, A. R., Dietze, M. C., Hall, R. J., Hogg, E. H., et al. (2012). Effects of biotic disturbances on forest carbon cycling in the United States and Canada. Global Change Biology, 18(1), 7–34. https://doi.org/10.1111/j.1365-2486.2011.02543.x

Hudiburg, T. W., Higuera, P. E., & Hicke, J. A. (2017). Fire-regime variability impacts forest carbon dynamics for centuries to millennia. Biogeosciences, 14(17), 3873–3882. https://doi.org/10.5194/bg-14-3873-2017

Hudiburg, T. W., Law, B. E., Moomaw, W. R., Harmon, M. E., & Stenzel, J. E. (2019). Meeting regional GHG reduction targets requires accounting for all forest sector emissions. Environmental Research Letters, 14(9), 095005.

Hudiburg, T. W., Law, B. E., Wirth, C., & Luyssaert, S. (2011). Regional carbon dioxide implications of forest bioenergy production. Nature Climate Change, 1(8), 419–423. https://doi.org/10.1038/nclimate1264

Hurteau, M., & North, M. (2009). Fuel treatment effects on tree-based forest carbon storage and emissions under modeled wildfire scenar-ios. Frontiers in Ecology and the Environment, 7(8), 409–414.

Hurteau, M. D., Liang, S., Martin, K. L., North, M. P., Koch, G. W., & Hungate, B. A. (2016). Restoring forest structure and process stabilizes forest carbon in wildfire-prone southwestern ponderosa pine forests. Ecological Applications, 26(2), 382–391.

IPCC. (2018). Summary for Policymakers. Global warming of 1.5°C. Geneva, Switzerland:IPCC.

Irvine, J., Law, B., Kurpius, M., Anthoni, P., Moore, D., & Schwarz, P. (2004). Age-related changes in ecosystem structure and function and effects on water and carbon exchange in ponderosa pine. Tree Physiology, 24(7), 753–763.

James, J. N., Kates, N., Kuhn, C. D., Littlefield, C. E., Miller, C. W., Bakker, J. D., et□al. (2018). The effects of forest restoration on ecosystem carbon in western North America: A systematic review. Forest Ecology and Management, 429, 625–641.

Katul, G., Lai, C.-T., Schäfer, K., Vidakovic, B., Albertson, J., Ellsworth, D., & Oren, R. (2001). Multiscale analysis of vegetation surface fluxes: from seconds to years. Advances in Water Resources, 24(9–10), 1119–1132.

Katul, G. G., & Albertson, J. D. (1999). Modeling CO2 sources, sinks, and fluxes within a forest canopy. Journal of Geophysical Research, 104(D6), 6081–6091.Körner, C. (2003). Carbon limitation in trees. Journal of Ecology, 91(1), 4–17.

Körner, C., Asshoff, R., Bignucolo, O., Hättenschwiler, S., Keel, S. G., Peláez-Riedl, S., et□al. (2005). Carbon flux and growth in mature deciduous forest trees exposed to elevated CO2. Science, 309(5739), 1360–1362.

Krogh, S. A., Broxton, P. D., Manley, P. N., & Harpold, A. A. (2020). Using process based snow modeling and lidar to predict the effects of forest thinning on the Northern Sierra Nevada Snowpack. Frontiers in Forests and Global Change, 3, 21.

Law, B. E., Arkebauer, T., Campbell, J. L., Chen, J., Sun, O., Schwartz, M., et al. (2008). Terrestrial carbon observations: Protocols for vegeta-tion sampling and data submission. Rome: FAO.

Law, B. E., Hudiburg, T. W., Berner, L. T., Kent, J. J., Buotte, P. C., & Harmon, M. E. (2018). Land use strategies to mitigate climate change in carbon dense temperate forests. Proceedings of the National Academy of Sciences, 115(14), 201720064.

Law, B. E., Hudiburg, T. W., & Luyssaert, S. (2013). Thinning effects on forest productivity: consequences of preserving old forests and mitigating impacts of fire and drought. Plant Ecology & Diversity, 6(1), 73–85. https://doi.org/10.1080/17550874.2012.679013

Li, Z., Kurz, W. A., Apps, M. J., & Beukema, S. J. (2003). Belowground biomass dynamics in the Carbon Budget Model of the Canadian Forest Sector: recent improvements and implications for the estimation of NPP and NEP. Canadian Journal of Forest Research, 33(1), 126–136.

Liang, S., Hurteau, M. D., & Westerling, A. L. (2018). Large-scale restoration increases carbon stability under projected climate and wildfire regimes. Frontiers in Ecology and the Environment, 16, 207–212. https://doi.org/10.1002/fee.1791

McCauley, L. A., Robles, M. D., Woolley, T., Marshall, R. M., Kretchun, A., & Gori, D. F. (2019). Large-scale forest restoration stabilizes carbon under climate change in Southwest United States. Ecological Applications, 29(8), e01979.

McDowell, N., Pockman, W. T., Allen, C. D., Breshears, D. D., Cobb, N., Kolb, T., et al. (2008). Mechanisms of plant survival and mor-tality during drought: why do some plants survive while others succumb to drought?. New Phytologist, 178(4), 719–739. https://doi.org/10.1111/j.1469-8137.2008.02436.x

McDowell, N. G., & Allen, C. D. (2015). Darcy's law predicts widespread forest mortality under climate warming. Nature Climate Change, 5(7), 669–672.

Means, J. E., Hansen, H. A., Koerper, G. J., Alaback, P. B., & Klopsch, M. W. (1996). BIOPAK. The Bulletin of the Ecological Society of Amer-ica, 77(2), 84–85. https://doi.org/10.2307/20168026

Meigs, G., Donato, D., Campbell, J., Martin, J., & Law, B. (2009). Forest fire impacts on carbon uptake, storage, and emission: the role of burn severity in the Eastern Cascades, Oregon. Ecosystems, 12(8), 1246–1267. http://dx.doi.org/10.1007/s10021-009-9285-x

Mitchell, S. R., Harmon, M. E., & O'Connell, K. E. B. (2012). Carbon debt and carbon sequestration parity in forest bioenergy production. GCB Bioenergy. http://dx.doi.org/10.1111/j.1757-1707.2012.01173.x

Muller, B., Pantin, F., Génard, M., Turc, O., Freixes, S., Piques, M., & Gibon, Y. (2011). Water deficits uncouple growth from photosyn-thesis, increase C content, and modify the relationships between C and growth in sink organs. Journal of Experimental Botany, 62(6), 1715–1729.

Naudts, K., Chen, Y., McGrath, M. J., Ryder, J., Valade, A., Otto, J., & Luyssaert, S. (2016). Europe's forest management did not mitigate climate warming. Science, 351(6273), 597–600.

North, M. P., & Hurteau, M. D. (2011). High-severity wildfire effects on carbon stocks and emissions in fuels treated and untreated forest. Forest Ecology and Management, 261(6), 1115–1120.

NRCS. (2010). Soil survey staff, natural resources conservation service, United States department of agriculture. Available online at http://soildatamart.nrcs.usda.gov

Pangle, R., Kavanagh, K., & Duursma, R. (2015). Decline in canopy gas exchange with increasing tree height, atmospheric evaporative demand, and seasonal drought in co-occurring inland Pacific Northwest conifer species. Canadian Journal of Forest Research, 45(8), 1086–1101.

Parton, W. J., Hartman, M., Ojima, D., & Schimel, D. (1998). DAYCENT and its land surface submodel: Description and testing. Global and Planetary Change, 19(1–4), 35–48. https://doi.org/10.1016/s0921-8181(98)00040-x

Reichstein, M., Rey, A., Freibauer, A., Tenhunen, J., Valentini, R., Banza, J., et□al. (2003). Modeling temporal and large-scale spatial variabil-ity of soil respiration from soil water availability, temperature and vegetation productivity indices. Global Biogeochemical Cycles, 17(4), 1104. https://doi.org/10.1029/2003GB002035,4

Ryan, M., Binkley, D., & Fownes, J. H. (1997). Age-related decline in forest productivity: Pattern and process. In M. Begon & A. H. Fitter (Eds.), Advances in Ecological Research (pp. 213–262). Elsevier. https://www.sciencedirect.com/science/article/pii/S006525040860001X

Ryan, M. G., Phillips, N., & Bond, B. J. (2006). The hydraulic limitation hypothesis revisited. Plant, Cell and Environment, 29(3), 367–381. https://doi.org/10.1111/j.1365-3040.2005.01478.x

Sala, A., Woodruff, D. R., & Meinzer, F. C. (2012). Carbon dynamics in trees: Feast or famine?. Tree Physiology, 32(6), 764–775.Schaefer, G. L., & Paetzold, R. F. (2001).

SNOTEL (SNOwpack TELemetry) and SCAN (soil climate analysis network). In Paper presented at the Proceeding of International Workshop on Automated Wea. Stations for Applications in Agr. and Water Resource Management.

Schlesinger, W. H., Dietze, M. C., Jackson, R. B., Phillips, R. P., Rhoades, C. C., Rustad, L. E., & Vose, J. M. (2016). Forest biogeochemistry in response to drought. Global Change Biology, 22(7), 2318–2328.

Schwalm, C. R., Williams, C. A., Schaefer, K., Anderson, R., Arain, M. A., Baker, I., et□al. (2010). A model-data intercomparison of CO2 exchange across North America: Results from the North American Carbon Program site synthesis. Journal of Geophysical Research, 115(G3), G00H05.

Schwalm, C. R., Williams, C. A., Schaefer, K., Baldocchi, D., Black, T. A., Goldstein, A. H., et□al. (2012). Reduction in carbon uptake during turn of the century drought in western North America. Nature Geoscience, 5(8), 551–556.

Sevanto, S., Mcdowell, N. G., Dickman, L. T., Pangle, R., & Pockman, W. T. (2014). How do trees die? A test of the hydraulic failure and carbon starvation hypotheses. Plant Cell and Environment, 37(1), 153–161.Skog, K. E. (2008). Sequestration of carbon in harvested wood products for the United States. Forest Products Journal, Vol. 58(6), 56–72.

Smith, J. E., Heath, L., Skog, K. E., & Birdsey, R. (2006). Methods for calculating forest ecosystem and harvested carbon with standard esti-mates for forest types of the United States gen. Tech. Rep. NE-343. PA: Newtown Square.

Sohn, J. A., Saha, S., & Bauhus, J. (2016). Potential of forest thinning to mitigate drought stress: A meta-analysis. Forest Ecology and Man-agement, 380, 261–273.

State of California Executive Department. (2018). Sacremento, CA. Retrieved from https://www.gov.ca.gov/wp-content/up-loads/2018/05/5.10.18-Forest-EO.pdf

Stenzel, J. E., Bartowitz, K. J., Hartman, M. D., Lutz, J. A., Kolden, C. A., Smith, A. M. S., et al. (2019). Fixing a snag in carbon emissions estimates from wildfires. Global Change Biology, 25. https://doi.org/10.1111/gcb.14716

Tague, C. L., Moritz, M., & Hanan, E. (2019). The changing water cycle: The eco-hydrologic impacts of forest density reduction in Mediter-ranean (seasonally dry) regions. WIREs Water, 6(4), e1350. https://doi.org/10.1002/wat2.1350

Tepley, A. J., Hood, S. M., Keyes, C. R., & Sala, A. (2020). Forest restoration treatments in a ponderosa pine forest enhance physiological activity and growth under climatic stress. Ecological Applications, 30, e02188. https://doi.org/10.1002/EAP.2188

Thornton, P., Thornton, M. N. W., Wei, Y., & Cook, R. B. (2012). Daymet: Daily surface weather on a 1 km grid for North America, 1980 - 2008. WOS:000319907800016

Tsamir, M., Gottlieb, S., Preisler, Y., Rotenberg, E., Tatarinov, F., Yakir, D., et al. (2019). Stand density effects on carbon and water fluxes in a semi-arid forest, from leaf to stand-scale. Forest Ecology and Management, 453, 117573.

U.S. Executive Office of the President. (2018). Promoting Active Management of America's Forests, Rangelands, and Other Federal Lands To Improve Conditions and Reduce Wildfire Risk (Executive Order 13855). Washington, DC.

van der Molen, M. K., Dolman, A. J., Ciais, P., Eglin, T., Gobron, N., Law, B. E., et al. (2011). Drought and ecosystem carbon cycling. Agri-cultural and Forest Meteorology, 151(7), 765–773. https://doi.org/10.1016/j.agrformet.2011.01.018

Van Wagner, C. E. (1968). The line-intersect method in furest fuel sampling. Forest Science, 14, 20–26.

Varhola, A., Coops, N. C., Weiler, M., & Moore, R. D. (2010). Forest canopy effects on snow accumulation and ablation: An integrative review of empirical results. Journal of Hydrology, 392(3–4), 219–233.

Wanek, W., Heintel, S., & Richter, A. (2001). Preparation of starch and other carbon fractions from higher plant leaves for stable carbon isotope analysis. Rapid Communications in Mass Spectrometry, 15(14), 1136–1140.

Ward, E. J., Domec, J.-C., King, J., Sun, G., McNulty, S., & Noormets, A. (2017). TRACC: An open source software for processing sap flux data from thermal dissipation probes. Trees, 31(5), 1737–1742.

Williams, N. G., & Powers, M. D. (2019). Carbon storage implications of active management in mature Pseudotsuga menziesii forests of western Oregon. Forest Ecology and Management, 432, 761–775.

Zeileis, A., Hothorn, T., & Hornik, K. (2008). Model-based recursive partitioning. Journal of Computational & Graphical Statistics, 17(2), 492–514.

Zhao, M., & Running, S. W. (2010). Drought-induced reduction in global terrestrial net primary production from 2000 through 2009. Science, 329(5994), 940–943.

Zhou, D., Zhao, S., Liu, S., & Oeding, J. (2013). A meta-analysis on the impacts of partial cutting on forest structure and carbon storage. Biogeosciences, 10(6), 3691–3703

Supplemental Information:

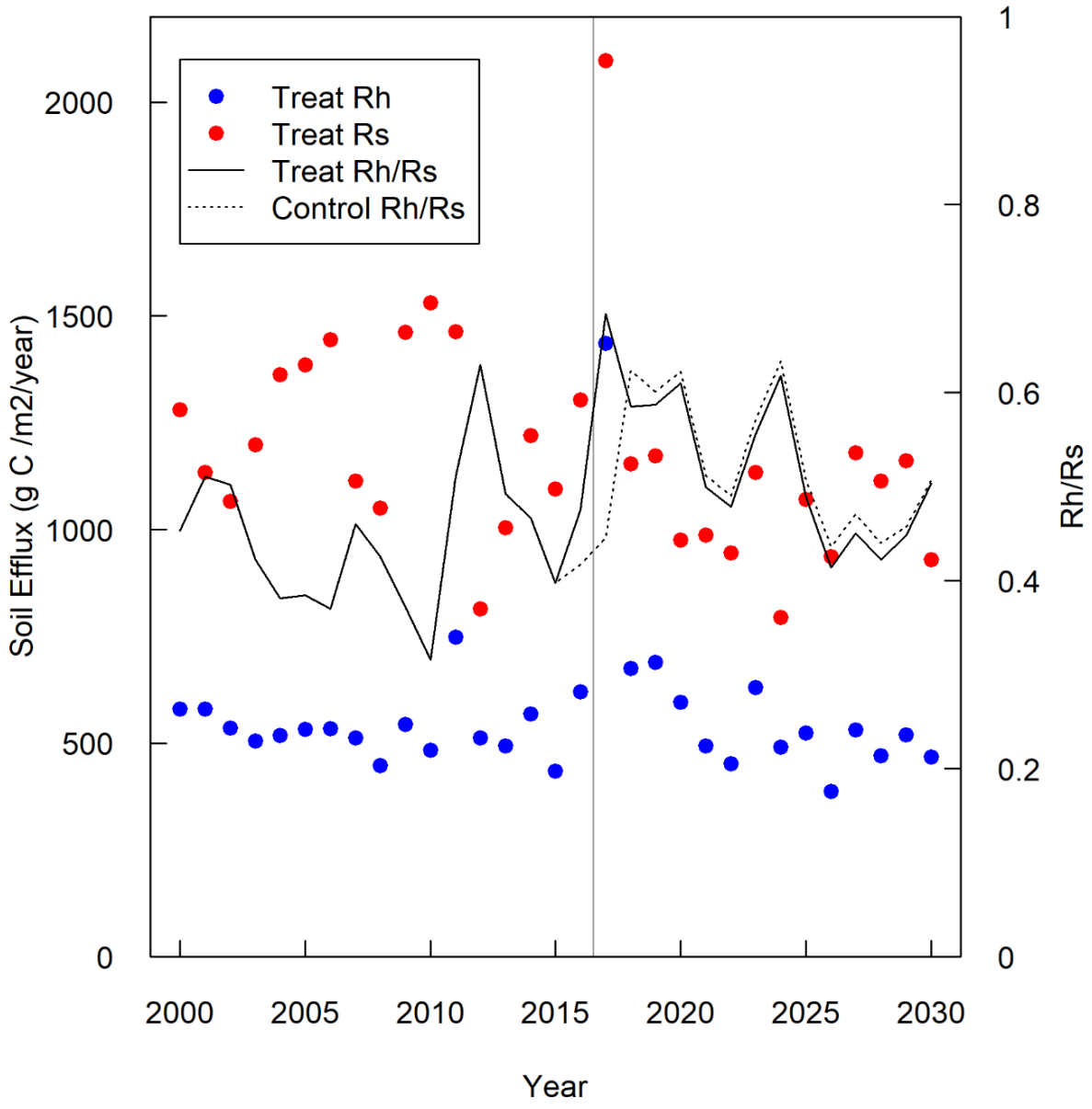

Figure S1. Daycent simulation total soil respiration (R_s) and heterotrophic soil respiration (R_h). Vertical gray line indicates treatment year.

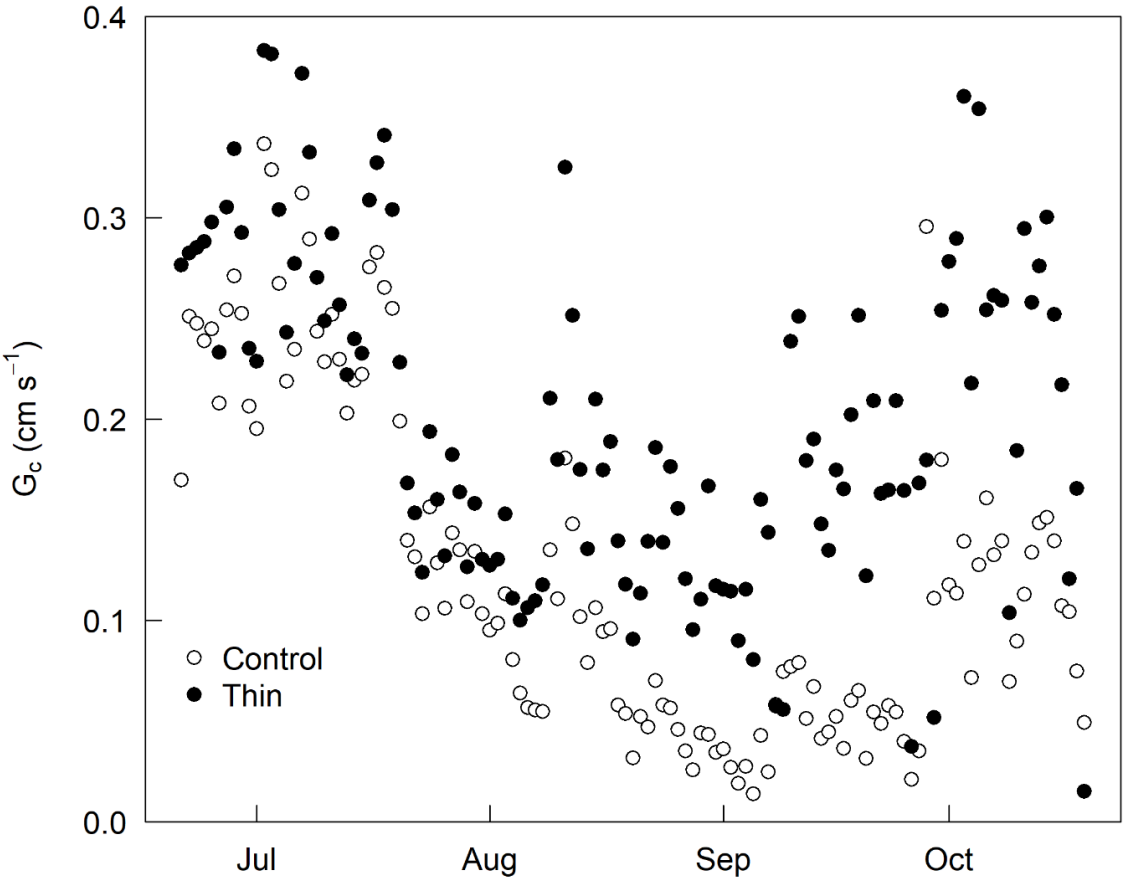

Figure S2. Treatment average canopy conductance, 2019.

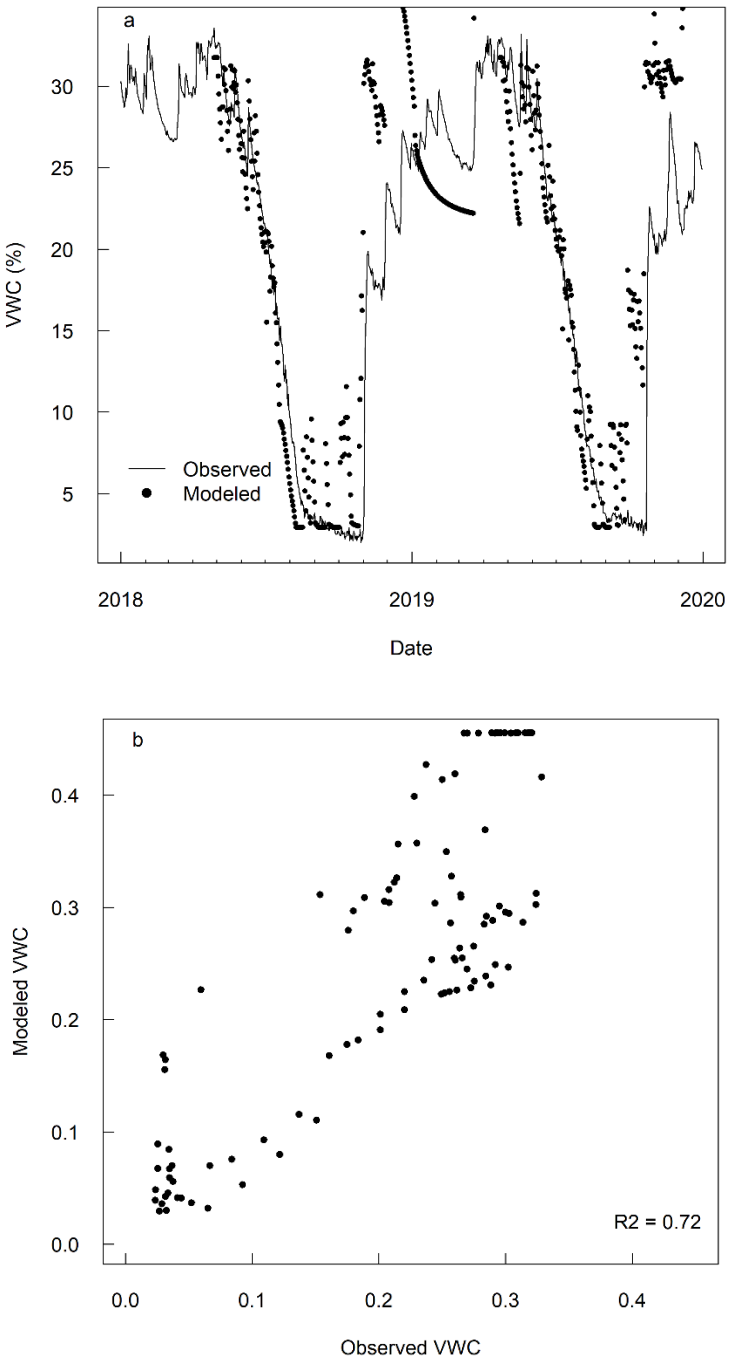

Figure S3. Model- Observation Comparison, soil VWC. Observed 20 cm Moscow Mountain Snotel VWC and Daycent simulated VWC (10-30cm), 2018-2019. **a.** Time series. **b.** Mean Weekly observed vs modeled VWC.

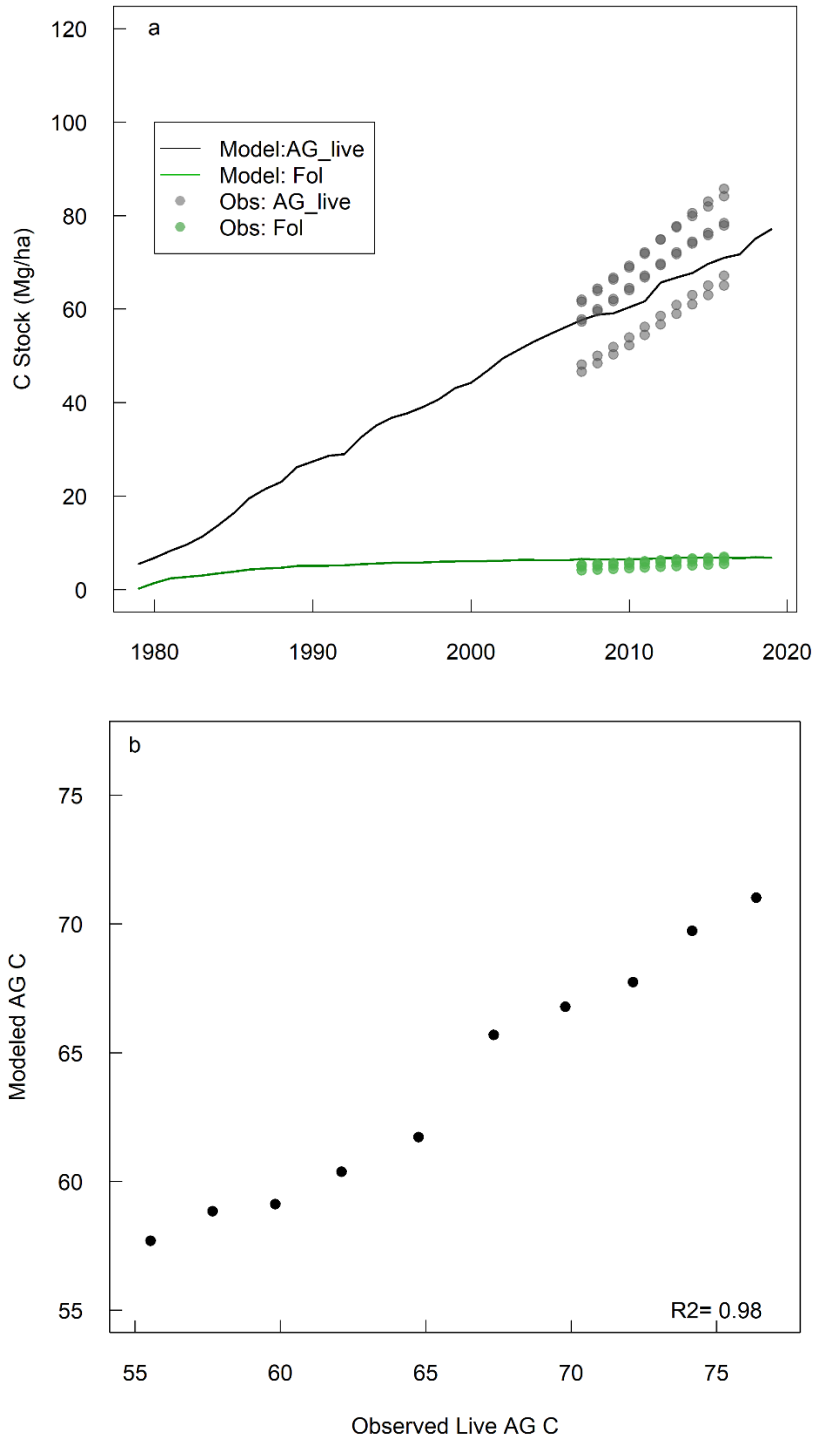

Figure S4. Model- Observation Comparison, live aboveground carbon stocks. **a.** Time series aboveground live C and foliage C, all plots. **b.** Modeled aboveground live c vs observed plot means.

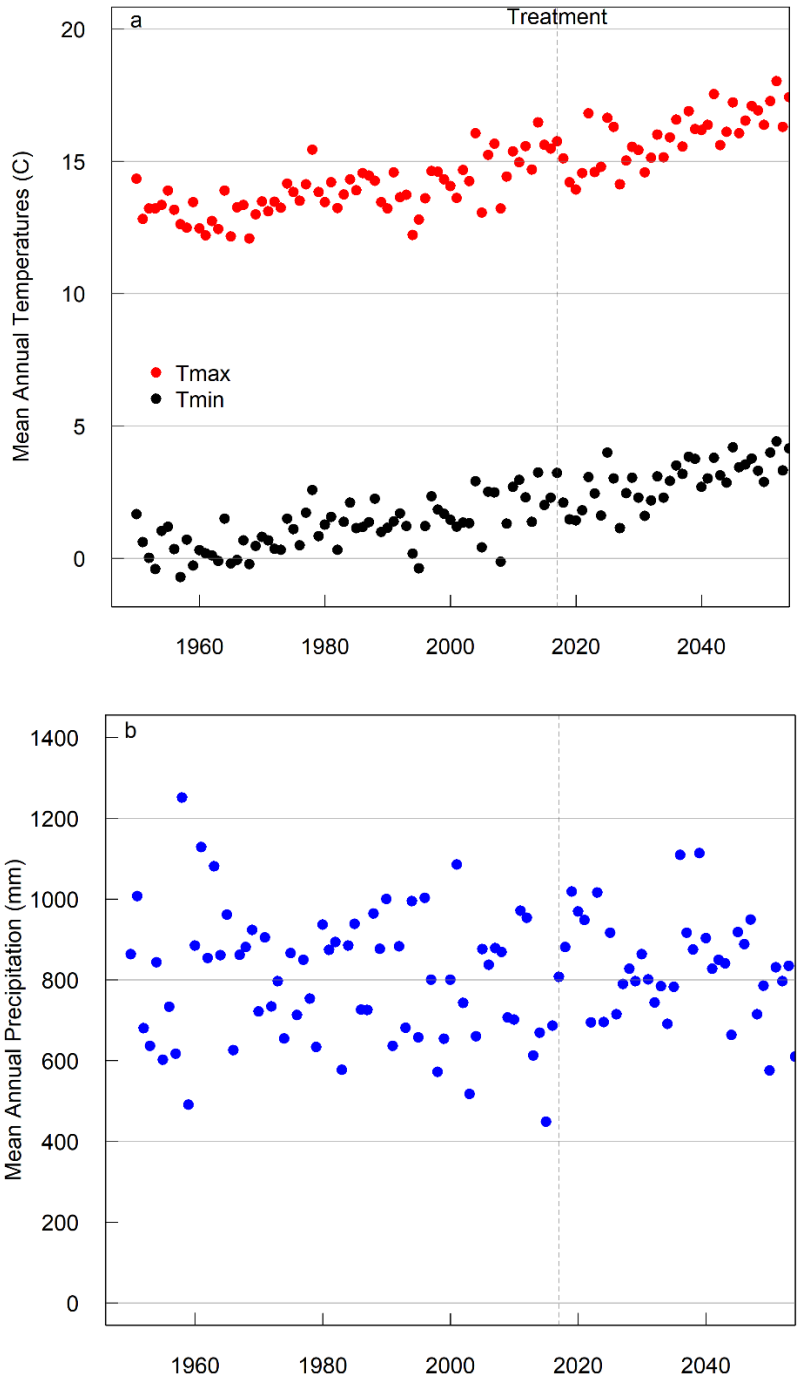

Figure S5. Model historical and future climate inputs, 1950-2050. **a.** Mean annual T_{max} and T_{min}. **b.** Mean annual precipitation.

Table S1. Daycent simulated stand mass mortality events in unthinned stands and carbon emissions relative to undisturbed control stands. *Note*: Mortality scenarios are intended to explore potential mortality as a result of unreduced density and were simulated without direct emissions (e.g. combustion) or site removals. Simulations allow for hypothetical 1:1 area comparisons with control and treatment stands but do not reflect likely landscape proportions that will follow each trajectory.

Event Year	Mortality (% Mass)	Live C (Mg/ha)	C emissions relative to control (Mg/ha)	Δ Live C from control (Mg/ha)
2021	50	149	11	-43
2021	75	130	15	-63
2021	90	119	16	-73
2026	50	141	14	-52
2026	75	118	18	-75
2026	90	106	19	-87
2036	50	125	18	-67
2036	75	94	26	-99
2036	90	76	29	-117
2046	50	100	19	-93
2046	75	56	27	-137
2046	90	29	33	-163

Table S2. Fixed Effect model parameters for pre-treatment Stand NPP_{wood} (g m^{-2} yr^{-1}), 2008-2019.

Stand NPP				
	β	**CI 5%**	**CI 95%**	**t**
(Intercept)	311.589	298.271484	324.816019	**40.004**
Year	-11.949	-14.024542	-9.882595	**-9.648**

Bold t values indicate a significant parameter based on 95% CI criterion.

Methods note: Variables examined but excluded by model selection (see Methods) included monthly and seasonal metrics of total and average precipitation, temperature, VPD, 30cm VWC. Timings included the initiation and cessation of rapid soil moisture depletion and recharge (calculated as weekly second differences). Period lengths included potential growing seasons defined by early (temperature) and late (soil moisture) thresholds within the growing season. Stand structure-relevant metrics examined included year (age), basal area, volume.

Table S3. LME tree model, 2018 survey soil respiration (R_s, g m^{-2} hr^{-1})

	Node 2				Node 4				Node 6				Node 7			
	Soil Temp <= 10.8 C				Soil Temp >10.8 C; VWC 30cm <=0.15				Soil Temp >10.8 C; VWC 30cm >0.15; VWC 30cm <=0.30				Soil Temp >10.8 C; VWC 30cm >0.30			
	Control	**Thinned**			**Control**	**Thinned**			**Control**	**Thinned**			**Control**	**Thinned**		
Sapflow (mean)	0.425	0.321			0.637	0.495			0.653	0.636			0.726	0.843		
	β	**CI 5%**	**CI 95%**	**t**	**β**	**CI 5%**	**CI 95%**	**t**	**β**	**CI 5%**	**CI 95%**	**t**	**β**	**CI 5%**	**CI 95%**	**t**
Intercept	-2.663353	-3.110	-2.218	**-9.478**	7.9237691	5.944	9.896	**6.375**	1.5674103	0.797	2.339	**3.231**	0.4774531	-0.489	1.439	0.787
Treatment	-0.182052	-0.370	0.005	-1.541	-0.177198	-0.353	-0.002	**-1.605**	-0.1220292	-0.319	0.075	-0.983	-0.092044	-0.382	0.198	-0.503
DOY	0.0035389	0.002	0.005	**5.072**	-0.020855	-0.027	-0.015	**-5.75**	-0.0020593	-0.007	0.003	-0.647	-0.001846	-0.010	0.006	-0.383
TempSoil	0.1629786	0.127	0.199	**7.241**	-0.060146	-0.103	-0.017	**-2.205**	0.0761471	0.018	0.135	**2.071**	0.1800165	0.045	0.317	**2.107**

Bold t values indicate a significant parameter based on 95% CI criterion.

Table S4. LME Tree Model, 2018-2019 weekly total sap flow (cm). Fixed effects are listed in table. Plot and tree are random effects. *Bold t values indicate a significant parameter based on 95% CI criterion.*

2018 Model

	Node 4				Node 5				Node 6			
	< 28 Weeks											
	VPD <= 0.77								VPD > 0.77			
	VWC 30cm <= 0.31				VWC 30cm > 0.31							
	Control	Thinned			Control	Thinned			Control	Thinned		
Sapflow (m	631.19	880.01			583.91	644.89			788.62	941.81		
	β	CI 5%	CI 95%	t	β	CI 5%	CI 95%	t	β	CI 5%	CI 95%	t
Intercept	-564.2	-2794.9	1666.4	-0.4	3458.0	1045.8	5871.6	**2.3**	-265.9	-3017.0	2486.0	-0.2
Treatment	248.4	167.4	329.3	**5.0**	110.0	29.2	190.6	**2.2**	139.1	56.1	222.0	**2.7**
Time	15.3	-22.9	53.6	0.6	-16.0	-26.8	-5.1	**-2.4**	36.1	18.3	53.9	**3.3**
VWC.30	764.5	-4404.6	5934.1	0.2	-7119.0	-9237.2	-5002.7	**-5.4**	1258.0	-2279.4	4793.2	0.6
VPD	938.0	629.7	1246.2	**4.9**	618.9	392.2	845.3	**4.4**	323.4	39.5	607.1	**1.8**

	Node 10				Node 11				Node 12				Node 14				Node 15			
	>28 Weeks																			
	<= 39 Weeks								VWC 30cm >0.15				> 39 Weeks							
	VWC 30cm <= 0.15												<= 43 Weeks				>43 Weeks			
	<= 32 Weeks				> 32 Weeks															
	Control	Thinned			Control	Thinned			Control	Thinned			Control	Thinned			Control	Thinned		
	465.27	1052.08			140.98	541.09			840.37	1212.69			45.19	262.97			17.79	75.56		
	β	CI 5%	CI 95%	t	β	CI 5%	CI 95%	t	β	CI 5%	CI 95%	t	β	CI 5%	CI 95%	t	β	CI 5%	CI 95%	t
	203800.0	55149.3	352351.6	**2.2**	-5614.0	-11264.5	33.8	-1.6	7343.0	-23251.2	37923.4	0.4	4437.0	855.3	8020.5	**2.0**	1341.0	-1583.3	4264.7	0.7
	585.2	493.2	677.0	**10.2**	391.9	316.6	467.1	**8.4**	357.4	268.0	446.6	**6.4**	224.2	144.5	304.0	**4.5**	2.6	-93.7	98.7	0.0
	-4599.0	-7977.4	-1216.8	**-2.2**	57.3	-6.4	121.0	1.4	-70.8	-794.0	652.9	-0.2	-21.4	-48.3	5.5	-1.3	-15.8	-76.3	44.6	-0.4
	-437000.0	-757075.7	-116584.8	**-2.2**	34770.0	10288.2	59269.1	**2.3**	-13500.0	-57277.2	30282.3	-0.5	-27060.0	-53054.6	-1090.8	-1.7	-150.4	-7218.6	6918.3	0.0
	2136.0	405.7	3863.3	**2.0**	43.2	-33.7	120.1	0.9	-755.8	-1773.9	261.8	-1.2	95.7	-19.4	210.8	1.3	231.0	-477.6	939.9	0.5

2019 Model

	<= 28 Weeks								>28 Weeks							
	<= 22 Weeks				> 22 Weeks				<= 36 Weeks				> 36 Weeks			
	Node 3				Node 4				Node 6				Node 7			
	Control	Thinned			Control	Thinned			Control	Thinned			Control	Thinned		
Sapflow (m	547.1	660.3			813.3	1004.9			383.9	730.8			131.7	298.3		
	β	CI 5%	CI 95%	t	β	CI 5%	CI 95%	t	β	CI 5%	CI 95%	t	β	CI 5%	CI 95%	t
Intercept	-2351.3	-3494.3	-1207.7	**-3.3**	-12135.7	-21122.1	-3152.3	**-2.2**	8281.9	5353.8	11213.3	**4.6**	-135.2	-5328.2	5060.2	0.0
Treatment	133.8	9.1	258.5	**1.7**	192.8	67.5	318.0	**2.5**	279.1	154.1	404.0	**3.6**	124.3	-9.5	258.1	1.5
Time	18.3	7.6	28.9	**2.8**	426.4	157.1	695.8	**2.6**	-148.3	-201.2	-95.4	**-4.5**	-18.5	-62.6	25.6	-0.7
VWC.30	17407.3	11390.8	23420.7	**4.7**	17334.6	10319.0	24351.8	**4.0**	11609.7	3898.3	19320.4	**2.4**	25724.4	-30319.8	81730.1	0.7
VWC.5	-13869.6	-18175.5	-9561.6	**-5.2**	-4825.4	-9294.6	-355.2	**-1.8**	-24324.9	-38278.2	-10386.8	**-2.8**	284.8	-2532.3	3104.4	**0.2**
VPD	472.3	340.7	603.9	**5.8**	670.4	501.6	839.1	**6.4**	-258.7	-375.3	-142.2	**-3.6**	649.6	-173.1	1473.0	1.3

Table S5. LCA carbon pool parameters

Pool	mass proportion	half life (years)
long-lived	0.6	75
waste	0.12	1
paper	0.28	2.5

Table S6. Model – Observation (mean) comparison, carbon stocks and NPP. Before thinning period (2016) and after thinning (2017-2018).

	Before Thinning		After Thinning	
Variable	Modeled	Observed	Modeled	Observed
Aboveground Live C (Mg C ha^{-1})	71	76	30	32
NPP (g C m^{-2} yr^{-1})	795	785	611	550
Total C (Mg C ha^{-1})	275	222	217	183
Soil C (Mg C ha^{-1})	49	53		

Table S7. Daycent site and tree characteristics and parameter values.

Site	
Latitude, Longitude	46.84°, -116.74° (UIEF)
Soil Texture	Silty loam (Sand: 32%; Silt: 53%; Clay: 15%)
Bulk Density	0.9 (g cm^{-3})
Mean Annual Precipitation	883 mm (1988-2017 mean)
Mean annual temperature	8.3° C (1988-2017 mean)
Mean N deposition	3.0 kg N ha^{-1} yr^{-1}
Site History	Clear cut mixed conifer stand in 1978. Followed by ponderosa pine planting. Study thinning treatment in Winter-Spring 2017.

Tree	
leaf C:N minimum	43
leaf C:N maximum	49
PRDX(2) (potential production coefficient)	0.7
Leaf retention time	3 yr
lai : biomass	0.0045
live wood background death rate	0.03% $month^{-1}$
course root : stem allocation	0.28

Chapter 3: Forest thinning and drought dynamics with CLM-FATES: Towards more mechanistic modeling of interacting disturbance and dynamic vegetation at a landscape scale.

Abstract:

Global change in the 21st century will impact the function of much of the Earth's forest cover, altering the state of large pools of sequestered biomass carbon and feeding back to further disturbance. However, the representation of dynamic forest disturbance history has only recently started to be incorporated into Earth System Models (ESMs) that are used for climate projections. Here, we examine the post-disturbance representation of carbon cycling and stand structure following selective forest harvest in CLM – FATES, the dynamic vegetation model of the CESM ESM. Simulations are parameterized and evaluated against field observations from a 2017 pre-commercial thinning operation in a 40 year old ponderosa pine plantation in the Northern Rocky Mountain ecoregion. Experiments examine the impacts of variable harvest intensity, historical and future climate, and variation of key model parameters. We find that selective harvest results in carbon deficits relative to control throughout all 70 year simulations and ranges from 10-62 Mg ha^{-1} by 2050 for historical stands despite recovery of Net Primary Production (NPP) after lower intensity harvests. In future scenarios, leaf area, NPP and live biomass accumulation decline after 2075 because of increasing growing season temperatures and vapor pressure deficits (VPD). We find that post-disturbance stand structure reorganization and recovery trajectories are dependent on several FATES parameters that control horizontal gap creation and canopy plasticity in response to changing light competition. Our results both indicate that FATES post-disturbance dynamics improve upon previous model representations of field-observed processes and highlight several FATES dynamics should be refined prior to regional application. Study findings will serve as bases for scaling to regional-scale, multi-disturbance simulations that explore the

carbon balance tradeoffs of natural disturbance and human management interventions through the 21st century.

Introduction:

Forests dynamics impact human societies in many ways, including the modulation of the earth's energy, water, and carbon balances; provisioning of resources; and direct disturbance impacts on communities (Bonan, 2008; Bowman et al., 2017). Because global disruptions are impacting essential forest processes, societies are seeking to design and implement ecosystem management strategies that mitigate disturbances such fire, drought, and insect outbreaks (Forest Climate Action Team, 2018; State of California Executive Department, 2018). The large scale and complexity of these impacts means that modeling studies are necessary due to the infeasibility of landscape level experimental treatments and measurements (Campbell & Ager, 2013). Models need to have sufficient mechanistic complexity to represent disturbance drivers and impacts in the context of novel conditions (e.g. climate). This includes model representation of land-atmosphere physical and chemical coupling, vegetation structure and function, and realistic management prescriptions among human land use and land cover change impacts (Foley et al., 1996; P. J. Lawrence et al., 2012).

Forest thinning—the harvest and disposal of a fraction of aboveground stand trees – is increasingly being implemented as a strategy to mitigate disturbance (Franklin & Johnson, 2013; James et al., 2018a; U.S. Executive Office of the President, 2018). Particularly, wildfire mitigation is in focus due to sharp increases in burned area in recent decades (Abatzoglou & Williams, 2016) as well as the direct and visible impacts of fire to communities (Bowman et al., 2017). Thinning may directly impact fire dynamics via increasing the height to the forest canopy (reducing torching) and decreasing canopy density (reducing crown fire spread);

indirectly, thinning may promote the growth of larger, more fire resistant individuals by decreasing competition (Agee & Skinner, 2005). Additionally, fire behavior can be modified via coordinated or separate surface fuels reduction treatments, including prescribed burning, (Kolden, 2019). Besides being fuels reduction strategies, thinning treatments are inherently forest mass-mortality events, altering the structure and function of live biomass remaining on site and creating fluxes of killed biomass to onsite ecosystem pools, to offsite waste and product pools, and to the atmosphere via decomposition and combustion (Hudiburg, Law, Moomaw, Harmon, & Stenzel, 2019; B E Law & Waring, 2015). As a result, terrestrial carbon stocks and atmospheric greenhouse gas (GHG) concentrations encounter treatment legacies from seconds to centuries (Beverly E. Law et al., 2018). Disturbance-prone forests of the western United States currently store large amounts of carbon (Pan et al., 2011). However, the potential carbon balance impacts of regional thinning treatments are substantially complicated by the spatial complexity of the region, changes to climate, and ongoing impacts from human land use and land cover change, precluding "one size fits all" analyses (Brown, Agee, & Franklin, 2004; DellaSala et al., 2013).

The immediacy of annual forest fire seasons in the western U.S. as well as narrowing routes to meeting greenhouse gas targets (Intergovernmental Panel on Climate Change, 2018) have led to many previous modeling studies on the subject of regional forest thinning and resulting net emissions (James et al., 2018b). However, a relative dearth of long term experimental measurements (Stenzel, Berardi, Walsh, & Hudiburg, 2021; Williams & Powers, 2019) in combination with insufficient vegetation modeling capabilities mean that there are clearly identifiable shortcomings to previous approaches. Until recently, earth systems models—models that couple atmosphere, ocean, land, and ice – have represented the physical

and chemical mechanisms that enable feedbacks with forest processes (D. M. Lawrence et al., 2019), but have not represented dynamic land cell vegetation, including patches and cohorts with variable disturbance history (Fisher et al., 2015). In the context of thinning, for instance, this means that a prescribed harvest may shrink the mass pool sizes of a vegetation 'column' and create tree pools that are on average 'smaller' (i.e. just reduce LAI and therefore GPP), but not generate representations of new gaps in function associated with disturbed patches. In contrast, ecosystem demography models enable prognostic vegetation composition within model cells but may not include the biophysics and biogeochemistry necessary for mechanistic representation of the evolving earth system. For instance, the biogeochemical portion of the forest landscape model, LANDIS II, does not explicitly model radiative transfer in vegetation or photosynthesis, instead calculating Net Primary Production (NPP, i.e. photosynthesis minus autotrophic respiration, approximately biomass growth) as an empirical function of a maximum production modified by temperature, soil moisture, and potential monthly incident radiation at the land surface. Combining mechanistic earth systems modeling and dynamic cell vegetation composition in dynamic global vegetation models (DGVM), as well as robust, prognostic disturbance is necessary for modeling forest management scenarios under novel future forcings.

This study examines site scale thinning treatment impacts within the Community Land Model 5 (CLM; D. M. Lawrence et al., 2019), Functionally Assembled Terrestrial Ecosystem Simulator (FATES), a model configuration which addresses many of the previous deficiencies discussed above. FATES with CLM is a dynamic global vegetation model (DGVM), representing the competition of cohorts of tree species and ages within disturbance-history patches at each model cell (Fisher et al., 2015; Moorcroft, Hurtt, & Pacala, 2001). An updated

selective logging (i.e. thinning) module has recently been implemented (Huang et al., 2020) that allows for variably designed thinning treatments across space and time. Critically, FATES is integrated with the biogeophysics and biogeochemistry of its land model (CLM), which in turn can run with a coupled earth system model (CESM). To date, the selective logging module of CLM FATES has been utilized in a single, published tropical study (Huang et al., 2020) and there are no published results in the Western United States. This study includes initial simulations of FATES at a Northern Rocky Mountain experimental forest site, representative of species demographics, climate, and topography found in the region. It assesses the impacts of model representation of ecosystem heterogeneity and treatment prescriptions as well as variation of sensitive ecosystem and plant functional type (PFT) parameters. We ask the following questions: 1) How does selective thinning in FATES impact ecosystem component carbon fluxes at an ecosystem scale, including mortality? 2) When and if is carbon parity of thinned vs unthinned stands achieved across a range of thinning designs (structure and timing)? 3) What varying impacts do historical and future climate forcings have on the relative carbon balance of control/treatment stands, including mortality from carbon starvation?

Materials and Methods:

Model description

Experiments were performed with the Community Land Model 5 (CLM5; Lawrence et al., 2019) with the Functionally Assembled Terrestrial Ecosystem Simulator (FATES) module (Fisher et al., 2015). FATES introduces dynamic vegetation to CLM and its broader earth

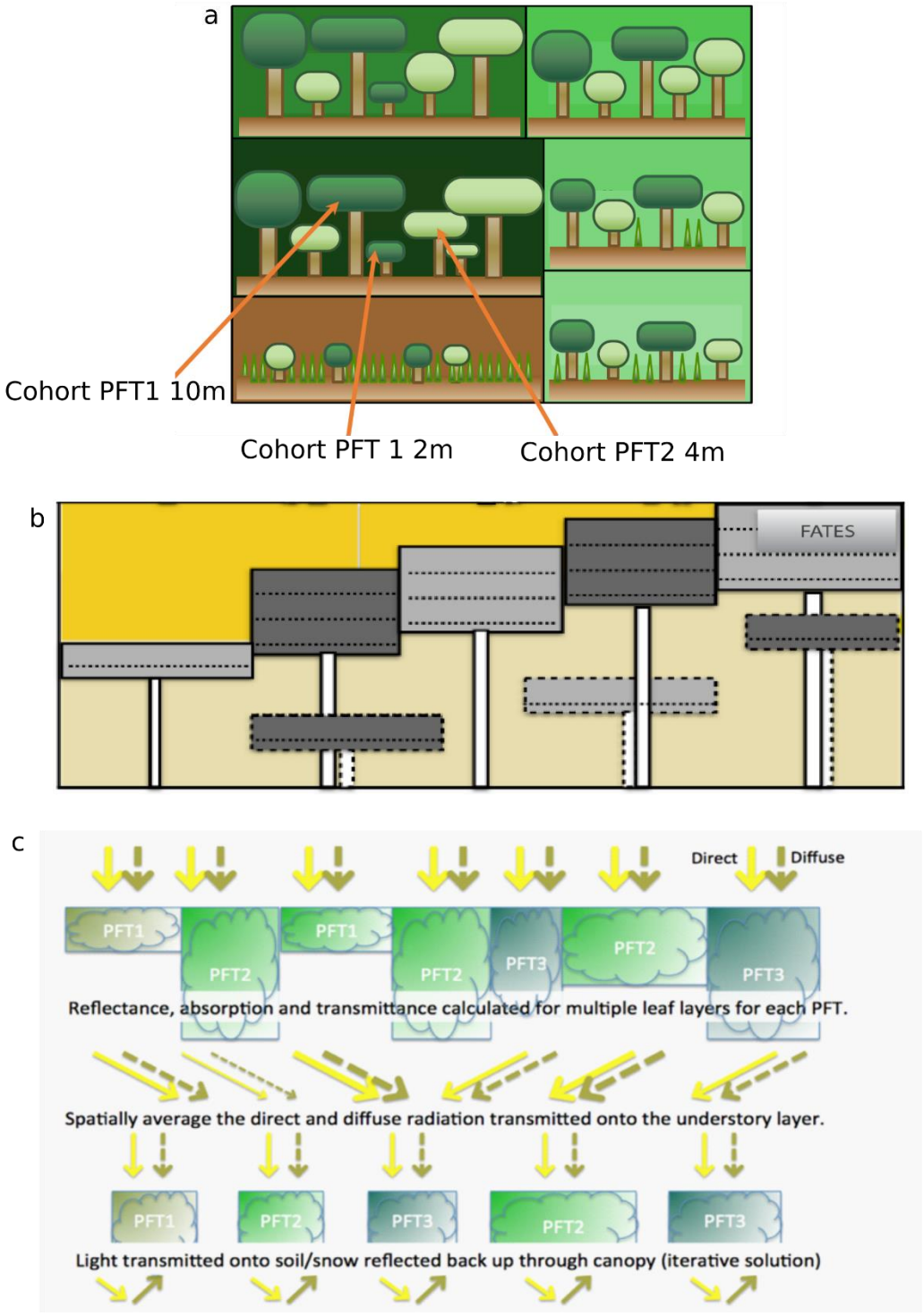

Figure 1. FATES conceptual diagrams. **a**. Vegetated column sub-column patch and cohort organization. Cohorts include multiple PFTs and height classes. **b**. Patch cohort canopy structure. Common PFTs share the same shading. Understory is denoted by "average trees" in the light yellow sub-canopy environment. Cohort leaf layers are separated by dotted lines. **c**. Light transmission across canopy layers. Source: Figure panels modified from NCAR FATES tutorial, 2019, C. Koven.

system model (ESM)—the Community Earth System Model (CESM). FATES represents dynamic disturbance patches within each land grid-cell, tracking shifting cohorts of trees characterized by size (and related canopy position), plant functional type (PFT), and disturbance patch (Fig 1). Presently, cohorts compete explicitly for light within the canopy and implicitly for soil water.

Biogeochemical models (e.g. Daycent; Parton, Hartman, Ojima, & Schimel, 1998; Stenzel et al., 2019) have traditionally represented ecosystem disturbances as combinations of reduced primary production and reduced biomass-pool size. Prescribed or prognostic disturbances such as harvest or fire cause transfers of live biomass to dead pools, resulting in reduced production due to effectively smaller pool-averaged tree organs (e.g. leaf biomass and LAI), not gaps in function. Less-acute sources of mortality, including stresses from limited access to light, water, or nutrients, are often simply implied by static, user-determined background mortality rate parameters. FATES can represent ecosystem disturbance by generating new grid-cell patches (i.e. gaps) as well as variable impacts to existing-patch cohorts. Prognostic mortality results from fire (Spitfire; Pfeiffer, Spessa, & Kaplan, 2013; Thonicke et al., 2010), carbon starvation, freezing, hydraulic failure, and tree size. Mortality rates related to cohort age, harvest, and background mortality are prescribed by the user. Prognostic mortality is variably mechanistic—explicit structural and storage carbon budgets drive carbon starvation, while hydraulic failure is empirically related to soil water potentials due to the lack of explicit plant hydraulic pathway in FATES. Fire impacts, including mortality, are driven by the SPITFIRE model; crown damage is a function of scorch height and fire intensity, while cambial damage and direct tree mortality are a function of bark thickness, fire intensity, and fire duration.

FATES simulates canopy direct and diffuse radiation transfer and the effects of variable canopy and leaf layer light absorption on cohort competition (Fig 1c). Cohort growth and resulting light access is determined by both PFT physiological characteristics (e.g. Specific leaf area, allometry, V_{cmax},, and maintenance respiration) and stand characteristics, including canopy stratification and variable crown geometry (and self-shading) as the canopy closes. Competition for moisture is implicit; during each time step, cohorts independently extract water based on root distribution and demand modified by moisture availability. Resulting soil column fluxes of water to the atmosphere are the weighted averages of cohort use, meaning that future time step soil water pools are impacted by coexisting cohorts. Nitrogen cycling and related competition is not yet represented, though PFT nitrogen stoichiometry parameters impact photosynthesis.

Parameterization and input data

CLM input variables include sub-daily surface air temperature, humidity, precipitation, incoming solar radiation, and windspeed. 3-hourly, 4 km inputs of observation-based (1950-2016) and MIROC5 historical and RCP 8.5 (1950-2099) climate were extracted for the simulation point domain (46.8125, 243.2292) from existing data products (Buotte et al. 2019). In Buotte 2019, 3-hr historical climate was interpolated from 4 km METDATA/GRIDMET datasets (Abatzoglou, 2013). GCM climate was generated from 3 hourly outputs of MIROC5 historical and RCP 8.5 experiments (CMIP5; (Taylor, Stouffer, & Meehl, 2012) and spatially downscaled, 4km daily MACA datasets (Abatzoglou & Brown, 2012). CLM requires input surface datasets, including grid cell cover types (e.g. natural vegetation, lake, glacier, crop, urban), slope, soil depth, soil texture, soil color, and elevation. These sets were also obtained from P. Buotte (Buotte et al., 2019), with soil depth-to-bedrock

Table 1. Key parameters, historical stand model control (control 1). Variable definitions directly from parameter file. All definitions are available at: https://github.com/NGEET/fates/blob/master/parameter_files/fates_params_default.cdl

Name	Definition	Unit	Value
seed_dbh_repro_threshold	the diameter (if any) where the plant will start extra clonal allocation to the seed pool	cm	30
mort_bmort	background mortality rate	1/yr	0.0025
allom_l2fr	Allocation parameter: fine root C per leaf C	gC/gC	1.35
allom_agb_frac	Fraction of woody biomass that is above ground	fraction	0.8
comp_excln	IF POSITIVE: weighting factor (exponent on dbh) for canopy layer exclusion and promotion, IF NEGATIVE: switch to use deterministic height sorting	none	-1
fates_recruit_initd	initial seedling density for a cold-start near-bare-ground simulation	stems/m2	0.1
canopy_closure_thresh	tree canopy coverage at which crown area allometry changes from savanna to forest value	unitless	0.8
mort_scalar_cstarvation	maximum mortality rate from carbon starvation	1/yr	0.15
alloc_storage_cushion	maximum size of storage C pool, relative to maximum size of leaf C pool	fraction	1.5
mort_disturb_frac	fraction of canopy mortality that results in disturbance (i.e. transfer of area from new to old patch). NOTE: For non-logging mortality	fraction	0
phen_evergreen	Binary flag for evergreen leaf habit	unitless	1
allom_d2ca_coefficient_max	max (forest) dbh to area multiplier factor where: area = n*d2ca_coeff*dbh^beta	m2 cm^(-1/beta)	0.3
allom_d2ca_coefficient_min	min (forest) dbh to area multiplier factor where: area = n*d2ca_coeff*dbh^beta	m2 cm^(-1/beta)	0.2
leaf_long	Leaf longevity (ie turnover timescale)	yr	3
leaf_slatop	Specific Leaf Area (SLA) at top of canopy, projected area basis	m2/gC	0.0079
prt_nitr_stoich_p1, leaf	nitrogen stoichiometry	gN/gC	0.022
leaf_vcmax25top	maximum carboxylation rate of Rub. at 25C, canopy top	umol CO2/m^2/s	43
leaf_stomatal_model	switch for choosing between Ball-Berry (1) stomatal conductance model and Medlyn (2) model	unitless	1
leaf_stomatal_intercept	Minimum unstressed stomatal conductance for Ball-Berry model and Medlyn model	umol H2O/m^2/s	10000
leaf_stomatal_slope	stomatal slope parameter, as per Ball-Berry	uniteless	8
smpsc	Soil water potential at full stomatal closure	mm	-255000
smpso	Soil water potential at full stomatal opening	mm	-66000

modified for the region from the upland soil depths of a global 1km soil thickness dataset (Pelletier et al., 2016). CLM dynamic cover and land use is implemented via timeseries surface datasets, including the year and location of harvests that are then implemented by FATES selective logging. The FATES module then requires >200 input parameters that impact sub-gridcell disturbance dynamics and PFT physiology.

Initial PFT parameters for a single ponderosa pine PFT were obtained from an in-progress parameter evaluation project of P. Buotte. Site parameterization for this study was then performed based on field site measurement from 2015-2020 (see site information below), including leaf nitrogen concentrations, leaf retention time, and tree allometry (Table 1). Initial parameter evaluation experiments (not detailed in results) were performed using the METDATA-based climate product (observation based). Parameter evaluation for 1979-2020 was performed based on study site measurements of carbon stocks and fluxes, including component Net Primary Production (NPP), and stand structure, including the size (diameter at breast height, DBH) and number of canopy and understory trees (Table 2, results section).

Experiments

Two categories of modeling experiments were performed: 1) Model sensitivity assessments and 2) assessments of treatment and natural disturbance impacts. Initial parameter evaluation experiments (~200) resulted in the default historical control stand parameter set reported in the results section. All experiments consisted of 72 year run lengths beginning from a model cold state (soil carbon stocks were not spun-up with pre-plantation vegetation). Historical stand experiments began with the germination of the ponderosa pine plantation in 1979 and proceeded through 2050. In future stand experiments, seed

germination occurred in 2028 and simulations ended in 2099. Thinning experiments prescribed single selective harvest events of varying intensity. Currently, CLM FATES selective harvest can be driven with a combination of spatiotemporal CLM land use timeseries harvest areal fraction inputs and FATES selective harvest parameters (e.g. size classes, direct, collateral, infrastructure mortality; see: https://github.com/NGEET/fates/wiki/Running-FATES-with-the-selective-logging-module-activated). Land use timeseries area inputs were set to 99% for the study site during the month of harvest. FATES selective harvest direct fraction was set to the selective harvest intensity fraction (e.g. 45%), with understory collateral mortality fraction set to 100%. Both the historical and future experiments reported in the results section were forced with the downscaled, temporally interpolated MIROC5 historical-RCP 8.5 product for dataset consistency across the boundary of past and future climate.

Results section experiments examined variable selective thinning intensity (low, moderate, and high), historical and future stands harvested at moderate intensity, and crown-area spread parameter variations, which evaluation experiments highlighted as critical to model outcomes. In all reported experiments, we examined carbon stock and flux impacts (net and component), stand structure (size, density, and canopy class), and mortality of control and experimental stands. We modeled low (25%), moderate (actual; 45%), and high (60%) levels of live biomass removal, comparing time-until-carbon parity (Mitchell, Harmon, & O'Connell, 2012) with control (i.e. unthinned) stands. We included 2 climate scenarios---historic and mid-21st century—to examine the impact of varying climate stress on thinning efficacy. Crown-area parameter experiments included 3 levels of variation for the maximum diameter-to-crown area parameter ('d2ca_max'), which determines the maximum crown area

by DBH when model canopy spread equals 1 (maximum) and determines canopy shape plasticity across canopy competitive conditions. Site canopy spread ranges from 0 to 1 and incrementally increases or decreases when site overstory canopy area is respectively higher or lower than a threshold closure threshold. Here, the closure threshold was set to 0.8 in all simulations. Spread value determines the degree to which tree canopies are horizontally vs vertically spread, with lower values resulting from site crown area competition and increasing canopy self-shading (Fisher et al., 2015). Study default 'd2ca_max' values were 150% of 'd2ca_min' (labeled '+50%' in this study). Variation levels included setting the maximum parameter equal to the minimum ('+0%) and to twice the minimum ('+100%).

Life cycle assessment:

The storage and emission of live biomass harvested and removed during thinning operations was modeled with a life cycle assessment in which biomass was separated into slash, waste, paper, and long-lived product pools. Off-site pool initial fractions from exported biomass and half-lives of product pools are the same as chapter 2 (see also: Dymond, 2012; Skog, 2008; Smith, Heath, Skog, & Birdsey, 2006; J. E. Stenzel, Berardi, Walsh, & Hudiburg, 2021). Only stem carbon is currently able to be exported with the FATES selective harvest module; To implicitly simulate on-site combustion of stem portions as slash within the year of harvest, 15% of harvested stem carbon was immediately subtracted from the model-exported fraction.

Field observations:

Stand stocks, fluxes, and structure were evaluated in part with field observations from a 40 year old (2020) ponderosa pine (*Pinus ponderosa*) plantation in the University of Idaho Experimental Forest (UIEF) in the northern rocky mountain ecoregion of Idaho (46.8125, 243.2292). Detailed descriptions of this evaluation site, study design, and measurements are provided in Chapter 2 of this dissertation (J. E. Stenzel et al., 2021). The site has been characterized by survey and automated carbon flux and stock measurements spanning the years immediately before and after a commercial thinning in winter 2016-2017.

Carbon cycle terminology:

Carbon cycle terms commonly referenced in this chapter include Gross Primary Production (GPP), Net Primary Production (NPP), Net Ecosystem Production (NEP) (Chapin et al., 2006) and carbon parity (Mitchell et al., 2012). GPP is the photosynthetic gain of ecosystem carbon resulting from fixation of atmospheric carbon by primary producers. NPP represents plant and ecosystem carbon gain minus autotrophic (plant) maintenance and growth respiration. NPP has traditionally be treated as plant carbon available for tissue growth, though can also be allocated to storage or export pools that may not ultimately result in plant growth (Körner et al., 2005). NEP is GPP minus ecosystem respiration (autotrophic and heterotrophic), or NPP minus heterotrophic respiration, and does not include horizontal transfers of carbon (e.g. harvest, water transport) or non-respiratory vertical transfers to the atmosphere (e.g. combustion). Finally, the terms of carbon debt and parity (Mitchell et al., 2012) between stands in this study refer to the relative masses of combined on and off site

terrestrial, stand-derived carbon. Carbon debts indicate relative decreases in terrestrial carbon storage and increases in atmospheric carbon.

Results:

Under simulated historical climate, control stand (Table 3) stocks and fluxes approximated observed 2019 field site carbon stock and flux variables (Table 2, Figure 2, version: control 1). During parameterization, stand dynamics were sensitive to allometric variables (number of allometric parameters = 27). Diameter-based allometrics determined recruit (i.e. sapling) starting mass upon germination, allocation to high turnover versus long-lived ecosystem biomass, ratio of diameter growth to structural biomass, and leaf and crown area. The parameters controlling minimum and maximum diameter-to-crown area determined canopy closure, canopy demotion (i.e. suppression), and overstory density in conjunction with tree count. The leaf-to-fine-root parameter strongly impacted NPP allocation to stem biomass and live biomass accumulation due to the highest turnover of any live biomass pool (50% yr^{-1}) and no positive feedback to production due to the plant hydraulics submodule being inactive in study experiments.

In the observed ponderosa pine field site, the 40 year old stand displayed negligible tree regeneration, cone production, or tree understory (Chapter 2, Stenzel, Berardi, Walsh, & Hudiburg, 2021). Prior to thinning, most available crown area was occupied. Measurements indicated that co -dominant tree growth, size, and physiology (e.g. sap flow) began to more strongly differentiate in the 2010s. With the assumption that these observations indicated the beginning of canopy layer stratification, historical control simulations were parameterized to begin canopy tree demotion in the 2010s (Table 3). Field observations included no overstory mortality except mild winter windthrow in thinned stands. The control simulation was

Table 2. Target stand variables. 2019 site observation vs model outputs. For model outputs, fluxes are 2016-2020 ranges.

Variable	Unit	Observation	Model
NPP	g/m2/yr	650-850	575-825
NPP_seed	g/m2/yr	0	0
Live C	Mg/ha	102	96
Fine root C	g/m2	400-500	378
Tree density	stem/ha	750-900	879
Mean DBH	cm	23	20-30 (class)
Lai	m2/m2	1.5-2.5	2.27
Timing, max Transpiration	Month period	May-July	June-July
Timing, min growing season transpiration	Month period	Sept+	None: Continual decline Aug+
Crown area	m2/m2	Near 1	1

Table 3. Experiments and results, carbon stocks, fluxes, and stand structure. Carbon stock units are Mg C ha^{-1}. Carbon flux units are g C m^{-2} yr^{2}.

run version	output year	harvest intensity	stand initiation	crown area-max:min	NPP	NPP wood	treeC	tree woodc	soilc	litter cwd	total eco c	offsite c	total c	lai	crown area index	cstarv	nplant can	nplant under
control 1	2020	none	1979	1.5	706	325	96	85	19	21	138	0	138	2.3	1	13	762	117
control 1	2035	none	1979	1.5	828	391	126	114	30	36	195	0	195	2.6	1	68	559	247
control 1	2050	none	1979	1.5	796	360	144	131	41	49	235	0	235	2.7	1	124	452	330
harvest 1	2020	moderate	1979	1.5	491	249	54	48	21	31	108	14.6	122	1.3	0.8	1	473	2
harvest 1	2035	moderate	1979	1.5	658	333	90	82	28	26	147	10.6	157	1.8	0.87	1	478	2
harvest 1	2050	moderate	1979	1.5	750	374	124	114	33	34	193	9.2	202	2.1	1	8	422	93
control 2	2020	none	1979	1	694	327	83	73	16	16	118	0	118	2.1	1	0	855	39
control 2	2035	none	1979	1	820	394	118	106	27	31	178	0	178	2.5	1	50	607	204
control 2	2050	none	1979	1	791	361	138	126	38	46	222	0	222	2.6	1	110	480	297
harvest 2	2020	moderate	1979	1	413	201	47	41	18	23	89	12.2	102	1.2	0.59	0	495	0
harvest 2	2035	moderate	1979	1	609	309	79	71	24	21	126	8.8	135	1.6	0.81	0	476	2
harvest 2	2050	moderate	1979	1	738	369	114	104	29	29	174	7.7	181	2.1	1	1	469	50
control 3	2020	none	1979	2	708	324	98	87	20	22	142	0	142	2.3	1	16	747	129
control 3	2035	none	1979	2	830	391	127	115	31	37	198	0	198	2.6	1	71	551	256
control 3	2050	none	1979	2	797	360	145	132	42	50	237	0	237	2.7	1	127	446	336
harvest 3	2020	moderate	1979	2	494	250	55	49	21	32	111	15	126	1.3	0.8	2	469	2
harvest 3	2035	moderate	1979	2	660	335	91	82	29	27	149	10.9	160	1.8	0.87	2	476	2
harvest 3	2050	moderate	1979	2	750	374	125	115	34	35	195	9.4	204	2.1	1	10	418	94
harvest 4	2020	low	1979	1.5	596	284	73	65	20	26	122	8.3	130	1.7	0.86	1	656	1
harvest 4	2035	low	1979	1.5	797	396	113	102	29	31	176	6	182	2.2	1	8	551	90
harvest 4	2050	low	1979	1.5	773	367	136	125	38	44	219	5.2	224	2.4	1	53	442	194
harvest 5	2020	high	1979	1.5	371	192	40	35	21	33	96	19.4	115	0.9	0.69	1	340	4
harvest 5	2035	high	1979	1.5	548	288	72	65	27	23	123	14	137	1.4	0.8	1	354	4
harvest 5	2050	high	1979	1.5	619	312	102	94	29	27	160	12.1	172	1.7	0.83	2	393	4
control 6	2070	none	2028	1.5	761	362	99	88	20	22	143	0	143	2.3	1	33	737	119
control 6	2085	none	2028	1.5	708	317	116	105	31	38	186	0	186	2.4	1	145	571	154
control 6	2099	none	2028	1.5	654	269	122	112	40	47	210	0	210	2.3	1	244	491	152
harvest 6	2070	moderate	2028	1.5	524	270	57	51	22	28	110	13.7	124	1.3	0.8	9	469	2
harvest 6	2085	moderate	2028	1.5	586	280	88	80	27	24	141	10.3	152	1.7	0.85	10	473	2
harvest 6	2099	moderate	2028	1.5	620	278	110	100	31	30	173	9	182	2	0.97	11	496	2

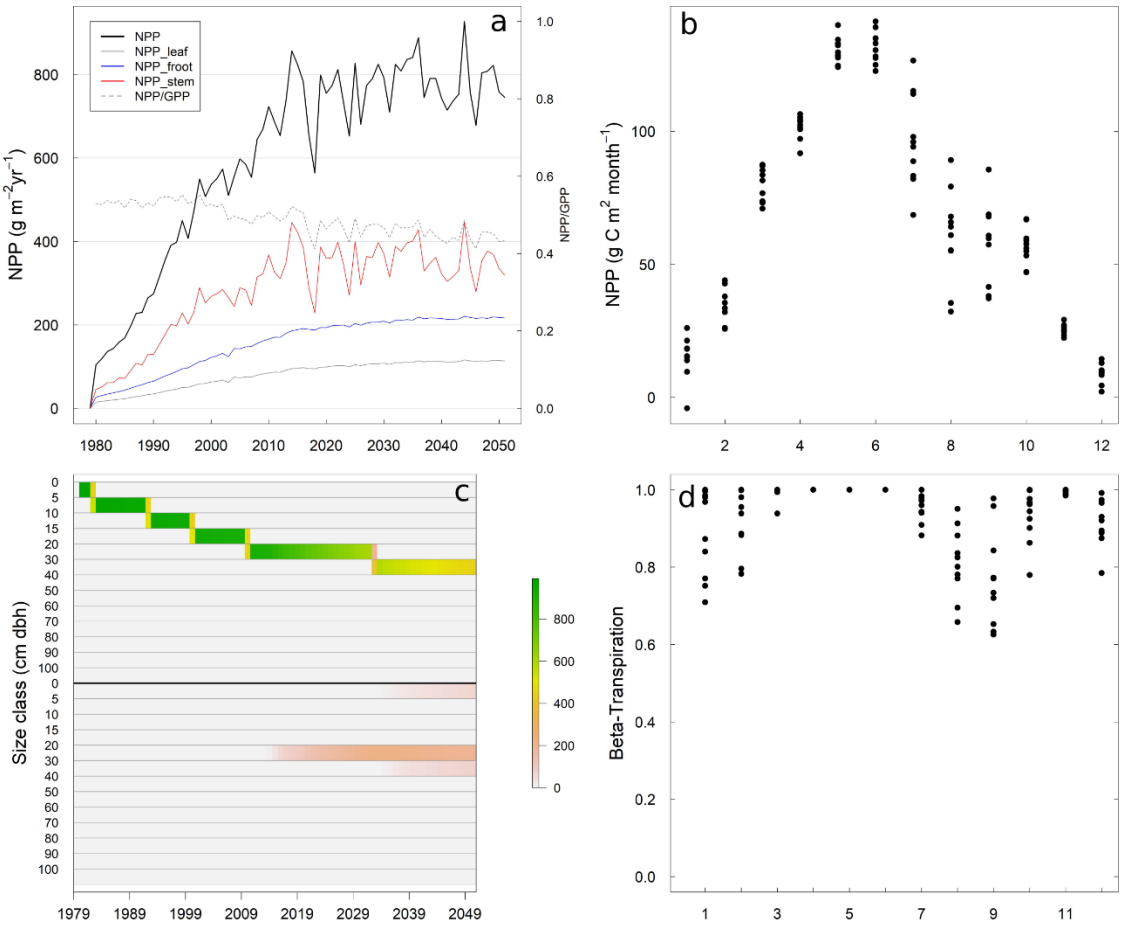

Figure 2. Historical control stand growth dynamics, 1979-2050 (control 1, Table 2). **a**. Tissue component NPP and carbon use efficiency (NPP/GPP). **b**. Monthly NPP, 2019-2029. **c**. Number of stems by size class. Top panel denotes overstory canopy layer, bottom panel denotes understory. **d**. Monthly β-Transpiration (soil moisture stress transpiration reduction factor), 2019-2029

therefore parameterized to prevent overstory carbon starvation morality in the observation period by increasing the carbon storage buffer (Table 3). The minimum necessary increase in carbon storage allowed carbon starvation of understory trees (Table 3), a hypothetical dynamic for the future stand. In 2020, the control run consisted of 20-30 cm DBH trees with a sparse initial understory generated from canopy closure and canopy-tree demotion (Table 3, Fig 2c). As in observations, NPP displayed an approximate plateau after 2010 (Fig 2a), varying between ~650-850 g C m^{-2} yr^{-1}. Modeled stem and course root wood allocation accounted for ~50% of stand NPP and did not decline through 2050. Carbon use efficiency (NPP/GPP) declined from ~0.55 to 0.45 between 1979 and 2050 because of increasing biomass and respiration without a proportional increase in GPP following canopy closure.

Though yearly model NPP was consistent with observations (Table 3), modeled downregulation of growth during the summer drought due to soil moisture stress was relatively mild. Field-observed volumetric water content through 80 cm soil depth displayed multi-month summer minimums of ~5% (Stenzel et al., 2021). Observed control stand stem circumference growth ceased in all years by August and daily sap flow declined by ~65% from the spring peak by August. Canopy conductance was reduced by ~80-90% of the observed peak from August through October. In comparison, modeled monthly NPP from 2019-2029 declined by ~50-60% from peak (June) to minimum (Aug-Oct). β-Transpiration (BTRAN), the model soil moisture stress factor that modifies stomatal conductance, declined on average from 1.0 (Spring) to 0.77 (September) (Figure 2d). BTRAN remained near 1 due to modeled soil matric potentials that did not fall below values necessary for PFT-specific stomatal closure.

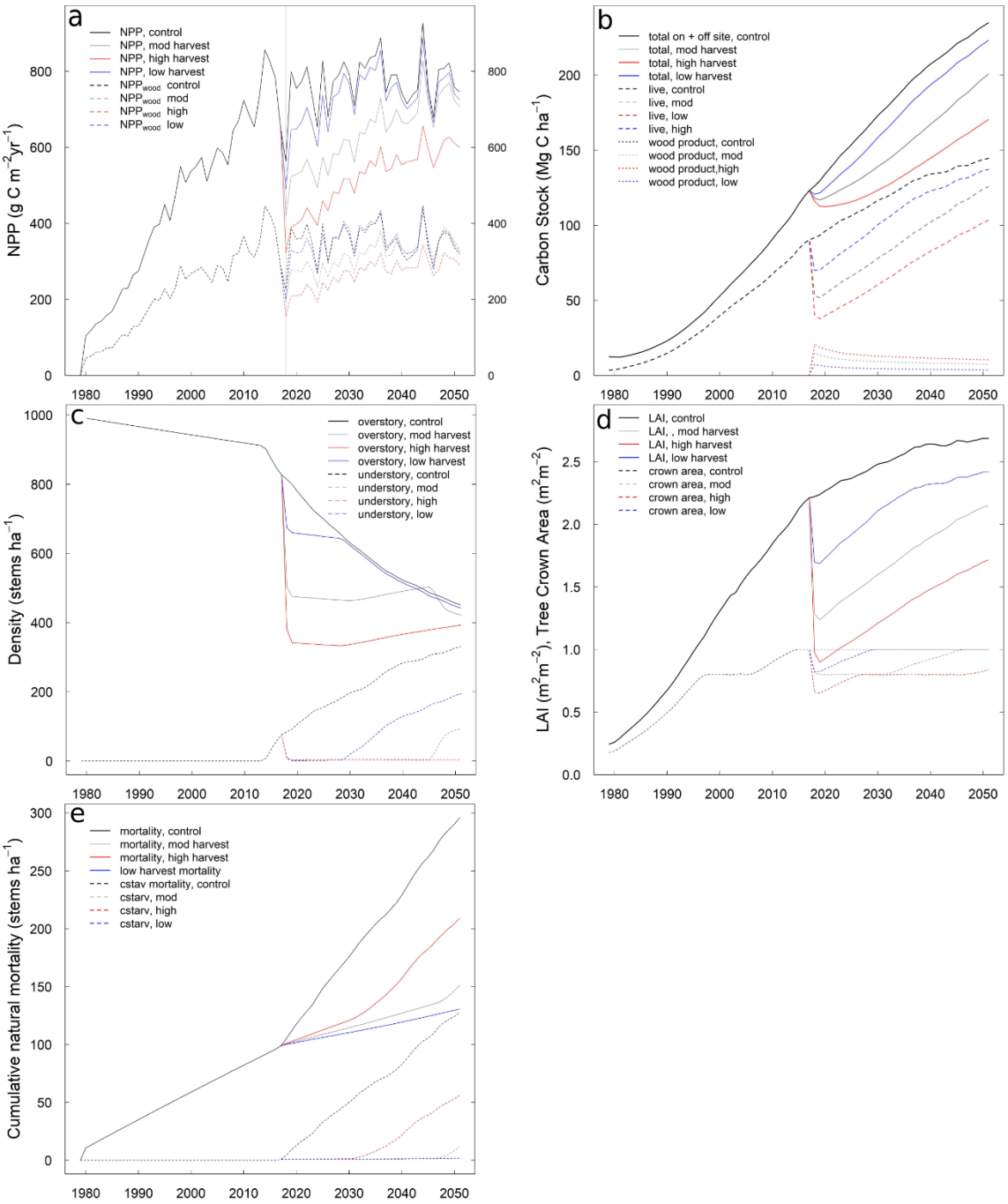

Figure 3. Selective thinning intensity experiments, stand dynamics, 1979-2050. Low harvest = 25%, Moderate harvest = 40%, High harvest = 60%. **a**. NPP and NPP_{wood}. **b**. Carbon stocks: total (on & off site), live biomass, and off site. **c**. Stand density, overstory and understory. **d**. Stand LAI and crown area. **e**. Cumulative natural mortality. Carbon starvation mortality as a component of total natural mortality is displayed additionally.

In selective harvest intensity experiments, stem density and live biomass were reduced by 25%, 40% (as implemented at the field site), and 60% in late-winter 2017. In all experiments, NPP was most reduced immediately after the thinning (Table 3, Fig 3). 2020 NPP was reduced by 16-55% over control from low to high intensity. NPP reductions relative to control were 21-34% in 2035 and 3-22% in 2050. In all experiments and periods, treatment reductions in NPP_{wood} were lower than NPP (Fig 3a). By 2050, NPP_{wood} was 2-4% higher than control in stands that had low and moderate thinning treatments. Lesser declines in structural NPP allocation resulted from increased average tree DBH in treated stands, which resulted from increased crown area per tree, decreased stand-level allocation to leaf and root mass, and increased diameter growth. Simulated 2020 NPP reduction in the harvested stand (30%) is less than reduction estimated from field observations for 2017-2019 (45%) (Stenzel et al., 2021). Field observations are consistent with lesser declines in simulation NPP_{wood} relative to NPP and increased stand-level allocation to wood.

Modeled canopy closure was reached prior to treatment (crown area index ~1; Table 3). Following treatment, a second closure occurred by 2035 and 2050 for low and moderate selective harvests (Fig 3d). Treatment LAI remained lower than control through 2050 at all intensities. As a result of a longer period of canopy closure and increased canopy tree demotion, 2050 control understory tree count was 330 stems ha^{-1} in comparison to 4-194 stems ha^{-1} in treatment plots.

Carbon stock parity (on and off site) was not achieved by any treatment stand by 2050 despite decreased natural mortality and long-lived off-site wood products (Table 3). Relative to control, the 2050 total carbon deficits in low, moderate, and high intensity treatment stands were 10, 42, and 62 Mg C ha^{-1}. In 2050, treatment stand live carbon stocks were 5-29% lower

than the control stand (Fig 3b). Compared to control, live carbon deficits decreased in thinned stands despite lower NPP due to increased structural allocation (i.e. reduced tissue turnover) and reduced mortality from the understory. Carbon starvation mortality increased in control and low harvest stands (Fig 3e) due to a positive relationship between mortality and understory density, overstory crown area and leaf area (i.e. decreased light transmission below the canopy), and duration of canopy closure (Table 3, Fig 3c). Control stand litter, coarse debris, and soil organic carbon pools were larger than all treatment stands due to greater live biomass stocks, background turnover (leaf, root, branch), and higher mortality. By 2050, the difference between control and treatment dead, on-site carbon pools was greater than treatment off-site wood-product pools. Though turnover-based dead biomass was subject to decomposition in the control stand, the earlier average timing and waste components of harvested biomass (left on site, combusted, or short lived) led to lower dead stocks in 2050.

FATES parameters ‘d2ca-min’ and ‘d2ca-max’ (corresponding to the minimum and maximum diameter-to-crown area values) determine realized tree crown area from DBH and site canopy area index (i.e. degree of canopy closure). During model evaluation, model canopy demotion, subsequent carbon starvation, and overstory mortality were sensitive to the values of this plastic canopy area range during either acute or accumulating disturbance. Low ‘d2ca’ ranges enacted the hypothesis that canopy-filling of open area only occurred with significant diameter growth and that crown architecture was static within size classes; non-zero ranges of ‘d2ca’ parameters allowed crowns to fill newly-opened canopy space to the maximum parameter value within several daily-time steps, representing near-perfect architecture plasticity even in the absence of structural growth.

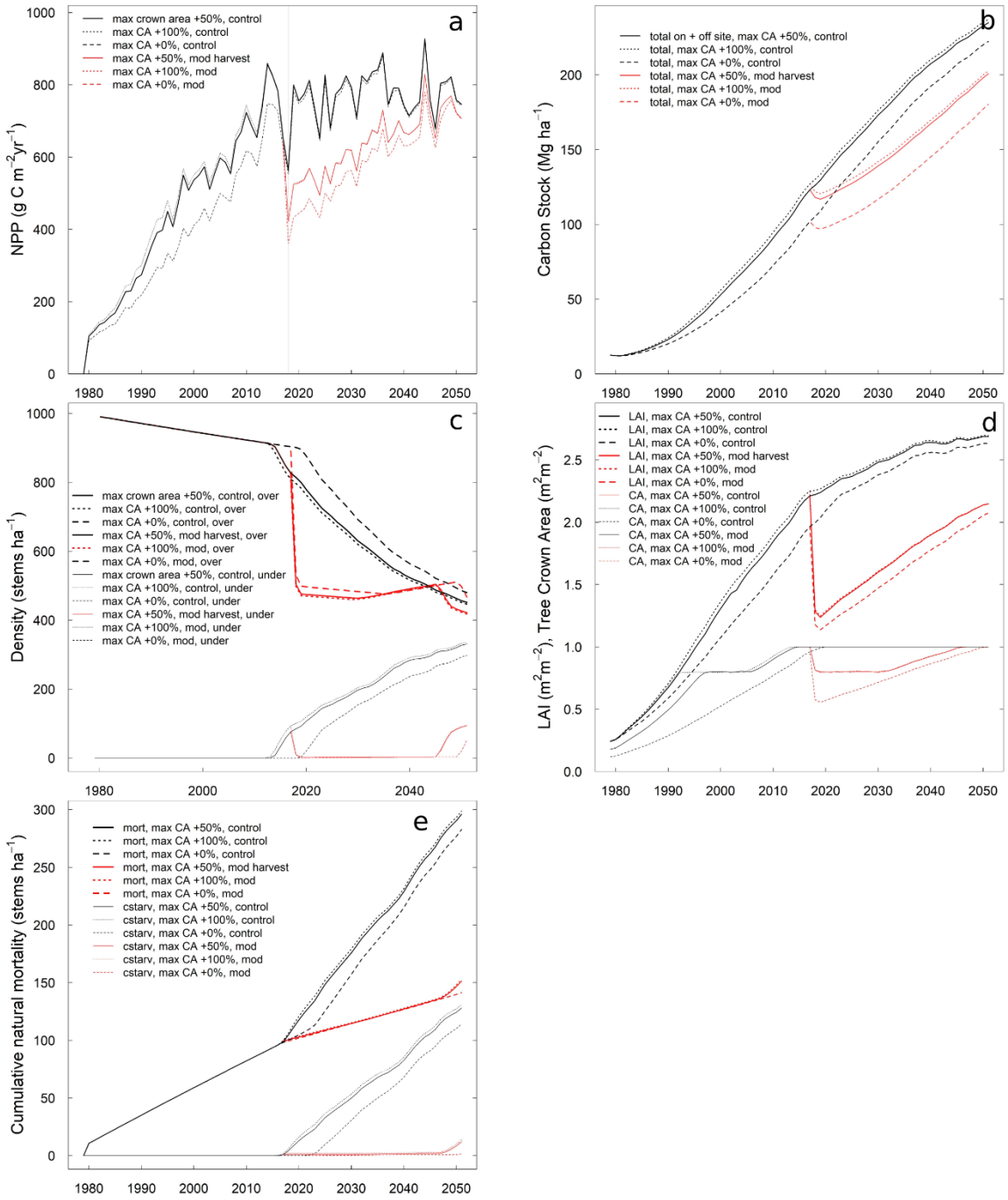

Figure 4. Canopy area parameter experiments, stand dynamics, 1979-2050. For harvest runs, intensity was moderate (observed). **a**. NPP **b**. Carbon stocks: total (on & off site), live biomass, and off site. **c**. Stand density, overstory and understory. **d**. Stand LAI and crown area. **e**. Cumulative natural mortality. Carbon starvation mortality as a component of total natural mortality is displayed additionally.

The impacts of variable ‘d2ca’ parameter ranges after harvest disturbances were demonstrated in combination with control and moderate thinning treatments (Fig. 4). At 40% density reduction, a ‘zero-range’ for ‘d2ca’ (representing persistent overstory gaps that were ‘grown into’ over time) led to reduced carbon stocks and fluxes through 2050 relative to both control and the initial ‘d2ca’ range (i.e. max d2ca ‘+50%’ greater than min d2ca). The ‘zero-range’ harvest simulation NPP was 16, 9, and 1% lower than the ‘+50%’ range harvest run in 2020, 2035, and 2050 (Table 2, Fig. 4a). 2020 ‘Zero range’ run NPP reduction relative to control was - 41% compared to - 30% for ‘+50%” and “+100%” ‘d2ca’ harvest runs; this larger reduction was similar to the 45% observed NPP reductions in 2017-2019 field plots (J. E. Stenzel et al., 2021). As a result, ‘zero-range’ live biomass carbon stocks were 15, 13, and 9% lower from 2020-2050, increasing stock deficits relative to the control stand (Fig. 4b). ‘d2ca’ ranges greater than the initial ‘+50%’ value had negligible impacts on total stand carbon stocks and fluxes through 2050. Like the ‘+50%’ run, the +100%’ run quickly reached the 80% canopy closure threshold, causing canopy spread per leaf biomass and LAI to decrease to it’s minimum and full closure to only occur when tree density reached a necessary level at ~2045. Near 2050, canopy tree demotion and understory development was delayed relative to ‘d2ca’ ‘+50%” and “+100%” runs by ~5 years.

Future control and harvest experiments simulated stands ‘planted’ ~50 years after historical stand plantations. Selective harvests occurred at the same stand age (i.e. 38 years, 2066 vs 2017). Across carbon stock, flux, and stand structure metrics, historical and future plantations displayed similar early post-thinning responses (Table 3, Fig 5). Divergence occurred at ~2075 (future stand year 50), when both future control and harvest stand NPP, total and live carbon stocks, and LAI decreased relative to historical plantation simulations

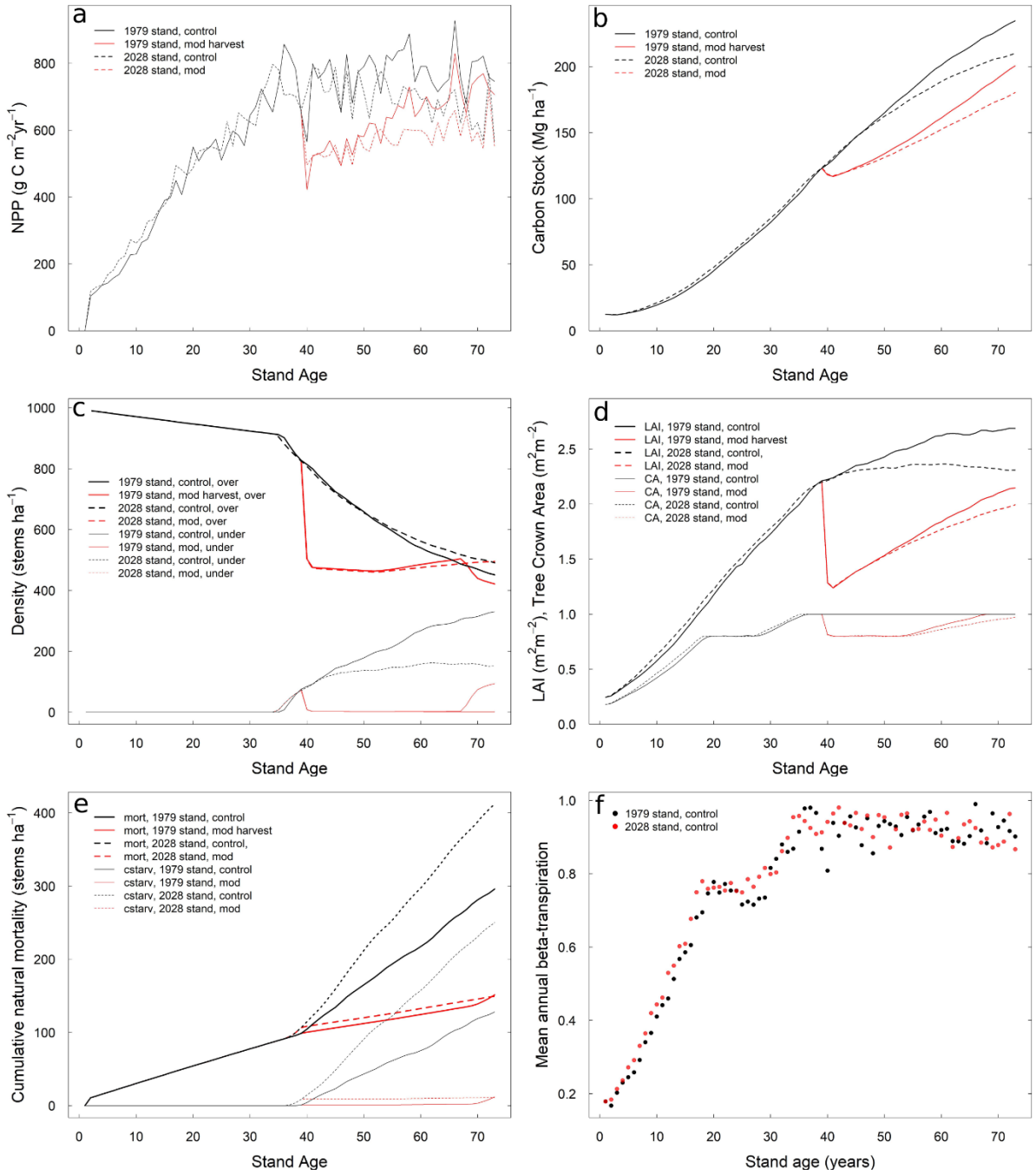

Figure 5. Historical and future stand initiation experiments, stand dynamics, 1979-2050 & 2028-2099. For harvest runs, intensity was moderate (observed). **a**. NPP **b**. Carbon stocks: total (on & off site), live biomass, and off site. **c**. Stand density, overstory and understory. **d**. Stand LAI and crown area. **e**. Cumulative natural mortality. Carbon starvation mortality as a component of total natural mortality is displayed additionally. **f**. 1979 and 2028 control stand yearly-average β-transpiration by stand age.

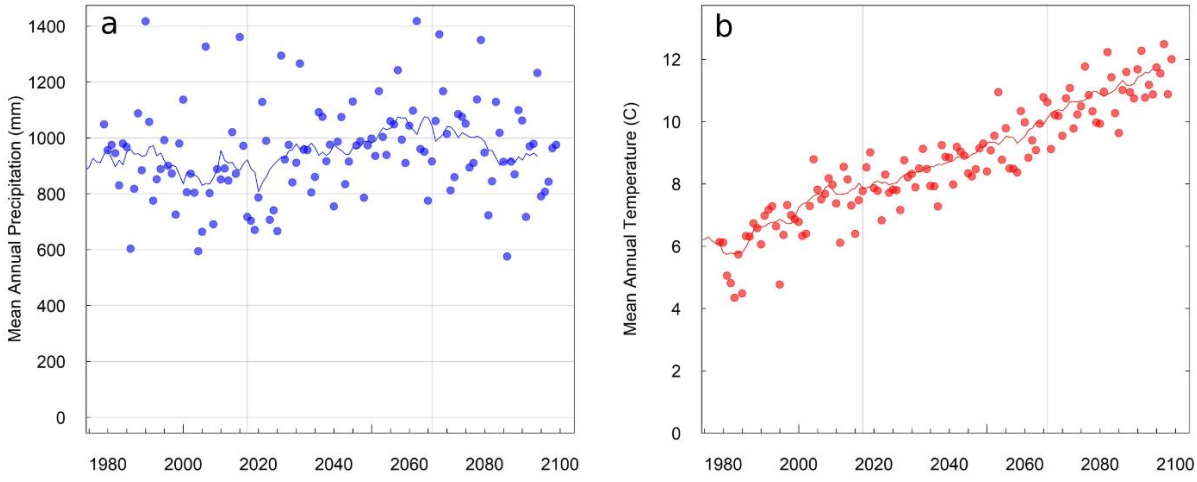

Figure 6. Miroc5 RCP 8.5-based FATES climate inputs, 1979:2099. Points indicate yearly averages; lines indicate 10 year, 2-sided rolling means. **a**. Mean annual precipitation **b**. Mean annual temperature.

(Fig 5 a,b,d). Divergence in carbon starvation mortality was minor (Fig 5e) and future stands demonstrated delayed understory development near year 70 (future stand ~2090-2099 ; Fig 5c). In the future harvest simulation, NPP and biomass recovery occurred, but were delayed compared to the historical stand harvest run. Future control plots, however, demonstrated declining NPP, LAI, and leaf biomass after peak values at ~50 years of age, with control and harvest NPP converging after 2090. In the absence of declining plant density, warming climate (increased temperature and VPD, Fig 6.) led to declining leaf biomass due increased understory mortality and decreased stand density.

The future harvested stand did not reach carbon parity with control. Live and total carbon stock deficits in 2099 were 13 and 29 Mg C ha^{-1}. Due to late-period convergence of NPP, carbon stock deficits were lower in than historical-stands (20 and 42 Mg C ha^{-1} for live and total stocks). Compared to their historical stands, future plantation total carbon stocks wer 25 and 20 Mg C ha^{-1} lower (10 and 10%) for control and treatment stands, though stocks continued to increase in all scenarios through the 72 year run length.

Discussion:

In all CLM-FATES experiments in a simulated UIEF Ponderosa pine plantation and across all time periods, selective harvest in the absence of subsequent stand-level disturbance caused carbon pool deficits (Mitchell et al., 2012), including total terrestrial (on + off site), live, and on-site dead. This finding is supported by observational studies of the carbon balance impacts of partial harvest (or restoration thinning) both within and beyond the western US (James et al., 2018a; Williams & Powers, 2019; Zhou, Zhao, Liu, & Oeding, 2013). Total terrestrial carbon deficits for harvested historical stands relative to control scenarios ranged from 16-41 Mg C ha^{-1} in 2020 and 10-62 Mg C ha^{-1} in 2050, representing

comparative increases in atmospheric carbon. These results are also consistent with the modeled 2050 deficit of 27 Mg C ha^{-1} in chapter 2 of this dissertation (Stenzel et al., 2021).

Near-maximum stand production (i.e. NPP) was simulated to continue through the late 21st century in all scenarios, despite increased canopy stratification and resulting understory mortality in control and low harvest intensity runs. Field observations from the study plantation also display high growth and stand-age-relative tree biomass compared to some other ponderosa pine forests in the Western U.S. (e.g. Campbell, Alberti, Martin, & Law, 2009; Law, Sun, Campbell, S, & Thornton, 2003), likely a result of the relatively wet site location. In control stand simulations, slow-decaying pools resulting from the death and turnover from stems and coarse roots led to persistent and increased dead ecosystem carbon that exceeded off-site wood product mass predicted by LCA. This relative dynamic resulted from high initial losses of harvest biomass to decomposition (leaves, fine roots) and combustion (branches burned as slash and product waste) (Dymond, 2012; Skog, 2008; Smith et al., 2006). Further, transfers of slow-decaying coarse root biomass to dead pools occurred earlier in harvest scenarios and therefore contributed to more complete run-period decay than the later, more gradual inputs resulting from tree competition and understory mortality, which represent future emissions past simulation periods.

Parity of thinned-stand NPP with control stands was approximately reached by stand ages of 60-70 years, or 20-30 years after harvest. In contrast, recovery of pre-thinning NPP occurred within several years in the Daycent projections of chapter 2 (J. E. Stenzel et al., 2021). This difference can be attributed to model structure. Daycent represents LAI that is not discretized by individual, cohort, or vertical leaf layers. Following disturbance that reduces biomass and LAI, LAI (and its direct scaling of NPP) can recover within several years if

woody biomass pools are large enough to support it based on an empirical equation (Parton et al., 1998). In effect, while Daycent simulates forest pools which have shrunken, it cannot represent horizontal gaps that would realistically result from a reduced density of the individuals that contribute to those pools. In contrast, FATES leaf area and spatial profile is restricted by the number and size of remaining trees, which determine allometric leaf biomass targets and maximum crown area (Fisher et al., 2015). In this study, we did not focus on comparisons of experiment NEP or ecosystem respiration because simulation soil carbon pools were not spun-up (i.e. the plantation was initiated from a cold state). However, the differences in total ecosystem carbons stocks between control and thinned stands decreased over time (Table 3), indicating relatively rapid NEP recovery within the context of these simulations, which is consistent with observations following multiple disturbance types in the western US (Amiro et al., 2010; Dore et al., 2010; Goetz et al., 2012). As such, the primary cause of carbon deficits legacies from harvest disturbances was the initial pulse of killed and then emitted ecosystem carbon.

In agreement with observational studies (Williams & Powers, 2019; Zhou et al., 2013), ecosystem and total carbon stocks were negatively related to the fraction of live trees harvested, while average overstory tree size increased with intensity across run periods. Low and moderate harvest intensity NPP and crown area recovered by year 2050 in historical-stand experiments. In experiments with stands planted in 2028, however, both control and thinned stands displayed declines in NPP relative to 50-70 year old historical stands. Decreases in GPP and NPP were attributable to increased temperature and VPD causing decreases in stomatal conductance and photosynthesis, as yearly average plant soil moisture stress did not increase. Decreases in assimilation led to increased mortality of understory trees with

exhausted carbon stores, as shown with the mid-century peak and then decline in control stand LAI and density. While stand carbon stocks did not reach equilibrium in any 70 year experiment, stock trajectories suggested that forest carbon carrying capacities (Keith, Mackey, Berry, Lindenmayer, & Gibbons, 2010) would be reduced by 2100 as a consequence of decreased leaf area and production.

Sensitivity experiments in which crown-area plasticity within DBH classes was varied (via the 'd2ca max' parameter) demonstrated that this parameter affects the timing of thinned-stand recovery, with decreased crown-area ranges increasing the carbon deficit between control and treatment areas. Decreased maximum crown area per DBH class led to more persistent crown area gaps following harvest, as tree canopies did not rapidly spread into available space. Though NPP reductions with decreased maximum crown area were closer to field observations in the several years after the 2017 thinning operation, the long-term accuracy of reduced canopy form plasticity is uncertain, as context-dependent crown morphology and allocation is a well-established component of forest growth (Pretzsch, 2014). It is likely that the rapidity of crown expansion with non-zero plasticity (i.e. days to months) in the absence of supporting growth is not possible; however, that degree of canopy space expansion becomes feasible several years after treatment. Finally, rapid canopy expansion was found to cause unexpected demotion and mortality in early parameter evaluation experiments when: 1) mortality created bare patches, 2) site-level crown area decreased below closure-behavior thresholds, and, 3) intact-patch canopy spread was triggered despite locally closed canopies. In effect, intact tree patches expansion was triggered by low canopy competition in horizontally separate space that intact patch trees were not able to access. This issue did not occur in the reported selective thinning experiments in this Chapter's results

because the model treatments were designed to transfer all thinned area to a new patch (e.g. harvest area = 100%, harvest fraction within area = intensity). In cases where patch number is allowed to increase, harvest or other mortality can trigger site-level canopy spread that leads to intact-forest canopy demotion and mortality. This behavior has not been previously reported, including with the FATES selective harvest module (Huang et al., 2020). This effect may have become apparent within this study's simulated stand due to low site reproduction and opportunistic canopy promotion, which, if present, could have mitigated low site canopy area and increased spread tendency resulting from bare patch creation.

Most simulated experiment mortality resulted from understory carbon starvation (Sevanto, Mcdowell, Dickman, Pangle, & Pockman, 2014) under study target carbon storage and mortality fraction parameters. Whether low overstory mortality and relatively consistent levels of stand NPP will occur as the actual stand matures and climate warms remains a key uncertainty that could alter carbon stock differences between control and treatment stands. Simulations lacked stochastic disturbances (e.g. insects or pathogens) that may stress carbon reserves of large, overstory trees that might otherwise remain vigorous under climate change alone (Bennett, Mcdowell, Allen, & Anderson-Teixeira, 2015). Additionally, because FATES represents cohorts of identical "average" trees (Fisher et al., 2015), individual mortality stochasticity is implied by a carbon starvation mortality fraction parameter, buffering against stand or canopy class-wide mortality during single extreme years that could shape real stand trajectories. Throughout most study experiments, control NPP did not significantly decline as stands matured, with only mild declines in carbon use efficiency (NPP / GPP; DeLucia, Drake, Thomas, & Gonzalez-Meler, 2007). In FATES, size-related (and therefore age-related) declines in NPP can occur gradually with increasing tissue respiration. Modeled stand NEP

and biomass can reach equilibriums due to first-order relationships between biomass stocks and turnover that balance saturated production. However, actual tree or stand GPP, NPP, and NEP may also decline in response to hydraulic limitations associated with size or changes to allocation and turnover (Bennett et al., 2015; Körner, 2003; Körner et al., 2005; McDowell et al., 2008; Pangle, Kavanagh, & Duursma, 2015; Ryan, Phillips, & Bond, 2006). Because these processes are not represented in FATES, NPP, the amount carbon available to be allocated to storage, and the storage pool buffer against starvation mortality could be overestimated as stands develop. Finally, FATES tree canopy layer demotion is based off of surface area filling given minimum crown area per DBH relationships; when canopy area is filled, a fraction of trees is demoted based in part on height. Therefore, there is a strong, immediate resolution of competitive differences and distinction between the light available to overstory trees versus recently demoted understory trees of the same size class. For this reason, photosynthesis limitations and their impact on carbon starvation mortality are exerted less heavily at a stand-wide scale during the stem exclusion phase of stand development (Waring & Running, 2010) than may be realistically expected with years of fractional changes to competitive characteristics.

CLM-FATES does not yet simulate mechanistic hydraulic failure and its existing, empirically based hydraulic failure mortality (from a soil water potential threshold and daily mortality fraction) did not contribute to mortality in this study's projections. In study simulations, summer reductions in photosynthesis were not driven primarily by soil moisture stress (as indicated by the 'beta-transpiration' output variable; Fig. 5f), but instead by stomatal conductance reductions based on an empirical relationship with vapor pressure deficit. Depletion of soil moisture to a multi-month summer minimum did not occur as in field

observations, in turn failing to trigger stomatal closure based on low soil matric potential. Currently, this issue may be related to a model issue in which soil depth cannot be restricted by bedrock depth to represent shallow uplands sites or to a model-wide low-bias for transpiration (D. M. Lawrence et al., 2019).

Conclusions:

In this study, we found that simulated young ponderosa pine stands treated with selective harvest did not reach carbon parity with control stands within 70 years in any experiment. Treatment stand NPP recovered in all but high intensity experiments and recovery time was positively correlated with thinning intensity. Further, thinned stands displayed higher structural allocation and average per tree NPP while experiencing decreased understory density and mortality. However, late 21st century stand NPP declined in both control and treatment experiments due to increased VPD, which caused decreased production and increased understory mortality.

Several observed model dynamics represent mechanistic improvements over the biogeochemical modeling reported in Chapter 2. Consistent with site observations, FATES simulated decreases in post-harvest NPP and recovery that exceeded multiple years due to generation of patches with decreased tree densities. Further, explicit space competition and carbon starvation mortality allowed for varied timing of canopy stratification and resulting understory stress between control and treatment stands. In contrast, dynamics that should be the focus of further improvement include a consistent sub-grid scale at which canopy competition and spread are implemented (i.e. site level crown filling vs patch level spread and demotion response) and more realistic soil moisture stress with increased summer moisture extraction. Finally, the target carbon storage parameter had a large impact on the timing and

canopy partitioning of carbon starvation mortality yet could not be validated directly with observations. Continued work will need to include sensitivity analyses that vary this and other important, parameter-associated hypotheses that may significantly determine the outcomes of treatments.

At a landscape scale, the carbon balance impacts of forest thinning are determined by treatment interactions with stochastic disturbances (including fire, insects, pathogens) and across environmental gradients (J. L. Campbell & Ager, 2013; J. L. Campbell, Harmon, & Mitchell, 2012). Stand scale results in this study demonstrate substantial, multi-decade carbon deficits in thinned stands in the absence of stand-level disturbance events. Anticipated future work with CLM-FATES includes introducing forest fire disturbance via the SPITFIRE module with region-scale model runs in which multiple new PFTs are parameterized. Previous work with CLM 4.5 has shown spatially variable forest carbon sequestration potential and vulnerability to drought and fire in the Northern Rocky Mountain ecoregion, indicating a range of preservation versus disturbance mitigation priorities (Buotte, Law, Ripple, & Berner, 2020; Buotte et al., 2019). Using CLM-FATES and SPITFIRE, more mechanistic representation of fire dynamics can be combined with dynamic vegetation to improve modeled representation of regional forest disturbances. As a result, management priorities – if, where, and when disturbance mitigation treatment should be applied for carbon storage and other benefits—can be better determined while considering regional complexity.

References:

Abatzoglou, J. T. (2013). Development of gridded surface meteorological data for ecological applications and modelling. *International Journal of Climatology*, *33*(1), 121–131. https://doi.org/10.1002/joc.3413

Abatzoglou, J. T., & Brown, T. J. (2012). A comparison of statistical downscaling methods suited for wildfire applications. *International Journal of Climatology*, *32*(5), 772–780. https://doi.org/10.1002/joc.2312

Abatzoglou, J. T., & Williams, A. P. (2016). Impact of anthropogenic climate change on wildfire across western US forests. *Proceedings of the National Academy of Sciences*, *113*(42), 11770–11775. https://doi.org/10.1073/pnas.1607171113

Agee, J. K., & Skinner, C. N. (2005). *Basic principles of forest fuel reduction treatments*. *211*, 83–96. https://doi.org/10.1016/j.foreco.2005.01.034

Amiro, B. D., Barr, A. G., Barr, J. G., Black, T. A., Bracho, R., Brown, M., … Xiao, J. (2010). Ecosystem carbon dioxide fluxes after disturbance in forests of North America. *Journal of Geophysical Research: Biogeosciences*, *115*(4). https://doi.org/10.1029/2010JG001390

Bennett, A. C., Mcdowell, N. G., Allen, C. D., & Anderson-Teixeira, K. J. (2015). Larger trees suffer most during drought in forests worldwide. *Nature Plants*, *1*(October), 1–5. https://doi.org/10.1038/nplants.2015.139

Bonan, G. B. (2008). Forests and climate change: forcings, feedbacks, and the climate benefits of forests. *Science*, *320*(5882), 1444–1449. https://doi.org/10.1126/science.1155121

Bowman, D. M. J. S., Williamson, G. J., Abatzoglou, J. T., Kolden, C. A., Cochrane, M. A., & Smith, A. M. S. (2017). Human exposure and sensitivity to globally extreme wildfire events. *Nature Ecology and Evolution*, *1*(3), 83844. https://doi.org/10.1038/s41559-016-0058

Brown, R. T., Agee, J. K., & Franklin, J. F. (2004). Forest restoration and fire: Principles in the context of place. *Conservation Biology*, *18*(4), 903–912. https://doi.org/10.1111/j.1523-1739.2004.521_1.x

Buotte, P. C., Law, B. E., Ripple, W. J., & Berner, L. T. (2020). Carbon sequestration and biodiversity co-benefits of preserving forests in the western United States. *Ecological Applications*, *30*(2), 1–11. https://doi.org/10.1002/eap.2039

Buotte, P. C., Levis, S., Law, B. E., Hudiburg, T. W., Rupp, D. E., & Kent, J. J. (2019). Near-future forest vulnerability to drought and fire varies across the western United States. *Global Change Biology*, *25*(1), 290–303. https://doi.org/10.1111/gcb.14490

Campbell, J., Alberti, G., Martin, J., & Law, B. E. (2009). Carbon dynamics of a ponderosa pine plantation following a thinning treatment in the northern Sierra Nevada. *Forest Ecology and Management*, *257*(2), 453–463. https://doi.org/10.1016/j.foreco.2008.09.021

Campbell, J. L., & Ager, A. A. (2013). Forest wildfire, fuel reduction treatments, and landscape carbon stocks: A sensitivity analysis. *Journal of Environmental Management*, *121*, 124–132. https://doi.org/10.1016/j.jenvman.2013.02.009

Campbell, J. L., Harmon, M. E., & Mitchell, S. R. (2012). Can fuel-reduction treatments really increase forest carbon storage in the western US by reducing future fire emissions? *Frontiers in Ecology and the Environment*, *10*(2), 83–90. https://doi.org/10.1890/110057

Chapin, F. S., Woodwell, G. M., Randerson, J. T., Rastetter, E. B., Lovett, G. M., Baldocchi, D. D., … Schulze, E.-D. (2006). Reconciling Carbon-cycle Concepts, Terminology, and Methods. *Ecosystems*, *9*(7), 1041–1050. https://doi.org/10.1007/s10021-005-0105-7

DellaSala, D. A., Anthony, R. G., Bond, M. L., Fernandez, E. S., Frissell, C. A., Hanson, C. T., & Spivak, R. (2013). Alternative Views of a Restoration Framework for Federal Forests in the Pacific Northwest. *Journal of Forestry*, *111*(6), 420–429. https://doi.org/10.5849/jof.13-040

DeLucia, E. H., Drake, J. E., Thomas, R. B., & Gonzalez-Meler, M. (2007). Forest carbon use efficiency: Is respiration a constant fraction of gross primary production? *Global Change Biology*, *13*(6), 1157–1167. https://doi.org/10.1111/j.1365-2486.2007.01365.x

Dore, S., Kolb, T. E., Montes-Helu, M., Eckert, S. E., Sullivan, B. W., Hungate, B. A., … Finkral, A. (2010). Carbon and water fluxes from ponderosa pine forests disturbed by wildfire and thinning. *Ecological Applications*, *20*(3), 663–683. https://doi.org/10.1890/09-0934.1

Dymond, C. C. (2012). Forest carbon in North America: annual storage and emissions from British Columbia's harvest, 1965-2065. *Carbon Balance and Management*, *7*, 1–20. https://doi.org/10.1186/1750-0680-7-8

Fisher, R. A., Muszala, S., Verteinstein, M., Lawrence, P., Xu, C., McDowell, N. G., … Bonan, G. (2015). Taking off the training wheels: The properties of a dynamic vegetation model without climate envelopes, CLM4.5(ED). *Geoscientific Model Development*, *8*(11), 3593–3619. https://doi.org/10.5194/gmd-8-3593-2015

Foley, J. A., Prentice, I. C., Ramankutty, N., Levis, S., Pollard, D., Sitch, S., & Haxeltine, A. (1996). An integrated biosphere model of land surface processes, terrestrial carbon balance, and vegetation dynamics. *Global Biogeochemical Cycles*, *10*(4), 603–628. https://doi.org/10.1029/96GB02692

Forest Climate Action Team. *F. C. A. California Forest Carbon Plan: Managing Our Forest Landscapes in a Changing Climate*. , (2018).

Franklin, J. F., & Johnson, K. N. (2013). A Restoration Framework for Federal Forests in the Pacific Northwest. *Journal of Forestry*, *110*(8), 429–439. https://doi.org/10.5849/jof.10-006

Goetz, S. J., Bond-Lamberty, B., Law, B. E., Hicke, J. A., Huang, C., Houghton, R. A., … Kasischke, E. S. (2012). Observations and assessment of forest carbon dynamics following disturbance in North America. *Journal of Geophysical Research: Biogeosciences*, *117*(2), 1–17. https://doi.org/10.1029/2011JG001733

Huang, M., Xu, Y., Longo, M., Keller, M., Knox, R. G., Koven, C. D., & Fisher, R. A. (2020). Assessing impacts of selective logging on water, energy, and carbon budgets and ecosystem dynamics in Amazon forests using the Functionally Assembled Terrestrial Ecosystem Simulator. *Biogeosciences*, *17*(20), 4999–5023. https://doi.org/10.5194/bg-17-4999-2020

Hudiburg, T. W., Law, B. E., Moomaw, W. R., Harmon, M. E., & Stenzel, J. E. (2019). Meeting GHG reduction targets requires accounting for all forest sector emissions. *Environmental Research Letters*, *14*(9). https://doi.org/10.1088/1748-9326/ab28bb

Intergovernmental Panel on Climate Change. (2018). Summary for Policymakers of IPCC Special Report on Global Warming of 1.5ºC approved by governments. *Ipcc*.

James, J. N., Kates, N., Kuhn, C. D., Littlefield, C. E., Miller, C. W., Bakker, J. D., … Haugo, R. D. (2018a). The effects of forest restoration on ecosystem carbon in western North America: A systematic review. *Forest Ecology and Management*, *429*(July), 625–641. https://doi.org/10.1016/j.foreco.2018.07.029

James, J. N., Kates, N., Kuhn, C. D., Littlefield, C. E., Miller, C. W., Bakker, J. D., … Haugo, R. D. (2018b). The effects of forest restoration on ecosystem carbon in western North America: A systematic review. *Forest Ecology and Management*, *429*(August), 625–641. https://doi.org/10.1016/j.foreco.2018.07.029

Keith, H., Mackey, B., Berry, S., Lindenmayer, D., & Gibbons, P. (2010). Estimating carbon carrying capacity in natural forest ecosystems across heterogeneous landscapes: addressing sources of error. *Global Change Biology*, *16*(11), 2971–2989. https://doi.org/10.1111/j.1365-2486.2009.02146.x

Kolden, C. A. (2019). We're not doing enough prescribed fire in the western united states to mitigate wildfire risk. *Fire*, *2*(2), 1–10. https://doi.org/10.3390/fire2020030

Körner, C. (2003). Carbon limitation in trees. *Journal of Ecology*, *91*(1), 4–17. https://doi.org/10.1046/j.1365-2745.2003.00742.x

Körner, C., Asshoff, R., Bignucolo, O., Hättenschwiler, S., Keel, S. G., Peláez-Riedl, S., … Zotz, G. (2005). Ecology: Carbon flux and growth in mature deciduous forest trees exposed to elevated CO2. *Science*, *309*(5739), 1360–1362. https://doi.org/10.1126/science.1113977

Law, B., Sun, O. J., Campbell, J., S, V. T., & Thornton, P. (2003). Changes in carbon storage and fluxes in a chronoseuence of ponderosa pine. *Global Change Biology*, *4*(4), 510–524. https://doi.org/10.1046/j.1365-2486.2003.00624.x

Law, B E, & Waring, R. H. (2015). Carbon implications of current and future effects of drought, fire and management on Pacific Northwest forests. *Forest Ecology and Management*, *355*, 4–14.

Law, Beverly E., Hudiburg, T. W., Berner, L. T., Kent, J. J., Buotte, P. C., & Harmon, M. E. (2018). Land use strategies to mitigate climate change in carbon dense temperate forests. *Proceedings of the National Academy of Sciences*, (12), 201720064. https://doi.org/10.1073/pnas.1720064115

Lawrence, D. M., Fisher, R. A., Koven, C. D., Oleson, K. W., Swenson, S. C., Bonan, G., … Zeng, X. (2019). The Community Land Model Version 5: Description of New Features, Benchmarking, and Impact of Forcing Uncertainty. *Journal of Advances in Modeling Earth Systems*, *11*(12), 4245–4287. https://doi.org/10.1029/2018MS001583

Lawrence, P. J., Feddema, J. J., Bonan, G. B., Meehl, G. a., O'Neill, B. C., Oleson, K. W., … Thornton, P. E. (2012). Simulating the biogeochemical and biogeophysical impacts of transient land cover change and wood harvest in the Community Climate System Model (CCSM4) from 1850 to 2100. *Journal of Climate*, *25*(9), 3071–3095. https://doi.org/10.1175/JCLI-D-11-00256.1

McDowell, N., Pockman, W. T., Allen, C. D., Breshears, D. D., Cobb, N., Kolb, T., … Yepez, E. a. (2008). Mechanisms of plant survival and mortality during drought: Why do some plants survive while others succumb to drought? *New Phytologist*, *178*(4), 719–739. https://doi.org/10.1111/j.1469-8137.2008.02436.x

Mitchell, S. R., Harmon, M. E., & O'Connell, K. E. B. (2012). Carbon debt and carbon sequestration parity in forest bioenergy production. *GCB Bioenergy*, *4*(6), 818–827. https://doi.org/10.1111/j.1757-1707.2012.01173.x

Moorcroft, P. R., Hurtt, G. C., & Pacala, S. W. (2001). A method for scaling vegetation dynamics: The ecosystem demography model (ED). *Ecological Monographs*, *71*(4), 557–586. https://doi.org/10.1890/0012-9615(2001)071[0557:AMFSVD]2.0.CO;2

Pan, Y., Birdsey, R. A., Fang, J., Houghton, R., Kauppi, P. E., Kurz, W. A., … Hayes, D. (2011). A large and persistent carbon sink in the world's forests. *Science*. https://doi.org/10.1126/science.1201609

Pangle, R., Kavanagh, K., & Duursma, R. (2015). Decline in canopy gas exchange with increasing tree height, atmospheric evaporative demand, and seasonal drought in co-

occurring inland Pacific Northwest conifer species. *Canadian Journal of Forest Research*, *45*(8), 1086–1101. https://doi.org/10.1139/cjfr-2014-0551

Parton, W. J., Hartman, M., Ojima, D., & Schimel, D. (1998). *Daycent description and testing*. 35–48.

Pelletier, J. D., Broxton, P. D., Hazenberg, P., Zeng, X., Troch, P. A., Niu, G., … Gochis, D. (2016). Global 1-km gridded thickness of soil, regolith, and sedimentary deposit layers. *ORNL DAAC*.

Pfeiffer, M., Spessa, A., & Kaplan, J. O. (2013). A model for global biomass burning in preindustrial time: LPJ-LMfire (v1.0). *Geoscientific Model Development*, *6*(3), 643–685. https://doi.org/10.5194/gmd-6-643-2013

Pretzsch, H. (2014). Canopy space filling and tree crown morphology in mixed-species stands compared with monocultures. *Forest Ecology and Management*, *327*, 251–264. https://doi.org/10.1016/j.foreco.2014.04.027

Ryan, M. G., Phillips, N., & Bond, B. J. (2006). The hydraulic limitation hypothesis revisited. *Plant, Cell and Environment*, *29*(3), 367–381. https://doi.org/10.1111/j.1365-3040.2005.01478.x

Sevanto, S., Mcdowell, N. G., Dickman, L. T., Pangle, R., & Pockman, W. T. (2014). How do trees die? A test of the hydraulic failure and carbon starvation hypotheses. *Plant, Cell and Environment*, *37*(1), 153–161. https://doi.org/10.1111/pce.12141

Skog, K. E. (2008). Sequestration of carbon in harvested wood products for the United States. *Forest Products Journal*, *58*(6), 56–72.

Smith, J. E., Heath, L. S., Skog, K. E., & Birdsey, R. a. (2006). Methods for Calculating Forest Ecosystem and Harvested Carbon with Standard Estimates for Forest Types of the United States. *USDA Northern Research Station, General Te*, 216. Retrieved from http://www.nrs.fs.fed.us/pubs/8192

State of California Executive Department. *Executive Order B-52-18*. , (2018).

Stenzel, J. E., Berardi, D. B., Walsh, E. S., & Hudiburg, T. W. (2021). Restoration thinning in a drought-prone Idaho forest creates a persistent carbon deficit. *Journal of Geophysical Research: Biogeosciences*, 1–18. https://doi.org/10.1029/2020jg005815

Stenzel, Jeffrey E, Lutz, J. A., Bartowitz, K. J., Hartman, M. D., Kolden, C. A., Smith, A. M. S., … Hudiburg, T. W. (2019). Fixing a snag in carbon emissions estimates from wildfires. *Global Change*, (March), 1–10. https://doi.org/10.1111/gcb.14716

Taylor, K. E., Stouffer, R. J., & Meehl, G. A. (2012). An overview of CMIP5 and the experiment design. *Bulletin of the American Meteorological Society*, *93*(4), 485–498. https://doi.org/10.1175/BAMS-D-11-00094.1

Thonicke, K., Spessa, A., Prentice, I. C., Harrison, S. P., Dong, L., & Carmona-Moreno, C. (2010). The influence of vegetation, fire spread and fire behaviour on biomass burning and trace gas emissions: results from a process-based model. *Biogeosciences*, *7*(6), 1991–2011.

U.S. Executive Office of the President. *Promoting Active Management of America's Forests, Rangelands, and Other Federal Lands To Improve Conditions and Reduce Wildfire Risk (Executive Order 13855)*. , (2018).

Waring, R., & Running, S. (2010). *Forest ecosystems: analysis at multiple scales*. Retrieved from https://books.google.com/books?hl=en&lr=&id=6YjhssXQ2AUC&oi=fnd&pg=PP2&dq=running+waring+forest+ecosystems&ots=bps4qI7IiG&sig=IH0iL0Gfuql9x8GCmEFQz3eqvT0

Williams, N. G., & Powers, M. D. (2019). Carbon storage implications of active management in mature Pseudotsuga menziesii forests of western Oregon. *Forest Ecology and Management*, *432*(September 2018), 761–775. https://doi.org/10.1016/j.foreco.2018.10.002

Zhou, D., Zhao, S. Q., Liu, S., & Oeding, J. (2013). A meta-analysis on the impacts of partial cutting on forest structure and carbon storage. *Biogeosciences*, *10*(6), 3691–3703. https://doi.org/10.5194/bg-10-3691-2013

Supplemental Information:

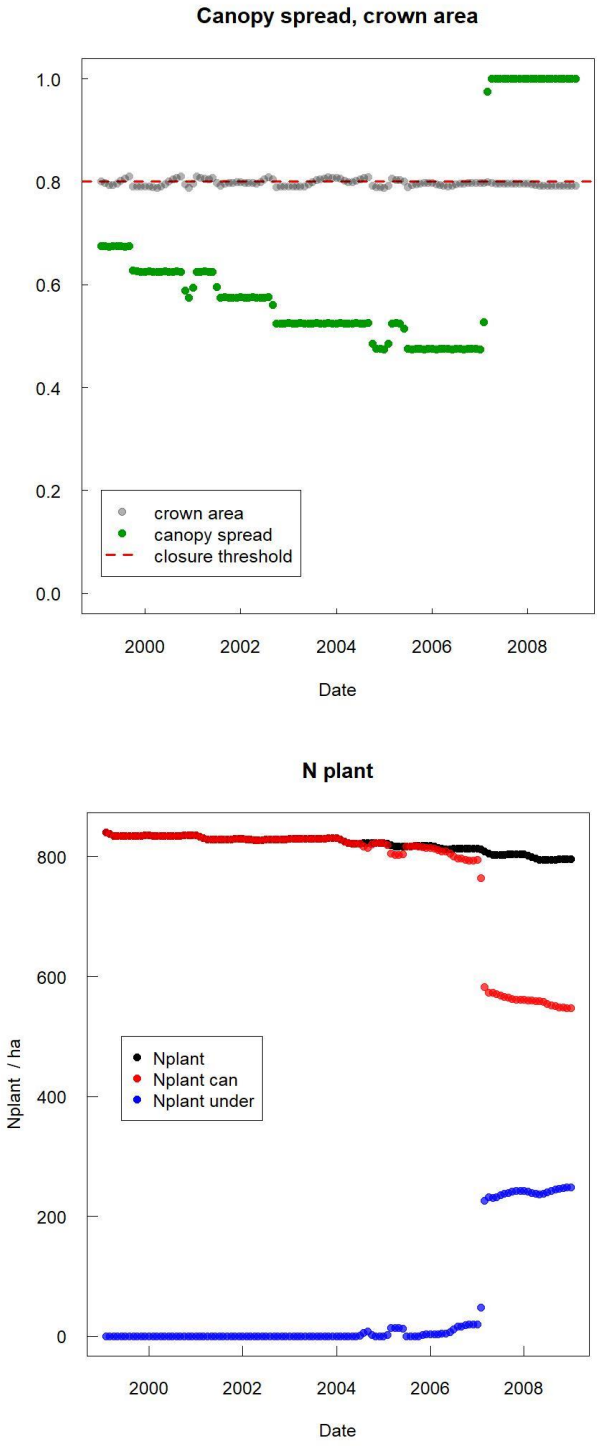

Figure S1. Example rapid canopy spread following threshold disturbance levels. Here, 'd2ca_max' is 200% of 'd2ca_min', with the same climate and initial density as the 'control 1' scenario (Table 2), but lower carbon storage targets/buffers, resulting in consistent overstory carbon starvation mortality. In **a**, sub-closure canopy area leads to rapid crown area expansion, resulting in rapid canopy closure, canopy tree demotion, and understory formation in **b**.